



Master Thesis

Hydrogeological 3D-modelling of Totes Gebirge karst basin supplying Lake Altaussee using VisualKARSYS platform

submitted by

Eric SMIT, BSc

in the framework of the Master programme

Kulturtechnik und Wasserwirtschaft

in partial fulfilment of the requirements for the academic degree

Diplom-Ingenieur

Vienna, June 2024

Supervisor

Priv.-Doz. Philipp Häuselmann, PhD
Institute of Applied Geology
Department of Civil Engineering and Natural
Hazards
University of Natural Resources and Life Sciences,
Vienna

Co-supervisors

Ass.Prof. Dipl.-Ing. Dr.techn. Erwin Heine
Department of Civil Engineering and Natural
Hazards
University of Natural Resources and Life Sciences,
Vienna

Dr. Pierre-Yves Jeannin
Swiss Institute for Speleology and Karst Studies
(SISKA)

Affidavit

I hereby declare that I have authored this master thesis independently, and that I have not used any assistance other than that which is permitted. The work contained herein is my own except where explicitly stated otherwise. All ideas taken in wording or in basic content from unpublished sources or from published literature, as well as those which were generated using artificial intelligence tools, are duly identified and cited, and the precise references included.

I further declare that this master thesis has not been submitted, in whole or in part, in the same or a similar form, to any other educational institution as part of the requirements for an academic degree.

I hereby confirm that I am familiar with the standards of Scientific Integrity and with the guidelines of Good Scientific Practice, and that this work fully complies with these standards and guidelines.


City, date

Eric SMIT (*manu propria*)

Acknowledgements

I would like to thank everyone that has helped me in the long process of my studies in general and during the research for and writing of this master thesis in particular. My sincerest gratitude to my supervisors, Dr. Philipp Häuselmann (BOKU, SISKa), Dr. Erwin Heine (BOKU) and Dr. Pierre-Yves Jeannin (SISKa). They accompanied me throughout and gave invaluable assistance and advice whenever necessary. Also from SISKa, Arnaud Malard introduced me to the workings of VisualKARSYS and answered any questions that remained.

I also owe thanks to the Walter Munk Foundation for the Oceans, especially to its president Mary Munk, for the warm welcome to the project and the wonderful meeting weekends in Altaussee.

From BOKU University, many thanks to Dr. Stephanie Neuhuber and Clemens Schmalfuß for pointers on literature and data, and to Prof. Dr. Rudolf Schwingenschlögl and Reinhard Gerstner for the vital help in the construction of the geological sections. It was also very useful to be able to use one of the  offered by the university library for thesis writing during the summer semester of 2023. From official Austrian institutions I also received a lot of assistance: the library employees of the Geological Survey of Austria (formerly GBA, now GeoSphere Austria) found any obscure piece of literature their online catalog gave me. DI Jutta Eybl of the Central Bureau of Hydrographics sent all information about tracer tests in the *Totes Gebirge* available, and Mag. Robert Stöffler of the Styrian federal administration, division 14, department for hydrography helped in uncovering the mystery of the orographic catchment without surface drainage. Thanks also go to Gerhard W. Mandl, Mario Habermüller and Oscar Fernández for pointers toward literature on Salzkammergut geology and cross sections.

Uncovering the mysteries of the *Totes Gebirge* caves would have been impossible without the help of the wonderful members of the CUCC, and Rob Watson especially, together with Robert Seebacher (VHO) and Lukas Plan (NHM) and all the cavers involved in discovering the depths of places the rest of us would not go anywhere near.

Last, but most certainly not least, a big thanks to my family and friends for their mental and material support and Anna, my wonderful girlfriend for many an evening of chatting with me, sitting in front of a screen and so much more.

Abstract

Lake Altaussee, Styria, Austria, is fed by underwater karst springs which drain a part of the surrounding massif, the Totes Gebirge. However, it is unknown how large and where this catchment is. It was thus the aim of this thesis to gain an understanding of the hydrogeological structure of the plateau and to delineate the catchment boundary of Lake Altaussee. The main methodological focus was the online, free hydrogeological karst modelling platform VisualKARSYS, developed by the Swiss Institute for Speleology and Karst Studies (SISKA). Its strengths lie in the uncomplicated construction of a geological model which can be iterated upon easily, and in the conceptual approach to karst aquifers, using the adjacent aquiclude topography and spring location and height to define vadose and phreatic zones within the karstified rock. On this basis, the catchment boundary can be drawn and flow condition-dependent connections between groundwater bodies can be recognised. To validate these results, a hydrological water balance model was implemented using two approaches and 48-year time series: First, the daily precipitation data from three weather stations was matched to the discharge from the lake under assumption of a flat evapotranspirative loss per year. This was compared to an estimation using a minimum specific discharge of mountainous karst catchments with the minimum discharge from the lake. Due to the poor quantity and quality of data, the results can only be understood as an order-of-magnitude estimation. Around 100 km² are estimated to feed the lake, only less than that. Seen as a synthesis of varied sources of data regarding the topic, the acquired body of knowledge could serve as a starting point for more focused research in the region. Three main areas of outstanding research spring to the fore: geological surveying, collection of precipitation and evapotranspiration data from the plateau, and modern tracer testing to prove hydraulic connections.

Kurzfassung

Der Altausseer See, Steiermark, Österreich, wird von Unterwasserkarstquellen gespeist, die einen Teil des umgebenden Toten Gebirges entwässern. Allerdings ist unbekannt, wie groß und wo dieses Einzugsgebiet ist. Daher lag der Fokus dieser Arbeit darauf, ein Verständnis für die hydrogeologische Struktur des Plateaus zu erwerben, und das Einzugsgebiet einzugrenzen. Der methodische Fokus hierzu war VisualKARSYS, eine offene Onlineplattform zur hydrogeologischen Karstmodellierung des Schweizer Instituts für Speläologie und Karstforschung (SISKA). Dessen Stärke liegt in der unkomplizierten, leicht zu iterierenden Erstellung geologischer Modelle und des konzeptionellen Karstverständnisses, bei dem die Topographie der Aquicluden sowie die Lage und Höhe der Quellen bestimmen, wo phreatische und vadosa Zonen des verkarsteten Gesteins liegen. So können Einzugsgebietsgrenzen gezeichnet und abflussabhängige Verbindungen zwischen Grundwasserkörpern erkannt werden. Um diese Resultate zu validieren wurde eine Wasserbilanzierung auf zweierlei Art durchgeführt: Zuerst wurden die Tagesniederschläge dreier Wetterstationen der Region, unter Annahme eines jährlichen Evapotranspirationsverlusts, mit dem Seenabfluss gegenübergestellt. Verglichen wurde dies mit einer Schätzung auf Basis eines minimalen spezifischen Abflusses aus Karstgebirgsgebieten und es minimalen Seenabflusses. Aufgrund der geringen Datenqualität und -menge können die Resultate nur eine Größenordnung der echten Gegebenheiten sein: Rund 100 km² entwässern durch den See, wahrscheinlich weniger. Der für diese Arbeit zusammengetragene Wissenskörper kann aber gut als Basis für weitere Forschungen dienen. Drei große Lücken tun sich hier auf: Geologische und meteorologisch-hydrologische Datenerhebung auf dem Plateau, sowie moderne Markierungsversuche, um hydraulische Verbindungen sicherzustellen.

Contents

Abstract	iii
Kurzfassung	iv
1 Introduction	1
1.1 Location - General description and characteristics	2
1.2 Scientific fundamentals in karst research	8
1.2.1 Geological framework	13
1.2.2 Hydrogeology and its application in karst	29
1.2.3 Karst hydrology	49
1.3 Research Questions	61
2 Methods and Materials	62
2.1 Data	62
2.1.1 Hydrological data	63
2.1.2 (Hydro-)Geological Data	69
2.2 Methodology	77
2.2.1 Water balance modelling	77
2.2.2 Hydrogeological modelling with VisualKARSYS	80
3 Results	96
3.1 Water balance modelling	96
3.2 Hydrogeological modelling	100
3.2.1 Geological sections drawn	100
3.2.2 Results from VisualKARSYS model	100
4 Discussion	108
4.1 Discussion of methodology and approach	108
4.1.1 Water balance modelling	108
4.1.2 Geology and hydrogeology	111

4.2	Discussion of the results	113
4.2.1	Hydrological water balance	113
4.2.2	VisualKARSYS model	114
5	Conclusions	123
5.1	Future outlook	124
	References	127
	List of Tables	140
	List of Figures	143
	Appendix A	144
	Appendix B	160

1 Introduction

When acclaimed oceanographer and geophysicist Walter Munk returned to Austria, his country of birth, in 2018, he visited Lake Altaussee, where he had spent many a happy holiday as a boy. Thinking of the pressures faced by alpine lakes due to climate change and pollution, he chose Lake Altaussee as an example, to be the object of scientific research encompassing all aspects of the lake's history and developments in geological, biological and hydrological terms. Analyses of microplastic dynamics, lake bed stratigraphy and water chemistry sampling are examples for the efforts undertaken by the Walter Munk Foundation for the Oceans and the involved scientists.

This thesis is also based on a research proposal of the project and aims to further the understanding of the lake's karst catchment. In a non-karstified watershed, catchment estimation usually starts and stops with a topographic catchment calculation. However, because karstified rock is characterised by strong underground channel flow across surface catchment borders, catchment size estimation in karst basins is more involved. For this thesis, at first an approximate watershed size is modelled by the means of the lake's water balance. The main part of the thesis is then a three-dimensional hydrogeological model, built in VisualKARSYS (SISKA, 2023), to arrive at an understanding of the spatial extension of the karst catchment.

To give an overview, Chapter 1 will introduce the reader to the lake itself, and the basics of hydrology, geology and hydrogeology as these topics pertain to the focus of this thesis. A background of previous findings from the relevant literature in the respective fields will also be given. In Chapter 2, the methods applied to hydrological and hydrogeological modelling for this thesis will be explained. Chapter 3 shows and describes the achieved results, which are then discussed in Chapter 4. A summary and concluding statements can be found in Chapter 5.

1.1 Location - General description and characteristics

The *Altausseer See*, or Lake Altaussee, is located in Austria, in the north-west of the federal state of Styria, very near the geographical centre of the country (see Figure 1.1). The larger cultural area it is situated in is called the *Salzkammergut*, boasting a long history of salt mining and picturesque alpine vistas. According to Beiwil and Mühlmann (2008) in their “Atlas of natural Austrian lakes with a surface area >50 ha”, Lake Altaussee has the following general and morphometric characteristics (see Table 1.1).

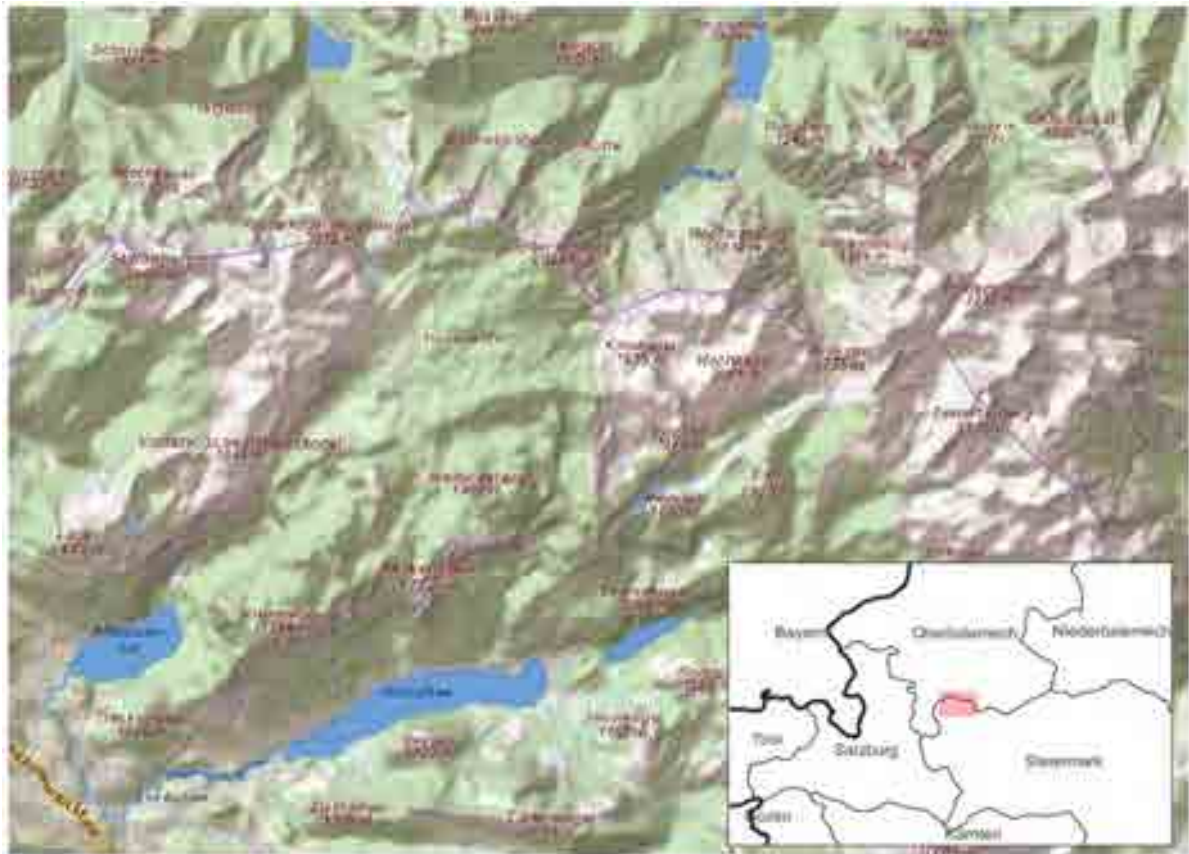


Figure 1.1: Map of the region of interest with shaded relief. Background map: Basemap (), shaded relief: ESRI.

As described above, the lake is fed from groundwater collected in the karst catchment. This is located inside the *Totes Gebirge*, or “Dead Mountains”, the limestone plateau massif that surrounds Lake Altaussee to the north, east and south-east. Owing to the rapid infiltration of precipitation into the karstified rock, little to no vegetation can survive on the plateau, hence the name.


The bathymetry of Lake Altaussee was the objective of a previous master’s thesis completed

Table 1.1: Collection of general and morphometric characteristics of Lake Altaussee according to Beiwl and Mühlmann (2008).

Water table elevation	712 m asl
Surface area	210 ha
Maximum length	2.6 km
Maximum breadth	1.0 km
Maximum depth	53 m
Average depth	35 m
Volume	$72.7 \times 10^6 \text{ m}^3$

for the project by Wagner (2021). A mixture of multibeam echo sounding in the deeper areas of the lake coupled with drone photogrammetry in the shallows was used, reaching an elevation precision of 0.5 m to 1 m. Although the bathymetric data could not be used in conjunction with VisualKARSYS for technical reasons, it still gives a good overview of the lake bed topography and clues about the karst system underneath. One such clue are a few funnels in the lake bed that reach up to 70 m in depth and show clear signs of water flowing up ~~and past~~ (e.g. no fine sediment, only larger gravel and rocks, crater walls built up around them (Harum et al., 2014)). These places are strongly assumed to be the inlets of karst groundwater into the lake. The area of their occurrence can be seen in Figure 1.2.

Physico-chemically, the water of Lake Altaussee has quite unique characteristics. In general, the lake shows dimictic, holomictic behaviour, meaning the entire water column mixes twice a year, in between of which the water stratifies based on temperature and therefore density. The temperature distribution over water depth shows a very rapid decline, from a summertime surface average of ca. 18 °C to 8 °C at a depth of 5 m, down to 4.6 °C under 15 m. This indicates a comparatively very shallow epi- and metalimnion, at 2 m and 5 m respectively. The hypolimnion, then, includes everything under about 10 m. The reasons for this structure are the lake's wind-sheltered location on the one hand, and the lack of a large surface-level input on the other hand. *Ödensee*, a different lake in the area, shows a similar water column structure with similar boundary conditions (Morton, 1932; Riedl et al., 2008).

Lake Altaussee's oxygen levels stay consistently high, with values directly  the spring mixing reaching a maximum of 15 mg L⁻¹ on the surface and an average of 11.5 mg L⁻¹ above the lake bed, corresponding to a 96 % O₂ saturation. In summer, when the phytoplankton is fully developed and photosynthesising, oversaturation levels of up to 138 % (14.8 mg L⁻¹)

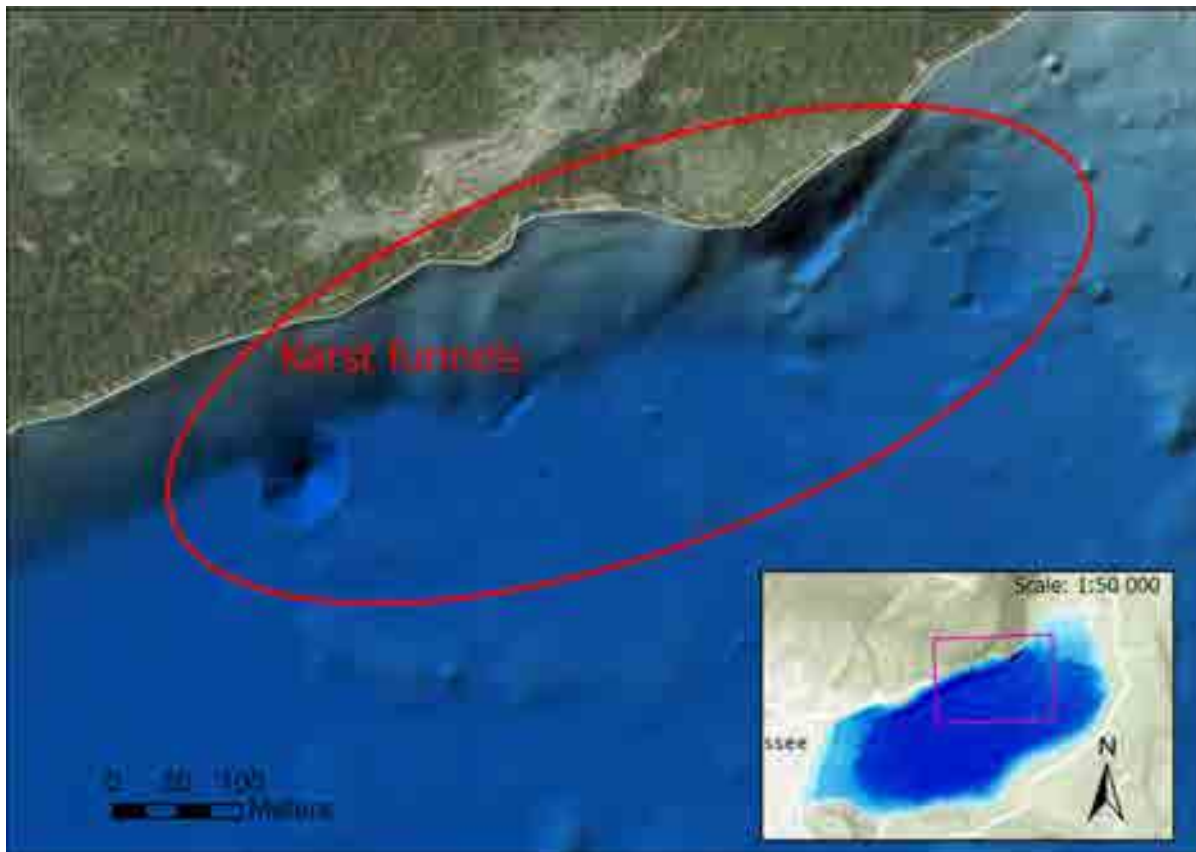



Figure 1.2: Visualisation of the bathymetry of Lake Altaussee assembled by Wagner (2021). The main area of karst funnel occurrence is marked, following Wagner (2021). Orthophoto of lake shore's source: GIS-Steiermark (2023).

have been measured at 5 m depth. On the surface, the higher temperatures cause lower O_2 levels of ca. 9.5 mg L^{-1} . However, even  m depth, 88 % O_2 saturation can be measured during summer. The pH-value of the lake varies from 7.2 to 8.6. For each sampling date, the corresponding value was homogeneous over depth and area, changing over time for as yet undescribed reasons (Morton, 1932; Riedl et al., 2008; Ruttner, 1937; Stundl, 1953). In a similar vein, the lake water's conductivity tends to remain quite constant over time, space and depth. From spring to summer, the values decline slightly, while at greater depth conductivity increases; in general, the levels range from $145 \mu\text{S}$ to $178 \mu\text{S}$. Concerning zoo- and phyto-nutritionally more interesting chemical compounds, e.g. nitrate, nitrite, ammonia, phosphorus and dissolved organic content (DOC), the oligotrophic nature of Lake Altaussee precludes levels large enough to sustain sudden algae blooms or similar phenomena. To be specific, nitrogen is present in the water mainly as nitrate (0.25 mg L^{-1} to 0.6 mg L^{-1} , average of 0.43 mg L^{-1}). Nitrite levels are so low as to have been largely undetectable by Riedl et al.

(2008), while ammonia peaked at 0.032 mg L^{-1} , an outlier probably caused by a miniscule input of organic matter. The levels of DOC ranged from 1.45 mg L^{-1} to 2.78 mg L^{-1} between 2004 and 2006. In general, the average surface concentrations were lowest, while larger variability and magnitude were found at the mesocline and below. Lastly, phosphorus acts as the ultimate plant growth inhibitor because of its scant occurrence in the lake's waters. Apart from random outliers, the average of total phosphorus in the upper 6 m of depth is $6.7 \mu\text{g L}^{-1}$ (Riedl et al., 2008). The stability with which Lake Altaussee and nearby *Grundlsee* stay oligotrophic can be seen in Figure 1.3.

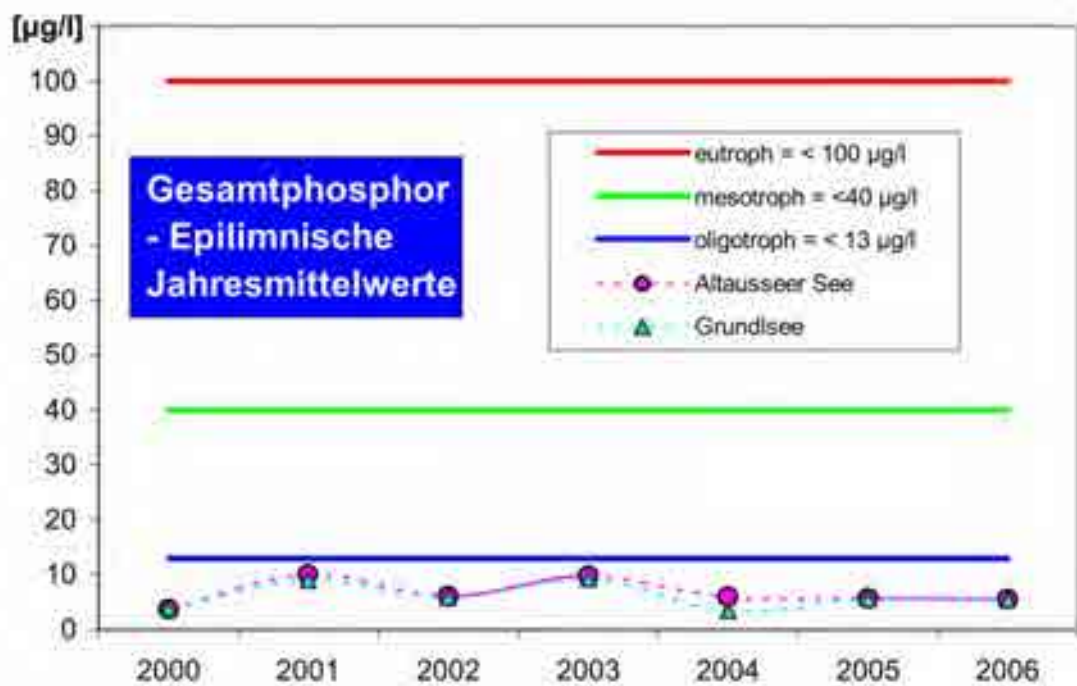


Figure 1.3: Graph taken from Riedl et al. (2008) showing the phosphorus content of Lake Altaussee in comparison to the threshold levels between trophic states (blue for oligotrophic, green for mesotrophic, red for eutrophic).


This water drains from the lake in the Altaussee Traun to the west-southwest, shortly afterwards joined by the Augstbach. Together with the Grundlseer Traun and the Kainischtraun it forms the Koppentraun, whose name changes to just Traun once it crosses federal state lines into Upper Austria and flows into Hallstätter See. Before becoming a tributary of the Danube, it flows through the Traunsee and most of the *Salzkammergut*. According to the Austria-Forum (https://austria-forum.org/af/AustriaWiki/Traun_%28Donau%29), in total its catchment is 4277 km^2 .

On the plateau of *Totes Gebirge*, the soil and vegetation cover is spotty and sparse. This,


of course, is due to the intensive karstification of the largely limestone constituting rock mass which leads to very rapid infiltration of rainwater, leaving little for soil formation or vegetation (Jennings, 1985). As can be seen in Figure 1.4, in large parts of the plateau the Normalized Difference Vegetation Index (NDVI) stays very low even in August, when the valley vegetation is at its maximum. However, there are also areas with obvious plant cover, in a range of one to two thirds according to Harlacher (2003). These occurrences are made up in part of mountain pines (E. Geyer et al., 2016) where there is enough soil for these to take hold. Otherwise, pioneer species form patches with alpine flowers and moss, before only lichen and algae can grow on bare rock (Mandl et al., 2012). Exceptions are local, red loam soils from the Tertiary that, along with the “Augensteine” described below, form a relict from that era. They are under increased protection, as their ability to store moisture allows for small-scale pasture farming on the otherwise infertile plateau (Mandl et al., 2012). Dinçer et al. (1972) note that the few small lakes that do exist, e.g. Wildensee, Elmsee and the Lahngang lakes, only do so because of the relative sealing property of the moraine sediments they lie on (see also Zojer, 1978). This ~~incredible~~ lack of water, coupled with the typical karst landscape forms, make the plateau accessible only to the determined and prepared, one of the reasons for the low density of good-quality geological data, as Schwingenschlögl (1986) attests to, having had a very difficult time lugging equipment and water throughout the plateau.


Beiwl and Mühlmann (2008, p. 116) also give an overview of the land use land cover (LULC) of the area in the orographic catchment of Lake Altaussee, which has an area of approx. 55 km². The vast majority, 70.3 %, are given as “open surfaces with little to no vegetation”, followed by 14.9 % covered by grasses, herbs and bushes and a further 10.1 % of wooded area. In absolute terms, these are 37.7 km², 8.0 km² and 5.4 km², respectively. Only a meager 0.4 km², or 0.8 %, are grasslands used for grazing.







Figure 1.4: Comparison of Normalized Difference Vegetation Index (NDVI) values for February and August 2023 over western *Totes Gebirge*. Images calculated by Nimbo service (Kermap, 2024) from Copernicus Sentinel satellite imagery; the greener, the larger the NDVI and therefore the more plant biomass is present. 

1.2 Scientific fundamentals in karst research

It was already mentioned above that Lake Altaussee discharges water that comes from a karst catchment ~~under the surrounding~~  *Totes Gebirge*. What, however, does that mean? In the following section, the phenomenon “karst” will be defined and explained for this context. Starting from the geological history of the Alps and the Northern Calcareous Alps (NCA) in general, and the *Totes Gebirge* in particular, the process of karstification and the development of karst catchments will be covered. Then, geological and hydrogeological modelling approaches will be dealt with. As the last step, the hydrology of karst areas and applicable hydrological modelling methods are given.

Historically, the word “karst” is eponymously derived from Slovenia's  *Kras*, a sparsely populated region which covers a quarter of the country's surface. This second-largest physiographic region's characteristic topography of hollow limestone shapes served as the resulting landscape name's origin for the natural scientists first mapping the area in the 18th century (Gosar et al., 2024). As given by the Encyclopedia Britannica (2024b), karst is defined as

"terrain usually characterized by barren, rocky ground, caves, sinkholes, underground rivers, and the absence of surface streams and lakes. It results from the excavating effects of underground water on massive soluble limestone." (Encyclopedia Britannica, 2024b)

This definition, ~~of the geomorphic variety as given by Worthington et al. (2017)~~, already includes the two domains of karst: the exokarst, which encompasses all forms visible from the surface of a karstified massif (e.g. karren, dolines, poljes)  (Bögli, 1980), and the endokarst, which in turn can be divided into different zones whose precise delineations differ ~~by author~~ . Following Ford and Williams (2007), the unsaturated zone, called the vadose zone, includes, with increasing depth, any covering soil, the subcutaneous zone (or epikarst), and the zone of transmission, in which infiltrating water can drain freely. Above the permanent karst water table, an intermittently saturated zone is situated, called the epiphreatic zone. Here, the level of saturation depends on rainfall events - after precipitation and resulting percolation, the groundwater table rises to build up the hydraulic gradient which increases discharge ~~from~~  the output point(s), decreasing the water table elevation again. ~~Under the~~  karst water table, the phreatic zone is permanently saturated, however, it can be subdivided into depths of decreasing circulation: the shallow phreatic zone's water content is frequently flushed after strong rainfall events, while the deep phreatic, or bathyphreatic, zone only shows exchange

after heavy recharge. The stagnant zone is practically never disturbed by subterranean currents.

Harlacher (2003) sees the epikarst, including the covering soil, as a self-contained unit and stresses its water storage capacity in the covering soil and/or faults, which is filled during precipitation events. Slowly but surely, this store is emptied into the vadose zone which stretches all the way to the permanent karst groundwater table. This term is defined more closely as the free water table in caves and conduits, to distinguish it from the often higher hydraulic gradient present in the matrix, or primary porosity of the rock itself. The distinction between primary porosity and the secondary (fault), as well as tertiary (dissolution conduit) porosities plays an important role in karst, with the latter acting as the main throughput route for rainfall and being the reason for the fast, (or “flashy” (Jeannin, 2014)) response of karst catchments to rain due to the high flow speeds, and the former providing long-term water storage in pores and draining freely during otherwise low-flow states (Ford and Williams, 2007; Hartmann et al., 2014).

The interplay between the fast-flowing conduit storage and the slow, but longer-term matrix pore water creates a dynamic of quite reliable base flows that are dwarfed in magnitude by precipitation event flow peaks. These large volumes of water are used by about 20 % to 25 % of the global population for a part or the entirety of its freshwater needs. In Austria, approximately one-third of the population depended on drinking water from karst systems in 1985 (Zötl, 1985, p. 237), and until 2001 this number had risen to 50 % (Kralik, 2001, quoted in Plan et al., 2009b, p. 285, C. Bauer and Plan, 2022)). Because the time the water spends underground is short, making the ground's cleaning effect relatively small and the speed of contaminant propagation high, and such a large population relies on the resource, vulnerability assessments and groundwater protection measures are of vital importance for the continued use of karst water. A variety of methods exist for different situations and data available (Laimer, 2005; Plan et al., 2009b). To show, on a global scale, which areas would come into question for karst water use, how to manage these resources and potentially protect them, the World Karst Aquifer Map (WoKAM) was created by the World-wide Hydrogeological Mapping and Assessment Programme (WHYMAP). This is a joint programme by a consortium which includes, among others, the UNESCO, its International Hydrological Programme (IHP) and the International Association of Hydrogeologists (IAH). As can be seen in Figure 1.5, all lithologically possible, i.e. carbonitic or evaporitic, outcropping formations are divided by their purity into continuous or discontinuous potential karst aquifers, as well as important karst springs and caves (WHYMAP, 2017). The concept and methodology for this map, as well as a sample map of European karst aquifers (see Figure 1.6) as developed by Chen et al.

(2017)).

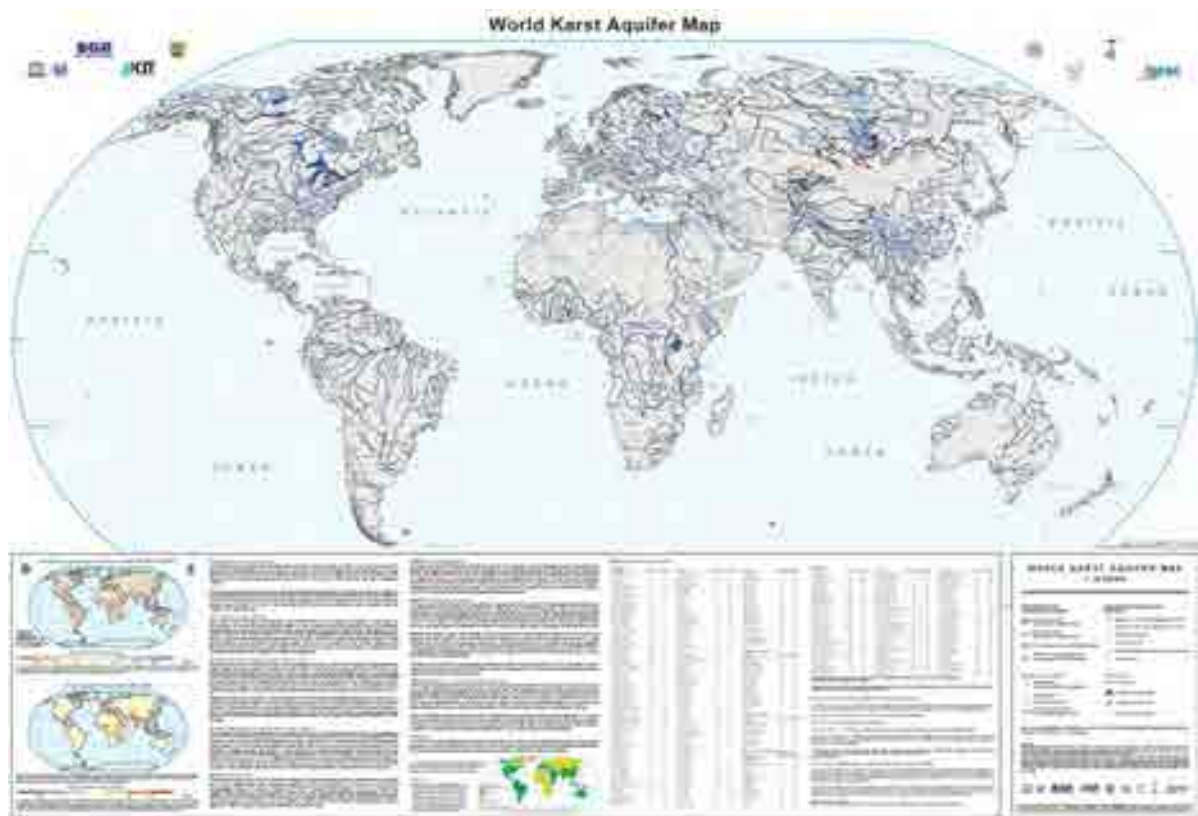


Figure 1.5: The World Karst Aquifer Map (WoKAM), developed by the World-wide Hydrogeological Mapping and Assessment Programme (WHYMAP) (WHYMAP, 2017) based on conceptualisation by Chen et al. (2017). In blue hues carbonate outcrops are shown and, under the assumption of karstification, thereby karst aquifers. Darker hues denote continuity (>65 % purity), lighter hues discontinuity (65 % to 15 % purity).

Inside of Austria, a similar large-scale lithological estimation of karstifiable rocks outcrops was undertaken; its result can be seen in Figure 1.7. It shows more or less the Austrian extents of the Northern and Southern Calcareous Alps (NCA, SCA resp.), as well as some additional specks of carbonate formations in the other regions of the Austrian Alps (Stummer, 1978, printed in Fink, 1978, p. 33).

As was shown, all around the world karst systems of all sizes, levels of complexity and of significance for local or regional water resource management have formed. However, the development of karst in a given soluble rock mass underlies a wide variety of different factors pertaining to a regions paleogeology and current geological setting, tectonic history, climate and other aspects. In the course of the study of karst and its phenomena, different scientific fields have developed many approaches to attempt to grasp the aforementioned complexities.

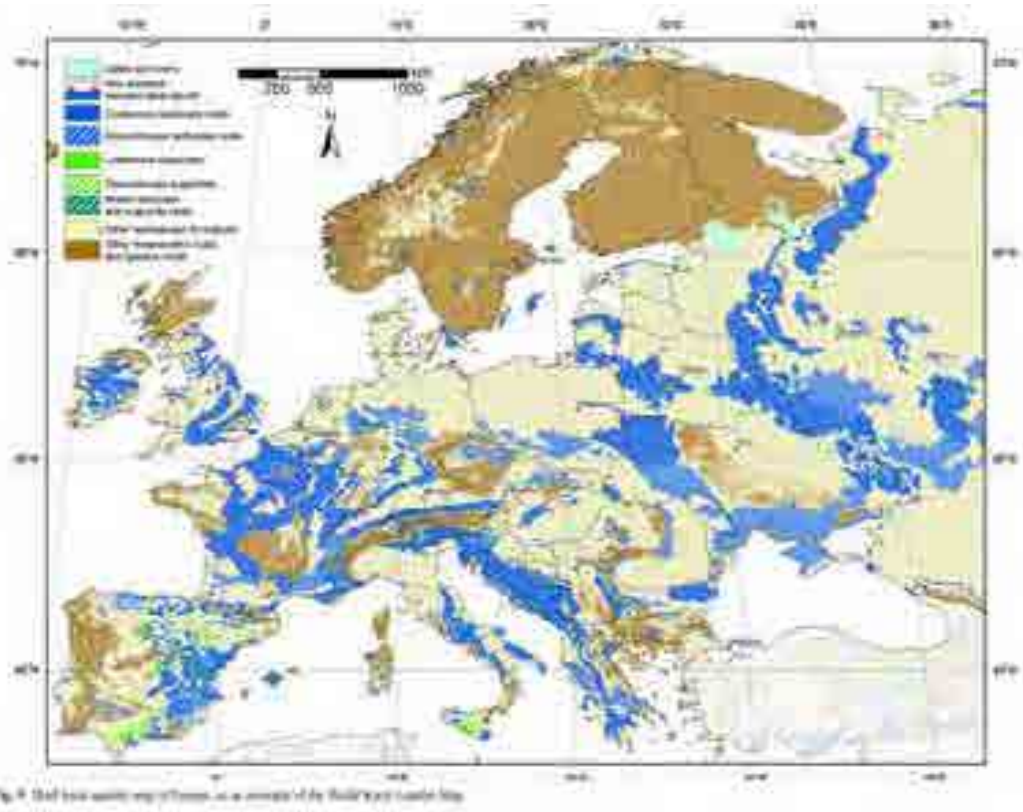


Figure 1.6: A draft version of the European extent (Chen et al., 2017, p. 781) of the World Karst Aquifer Map (WoKAM). In blue hues carbonate outcrops are shown and, under the assumption of karstification, thereby karst aquifers. Full darker hues denote continuity ($>65\%$ purity), striped with lighter hues discontinuity (65% to 15% purity).



Figure 1.7: A map of the Austrian extent of karstifiable rock formations (Stummer, 1978, printed in Fink, 1978, p. 33). Overlain is the map sheet layout of the Austrian map in the scale of 1:50000 (ÖK 50).

In the following sections, an overview will be given over the issues raised above.



1.2.1 Geological framework



Karst, as a description of a landscape type and its elements (Veress, 2022) and as a ~~water-soluble limestone landscape's~~ mainly underground drainage system, is highly dependent on a region's geological make-up and history in its genesis, development and continuing function (Mandl and Williams (2007)). For this reason, it is necessary to consider and describe the area of interest's geology thoroughly, to establish the basics necessary for any further investigation into its karst system.

The *Salzkammergut*, where the focus of this thesis lies, gained a lot of attention early on, as salt mining had been ongoing there for thousands of years already and was a major economic driver for the area. Mandl et al. (2012) gives a good overview of the first attempts to describe and classify that region and the Alps as a whole, often by the same actors involved in the creation of geology as a branch of science. In any case, many of the developing methods of geology, like biostratigraphy or international stratigraphic comparison, were applied in this area (Mandl et al., 2012). The founding in 1849 of the *Geologische Reichsanstalt*, or Geological Survey of the ~~Empire~~ ^{Empire}, in Vienna marks the beginning of state-sponsored institutional geological exploration and research in Europe in general (AEIOU, 2016). It also coincides with what is seen as the start of the so-called classical period of research in *Salzkammergut*: the classification of Dachsteinkalk as Triassic instead of Jurassic, following Alphons von Morlot in 1847 and Franz von Hauer in 1848 and their biostratigraphic work with ammonites (Mandl et al., 2012). During the following years, many carbonate formations were given names for their localities of first description that lay on the *Bad Ischl* map sheet, number 96, in the *Salzkammergut*. A few examples: the Hierlatz Fm., the Klaus Fm., the Hallstätter Fm., the Zlambach strata or the Plassen Fm (Mandl et al., 2012). The later director of the Geological Survey, Georg Geyer, spent a lot of time in the *Totes Gebirge* and published a monography about its hydrology, geology and touristic accessibility (G. Geyer, 1878) along with several other works about the area (G. Geyer, 1916; Vacek and G. Geyer, 1916).

In the effort to describe the geological history of the *Salzkammergut*, sheet tectonic concepts were developed there relatively very early on, and continue to be hotly contested. Specifically, the question of the paleogeographic relation between the Tirolic Dachstein-facies (= carbonate platform) massifs, the Juvavic Hallstatt-facies (= basin carbonate) areas and the Juvavic Dachstein thrust sheet was and is unclear, depending on regional tectonic model. From as early as 1904 onwards, nappists and autochthonists argued this point. While the former, in general, held the view that the basin sediments had formed outside of the carbonate platforms to the south and had then been moved north, the latter argued for intra-platform channels or basins. The nappists gave Jurassic sheet movements as the cause for today's facies mosaic

(Mandl et al., 2012). Recently, a salt-tectonics based modification of the autochthonist standpoint has been gaining momentum, emplacing Permian Haselgebirge salt diapirs inside the carbonate platforms (e.g. Fernández et al. (2021) and Leitner and Spötl (2017) and following). More details of the development of the Alps and the *Totes Gebirge* will be given in the following sections.

1.2.1.1 A short geological overview of the Alps

The mountain range of the Alps reaches from the shore of the Mediterranean Sea in the Southwest ~~until the~~ Vienna basin in the East, constituting parts of Italy, France, Switzerland, Liechtenstein, Austria and Slovenia on the way. The main chain of the Alps, also known as the Alpine divide for its orographic effect in delineating all catchments north or northwest of the range from those south or southeast, covers roughly 1200 km in length (Diem et al., 2024).

As a part of the Alpine mountain belt (see Figure 1.8), the Alps are amongst the youngest mountain ranges in Europe, with the earliest orogenic event (Eo-alpine orogeny) dating to the Cretaceous period. Preceding the Alps, the Variscan and the Caledonian mountain belts formed in the late and early Paleozoic, respectively. By the time of the formation of the Alps from the late Mesozoic onwards, erosion had largely worn down these previously massive ranges (Pfiffner, 2015). In Austria, the hills of the Bohemian massif to the north of the Danube in Lower and Upper Austria are direct remains of the Variscan orogeny, although Variscan metamorphism can be observed in basement units of the Eastern Alps (Schuster and Stüwe, 2022).

Beginning with the Permian period (from 285 Ma on), things started getting serious for the formation of the Alps. The supercontinent of Pangaea, along whose eastern shore the paleogeographic origin of the Alps lay, slightly to the North of the equator, was starting to break up in N-S expansion. The resulting continents of Gondwana and Laurasia were being driven apart from one another by a rift that started from the Tethys Ocean and propagated to the West. ~~This rift would later become the Atlantic Ocean.~~ Gondwana then moved in a counterclockwise direction and eastwards relative to Laurasia, continuing after the former lost the South American plate to its west and the latter being split into North America and Eurasia by the developing North Atlantic, itself widening along rifts either side of Greenland. Caused by the eastward movement of Africa, the Adriatic (or Apulian) plate also rotated counterclockwise (Schuster and Stüwe, 2010). To its east and south lay the Meliata-Hallstatt-Vardar Ocean, an embayment of the Tethys Ocean. Beyond the the Piemont-Ligurian Ocean to the northwest and Penninic Ocean to the north and northeast, the European plate lay. On

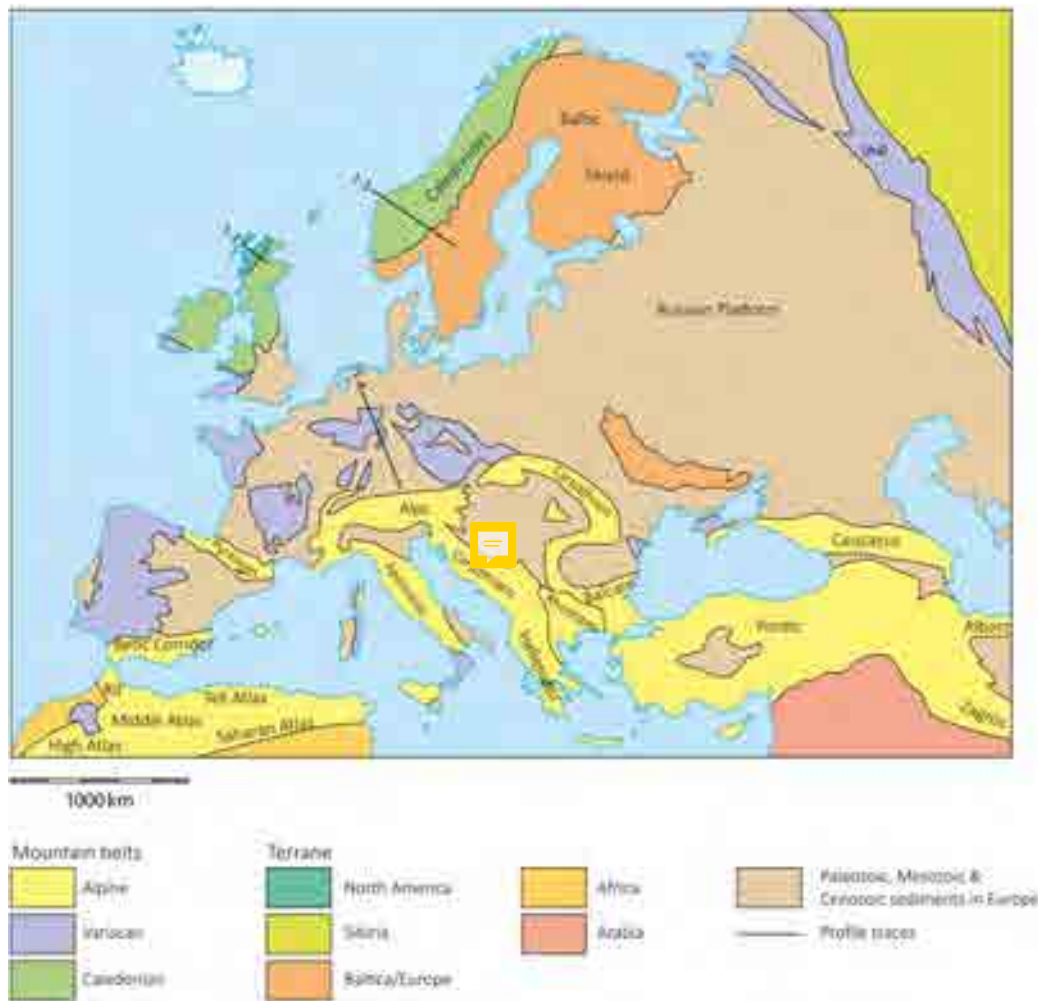



Figure 1.8: Large-scale tectonic map, modified from Pfiffner (2015), showing the three youngest mountain belt orogenies in and around Europe, as well as the terranes that constitute western Eurasia, the northern tip of Africa and the Near East.

both coasts were situated shelf zones of wide-spread carbonate and siliciclastic sedimentation from which, amongst others, the Northern and Southern Calcareous Alps or the Penninic masses formed (Pfiffner, 2015).

During the previously mentioned Permian rifting of Gondwana and Laurasia, the northern Adriatic continental lithospheric crust had been significantly thinned, while the mantle part had thickened and cooled only slowly. This combination of depths and densities can cause negative buoyancy to occur also in continental plates. Following Jurassic tectonic activity, a more southern part of the plate, unaffected by this development and therefore positively buoyant, moved along sinistral strike-slip faulting to confront the negative buoyancy in the north. Here, according to Stüwe and Schuster (2010), an intracontinental subduction zone

initiated in the Cretaceous as the first, Eo-alpine, orogenic event of the Eastern Alps (130 Ma to 80 Ma, (Schuster and Stüwe, 2022)) - the rock masses to become Central and Western Alps continued sedimenting in the oceanic Penninic and distal continental Dauphinois-Helvetic realms unperturbed (Pfiffner, 2015). The documented mid-Cenozoic metamorphic peak (45 Ma to 30 Ma, (Schmid et al., 2004)) was then caused by continental collision after the closure of the Penninic Ocean, along the same subduction suture.

Alternative theories postulate either only one long subduction of the oceanic plates under the Penninic Ocean, which does not account for the mentioned Eo-alpine eclogite metamorphism (Tollmann, 1977, in Stüwe and Schuster (2010, pp. 175-176)). Or, two successive oceanic subduction zones are put forth (first the Meliata-Hallstatt Ocean, then the Penninic Ocean), but the lack of lithologies related to oceanic subduction in the Eo-alpine metamorphic band, e.g. ophiolites, as well as “geometric problems with the removal of the mantle part of the lithosphere” (Stüwe and Schuster, 2010, p. 176) if the Austroalpine nappes were to have been stripped off their mantle entirely (Neubauer et al. (2000), in Stüwe and Schuster (2010, p. 176)). .

In the pro-wedge formed between the southwardly subducted European plate and the Adriatic plate's hanging wall, the Austroalpine nappes were the first to be involved and were pushed northwards on the top of the wedge. In the course of further subduction, the Penninic, Helvetic and Subpenninic nappes were sheared off northern, distal Adriatic, oceanic Penninic and southern, distal European lithosphere. The Alpine orogenic metamorphism peak (around 45 Ma to 30 Ma) formed eclogites and blueschist in some of the (Sub-)Penninic nappes (Schuster and Stüwe, 2022).

Throughout this time, the Alpine orogenic wedge experienced continuing build-up. At first by inclusion of the formations scraped off their lithospheric mantle, and then, when subduction of the European plate came to a halt and the two plates collided head-on in the Oligocene-Neogene, a further 28 % to 39 % of N-S shortening due to Adriatic underthrusting under the pro-wedge and backthrusting of the retro-wedge making up the Southern Alps. This pressure was released in 47 %, or up to 300 km (Pfiffner, 2015), W-E lateral extension of Eastern Alpine orogen toward the newly forming Pannonian basin, along sinistral strike-slip faults in the north (i.e. Salzach-Ennstal-Mariazell-Puchberg (SEMP) fault), in the south mainly the dextral Periadriatic strike-slip fault (PAF), and in the west the normal faults on either side of the Tauern Window (Brenner fault in the west and Katschberg fault in the east). Additionally, the faster rollback of the European slab in the Carpathian region due to strong slab-pull forces acting on the very dense Magura Basin lithosphere resulted in encouragement for eastward escape of Austroalpine units (Mroczek et al., 2023).

Previously, the accepted model of European plate mechanics in the Oligocene-Miocene held that the divergent forces between the denser, oceanic part and the lighter, continental part were released by the former breaking off at a relatively shallow depth. “Like a cork out of water” (Schuster and Stüwe, 2010, p. 17), the Alpine orogenic wedge gained substantial height and became the high mountain ridge we are familiar with today. Because the European slab was surprisingly shortened, the continuing northward movement of Adria led, in turn, to its north-dipping subduction under the European plate. However, as shown in geological transects in, for example, Schuster and Stüwe (2010, p. 12), Schmid et al. (2004, p. 101) or Schuster and Stüwe (2022, p. 10), this idea, coupled with the data already available that indicated an undisturbed southward subduction of the European plate in the Central and Western Alps, led to the implication of a subduction polarity switch. Mroczek et al. (2023) collected teleseismic data along previously unprobed transects and was able to show that the postulated break-off does not seem to have happened, as a flat Moho was detected to bridge the gap between the two steep Mohos of Europe and Adria (see Figure 1.9. Instead, around 32 Ma ago, asthenospheric mantle material could have started to well up and insert itself in the décollement between the thin, distal European slab’s mantle lithosphere and the Penninic and Subpenninic nappes being formed. The intrusion of this so-called Pannonian Moho would be able to explain the magmatism along the PAF from around 35 Ma, which previously was given as proof of shallow European slab break-off. The Pannonian Moho as an affectant of eastward lateral escape of Austroalpine units would also give a reason for the Early Miocene (around 20 Ma) shift from flysch- to molasse-type sedimentation in the Paratethys of the European Alpine foreland: the decrease in weight load with movement of Alpine nappes to the east would account for this change (Mroczek et al., 2023).

Ever since the Oligocene-Miocene uplift of the Alps, the endo- and exogenic forces of erosion have been at work. The many intra-alpine basins that opened up along strike-slip faults, e.g. the Vienna basin or the Styrian basin with the Klagenfurt basin as an appendix, were infilled with fluvial sediments of the drainage system establishing itself (Schuster and Stüwe, 2010). Continuing uplift, probably due to “processes in the upper mantle” (Schuster and Stüwe, 2022), further increased the erosional gradient. However, decreasing load on the lithosphere due to decreasing mountain mass again led to further uplift of the Alpine orogen, causing even more removal of exposed rock mass. Regional further tectonic uplift or subsidence movements, as well as differing lithological resistance to erosion and fault and contact erosion preference for streams and rivers resulted in locally and regionally divergent trends in mountain and valley elevations. For the Eastern Alps, Frisch et al. (2000), cited in Pfiffner (2015, p. 345), delineated five regions with differing characteristics regarding

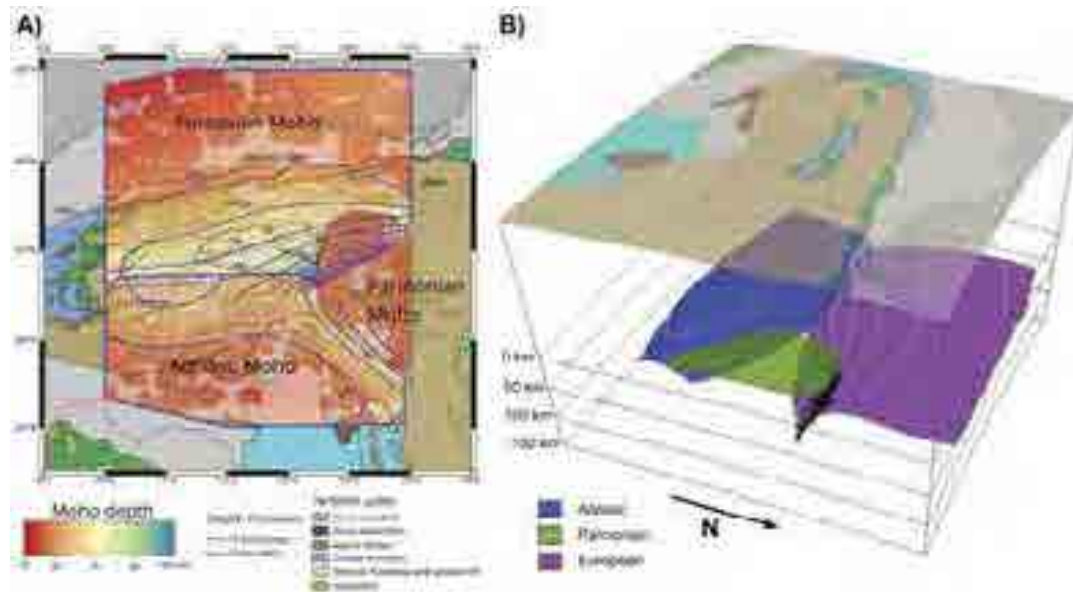


Figure 1.9: Diagram from Mroczek et al. (2023) of their teleseismic findings suggesting a flat Pannonian Moho reaching as far west as the Tauern Window. **A)** shows the depth contours of the European and Adriatic Mohos in the north and south, respectively, with the Pannonian Moho between them in their strong declines in the east, and **B)** gives a three-dimensional view of the spatial relation of the three slabs.

slope inclination and elevation a.s.l.: a high and rough relief could be found in areas that had been uplifted and eroded significantly since the Miocene, linked to the Cenozoic Alpine orogen. In contrast, areas in the east Eastern Alps, influenced strongly by the Miocene W-E lateral escape, show a more soft relief, also caused by the now exhumed, more strongly metamorphosed lithologies (Pfiffner, 2015).

The fluvial drainage system of the Alps experienced drastic changes throughout the Miocene and the Pliocene. From an entirely westward drainage of the Central Alps during the Mid Miocene, the formation of the Jura mountain range in modern Switzerland and France, from 10 Ma to 3 Ma, shifted this direction eastward. Affecting the southern Alpine catchment, the so-called Messinian salinity crisis dried out the Mediterranean Ocean completely, lowering dramatically the base level of all catchments draining toward the south. The consequent backcutting gave the large Piemontese and Lombardic lakes (Lagao Maggiore, Lago di Como, Lago d'Iseo and Lago di Garda) a thalweg of down to 700 m under sea level (Pfiffner, 2015), lower even than the current Adriatic sea floor (Schuster and Stüwe, 2010). The V-shape of the uneroded valley profiles is a sure sign for their fluvial origin. Geologically shortly afterwards, the flooding of the Mediterranean after the re-opening of the Strait of Gibraltar reached far inland along the recently so deeply cut valleys, leaving marine sediments in the area of Lake

Lugano, currently some 170 km away from the Mediterranean coast at Genoa.

The Alpine Quaternary has been marked by up to 15 climatic cold periods and their resulting wide-spread glaciations covering up to almost the entire Alpine mountain range with hundreds or thousands of metres of ice and snow, and their forelands and basins with the glacial sediments that can reach equal depths (Pfiffner2015). For example, the hole of Bad Aussee in Styria, Austria has sedimentary infill of at least 880 m, as found out by deep core drilling (van Husen and Mayr, 2007). This case also exemplifies the strong dependence of grain size distribution on alternating periods of glacial advance, cover, and retreat, glacier lake sedimentation, and the intervening warm periods. Schmalfuss et al. (2023) show that the provenance of sediment cover could also be changed by glaciers, depending on the flow direction and extents: a re-investigation of the drill core in the Bad Aussee basin showed beds with a much higher crystalline content than possible for the neighbouring carbonate outcrops of the Northern Calcareous Alps (NCA). Instead, the glacier must have brought the crystalline gravels from south of the Enns catchment, possibly crossing the current Traun-Enns watershed divide along the Salza gorge, against today's flow direction.

Currently, the Alps are, at least tectonically, a relatively quiet region. With the counter-clockwise Adria plate rotation having slowed to half a degree per million years around a point near Turino, and almost no northward translational movement anymore, the mountain range has quieted down. Any uplift movement left is caused in large part by pressure deloading due to erosional forces, which are keeping pace handily (Pfiffner, 2015; Schuster and Stüwe, 2010). In Figure 1.10, an intuitive overview of the tectonic makeup of the Alps can be seen which was drawn by Schuster and Stüwe (2010). It gives an unusual block-diagrammatical, orogen-parallel view which aids in the understanding of the processes that led to the present situation.

1.2.1.2 Geology of Northern Calcareous Alps and *Totes Gebirge*

Zooming in from the large-scale view of the entire Alps to the more small-scale extent of this thesis' spatial scope, the latter fits into the former geologically thus: being situated east of a N-S line, which itself is approximately between the 10° longitude in the east and the connection of Constance with Milano, it lies in the Eastern Alpine domain (Pfiffner, 2015). Additionally, as the plateau of *Totes Gebirge* is made up of Mesozoic carbonate sediments, and outside either the Tauern or the Lower Engadine Windows, it must be counted as part of the Austroalpine nappe stack, with its paleogeographic origin on the Adriatic tectonic plate (Mandl, 2000; Schuster and Stüwe, 2022). A classification as part of the Southern Alpine is not possible because Altaussee is well north of the Periadriatic Fault, the dividing



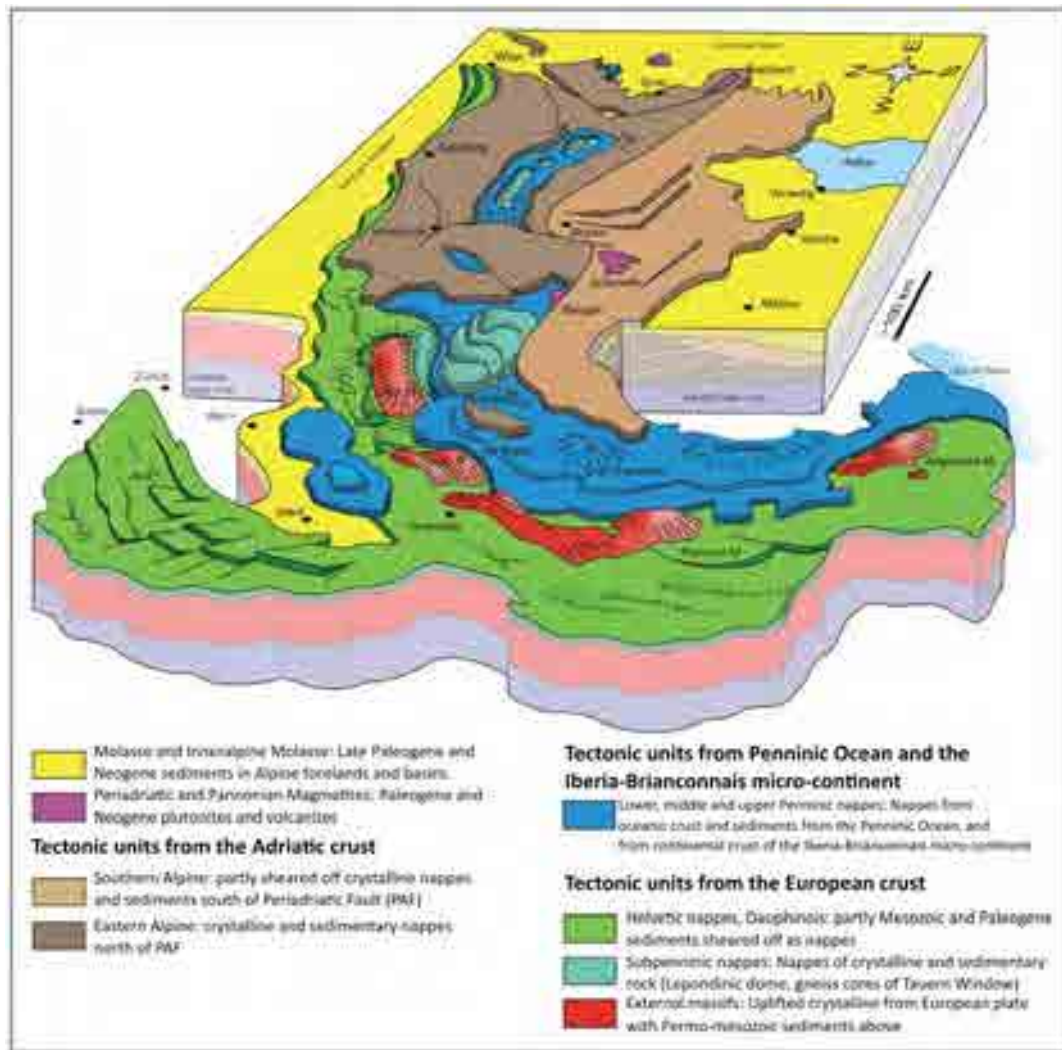


Figure 1.10: Block diagram modified from Schuster and Stüwe (2010) showing the current tectonic make up of the Alps, with geographic markers.

~~line between the Eastern and Southern Alpine domains.~~ Within the Austroalpine system, its Upper Austroalpine Subunit is made up of five units, the two lower-most of which are mostly metamorphic basement (Silvretta-Seckau and Veitsch-Silbersberg Nappe Systems). The thick Permo-Mesozoic sedimentary cover above, which forms the Northern Calcareous Alps (NCA), is made up of three nappes: the Bajuvaric, Tirolic-Noric and Juvavic nappes, from bottom to top. Their combined ~~un- to lowgrade metamorphosed~~ sediments reach up to 3200 m of thickness (Schuster and Stüwe, 2022). This naming convention also reflects the eponymous localities of their first description (Hahn (1912, 1923) cited in Mandl et al., 2012, p. 25): the Bajuvaric is named after the original name for the Bavarian, or Bajuvaric, inhabitants of the modern German federal state of Bavaria, the Tirolic after the Austrian federal state

of Tyrol, and the Juvavic after the Roman name for Salzburg, *Iuvavum*. The *Totes Gebirge* thrust sheet, which makes up the plateau, is part of the Tirolic nappe, although southwest of it Hallstatt-facies Juvavic nappes are close by (e.g. see Figure 1 (b) in Mandl, 2000, p. 62). Figure 1.11, from Leitner and Spötl (2017), shows the tectonic situation in the Eastern Alps and the NCA, with the latter also including outcrops of Permo-Triassic evaporites. The salt mine of Altaussee, in the Sandling mountain, shows the approximate location of this thesis' area of interest.

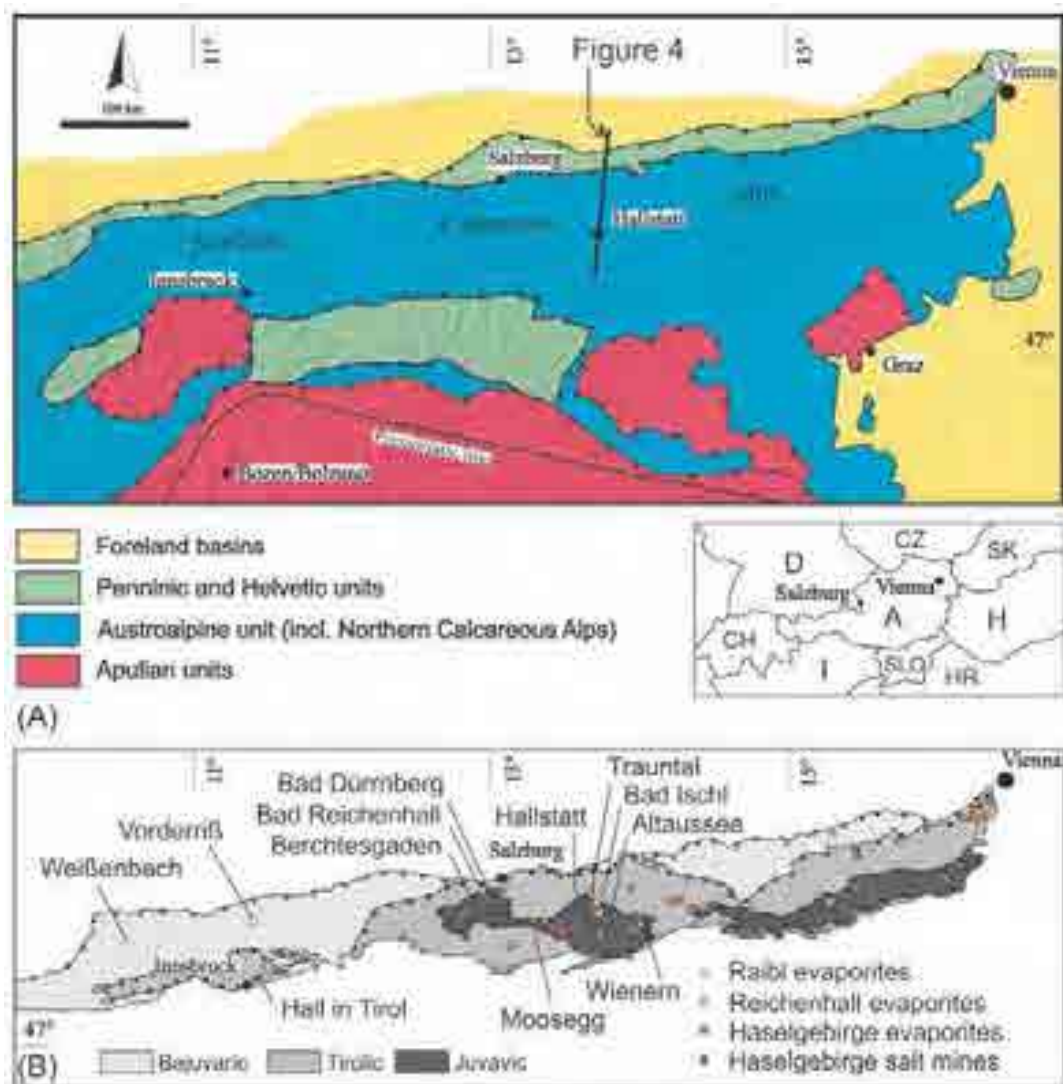







Figure 1.11: Tectonic maps of (A) Eastern Alps and (B) the NCA in particular, the latter with evaporite outcrops, from Leitner and Spötl (2017, p. 468)

Although the NCA themselves end west of Vienna, the carbonate mountain belt of the Alps-Carpathians-Pannonian (AlCaPa) block continue, underneath the Vienna basin, further

to the east  in the Carpathians (Mroczek et al., 2023). Vienna's drinking water is largely brought directly from the karstic catchments of *Rax*, *Schneeberg* and *Hochschwab*, ~~and has been~~ since the construction of the necessary infrastructure in the late 19th century (C. Bauer and Plan, 2022; Wien Geschichte Wiki, 2024).

As mentioned above, in recent years an alternative regional  geological model has been gaining momentum: according to Fernández et al. (2022, 2021, 2023, 2024) and Leitner and Spötl (2017), salt tectonics had a large impact on the Triassic and Jurassic stages of carbonate formation and sheet movement. Earlier models (Mandl, 2000; Mandl et al., 2012; Missoni and Gawlick, 2011; Schöllnberger, 1973, and older quoted therein) had the Hallstatt salt bodies, with overlying Hallstatt-facies Triassic and early to mid Jurassic carbonates, form in deeper basins further from the coast, to then slide as gravitational mass-transport deposits on top of the Tirolic platform nappes during Upper Jurassic tectonic activity. Here, the easily deformed layer of salt and evaporites was to act as the plastic sliding surface. While some of the earliest treatises on the geology of the area (e.g. G. Geyer, 1916; Vacek and G. Geyer, 1916) already emplace the *Hallstätterzone* of *Grundlsee* and *Tauplitzalm* as autochthonous units south of the Dachstein-facies limestone of *Totes Gebirge*, the evidence  used as basis for this assertion was already found to be faulty by Schöllnberger (Tollmann, 1960), cited in 1973)) and preceded modern theories of salt tectonics.

In contrast,  we propose that the Permian salt-bearing Haselgebirge might have actually undergone passive diapirism from the early Triassic onwards and ended in submarine salt extrusion in the Jurassic. This may have happened inside the carbonate platform domain, with the subsidenc  “basins or carapaces over a broadening diapir” (Fernández et al., 2021) sufficing for the Hallstatt-facies Triassic carbonates to be of deeper-water sedimentation type than the surrounding Dachstein-facies platform limestone. This theory of “relative autochthony” (Fernández et al., 2024) would have a large impact on the structure of (especially Juvavic) units in the NCA, but also on the relationship between units. This can be seen very clearly in Figures 7 to 9 in Fernández et al. (2024, pp. 266-268), for which the authors constructed two different geological sections along three traces crossing the central NCA from north to south, and then built reconstructions reaching back as far as the Late Triassic for each. The first of the two sections followed the classic theory of allochthony, with Hallstatt-facies carbonates and their underlying Permian evaporites and clastics moving tens of kilometres from a relative S position over Dachstein-facies Tirolic nappes to their modern position. In the second sections' case, a scenario of salt-rich structural development is followed. As described above, this includes diapirism inside the carbonate platform.

While this approach looks promising and offers exciting new interpretations, it does not

seem to have a large impact on the stratigraphy of the thrust sheet of the *Totes Gebirge* itself: even in the salt-rich scenario, the Permian unit begins only in large depths in areas with *Dachsteinkalk* cover, in the eastern part of the massif. More to the west of the plateau, even fewer evaporitic outcrops are mapped. Because of this thesis' scope being limited to only the *Totes Gebirge* nappe, and focusing on its hydrogeology, a methodological inclusion of this theory would exceed ~~said~~ scope and will therefore not be followed in the following description of the sheet's stratigraphy, nor will it be applied during geological section construction or three-dimensional modelling in VisualKARSYS.

Additionally, different authors have described the NE-SW or NNE-SSW fault systems of the plateau to be (more) important in its underground drainage (Kuffner, 1998). Maurin and Zötl (1964) note that while the springs in the area of Tauplitzalm and along the massif's eastern border are very much affected by hydrostratigraphy, in the northwest fault and cave springs are predominant. L. Geyer et al. (2016), Kuffner (1998), and Schwingenschlögl (1986) report that the plateau's karst caves follow fault systems in their general directions, which greatly influences karst catchment delineations (Ford and Williams, 2007). Dinçer et al. (1972) confirm that because formations that could act as aquitards, e.g. *Werfen* Fm. shales, are not strongly represented in the main massif's strata, the tectonic fault systems play the more important role in the karst catchment.

1.2.1.2.1 *Totes Gebirge*

The *Totes Gebirge* massif itself is a thrust sheet which is part of the Tirolic nappe stack (Mandl et al., 2012). Its oldest and basement layer is the **Haselgebirge Fm.** which crops out only very locally in the N of the massif, on map sheets 97 and 67, or *Bad Mitterndorf* and *Grünau im Almtal*, respectively (Egger and van Husen, 2007; Moser, 2019). While on the former map the formation is listed as a mélange of claystone and evaporites (gypsum and salt), the latter sees mainly gypsum-bearing colourful claystone, of Upper Permian age (Egger, 2007; Mandl et al., 2012). On map sheet 68 *Kirchdorf an der Krems*, no outcrops of the *Haselgebirge* are given (Griesmeier and Hornung, 2023), although it must be added that both 97 and 68 are geological maps of the GEOFAST series, for which only archival maps and data were amalgamated. The large salt bodies of the *Haselgebirge* Fm. involved in the salt tectonics of i.e. Fernández et al. (2021) are confined to the Juvavic nappes to the E and SE of *Totes Gebirge*.

Next up, the **Werfen Fm.**, of Lower Triassic age, comprises mainly sandy, micaceous schist strata which, toward the top, intercalate with very thin to dm-thick sandy limestone beds. On the lower end, the colour ranges from mainly red to green and grey. In terms of

thickness, 150 m is the maximum, with about one-third taken up by the calcareous top part (Mandl et al., 2012). On map sheet 67, *Werfen* Fm. outcrops only occur along faults and are rather of schistose silt- or sandstone with mica pieces on bedding planes (Egger, 2007).

Skipping the Reichenhall Fm. of the early Anisian, which should follow according to the Stratigraphic Table of Austria (STA 2004, Piller et al. (2004)), the **Gutenstein Fm.** (up to mid Anisian) is the next overlaying stratum. It is described as intercalated limestone and dolomite in thin, even to undulating beds of dark grey to black colour due to the bitumen content (Egger, 2007). The main extent of outcrops is on map sheets 67 and 68, in other words, to the north (Egger and van Husen, 2007; Griesmeier and Hornung, 2023). Locally, light, detrital *Steinalm* Lst. intercalations have been observed too; they are of shallow marine sedimentation. Thickness estimations for the *Gutenstein* Fm. range from a few tens of metres (Mandl et al., 2012) up to 150 m (Egger, 2007).

The **Reifling Fm.**, drawn onto map sheets 67 and 68 and with an estimated thickness of 100 m (Egger, 2007), is not covered by Mandl et al. (2012) and appears to only occur in the eastern *Totes Gebirge*, dipping S from the outcrops in the NE.

Overlaying, the **Wetterstein Fm.** can be found, first the limestone beds, and capping them, the Wetterstein dolomite, although the border between the two is very irregular, forming more of an interfingering zone (Mandl et al., 2012). Concerning the age, the formation covers the Ladinian and reaches into the Carnian; the older limestone strata reflect this in their rather grey colour, while the younger beds are often white or ivory (Egger, 2007). The dolomitised beds above, cropping out more to the south than the limestone on map sheets 67 and 68, are unstratified, in contrast to the thick beds of the limestone below. In colour, they are grey to white, and are easily eroded into a fine, white scree to sand (Mandl et al., 2012). In total, the *Wetterstein* Fm. is probably a few hundred metres thick (Egger, 2007).

The following strata have different names depending on where the focus is in the NCA: on map sheets 96 and 97, the term **Raibl Lyrs.** is used by Mandl et al. (2012) and Moser (2019), which is also the name given by Grottenthaler (1978), who wrote an extensive and authoritative paper about this formation. Although referencing the same formation, Egger and van Husen (2007) and Griesmeier and Hornung (2023), on their map sheets 67 and 68, respectively, call the brown sandstone and dark grey claystone layers *Lunz Lyrs.*, and the thinly bedded micritic limestone *Opponitz Fm.* However, it must be said that although *Opponitz Fm.* is given by Grottenthaler (1978) as an alternative name for *Raibl Lyrs.* east of the Salzach, both map sheets 67 and 68 only assign the 100 m to 300 m (Egger (2007) and Plöckinger (1980), resp.) thick formation in question to either the *Stauffen-Höllengebirge* thrust sheet in the Tirolic nappe stack, or other massif nappes in the Bajuvaric System. Thus,

the between 25 m to 50 m thick (Mandl et al. (2012) and Egger (2007), resp.) intercalating sandstone, claystone, shale and carbonate strata are only either *Raibl* or *Lunz* Lys. In *Totes Gebirge*, the so-called central facies (Grottenthaler, 1978) is predominant; it is defined by a bed of limestone in the upper third of the shale section, which itself is the first element of the facies stack. Above the shale, an oolite bed can be seen in *Totes Gebirge*, followed by Carnian to Norian dolomite strata. In some areas, i.e. that of *Offensee* (map sheets 97 and 67), *Raibl* Lys. were not formed in the first place, and in other parts of the northern slope of the massif they were tectonically squeezed out of the nappe stack (Grottenthaler, 1978). This explains why the narrow band of outcropping *Raibl* Lys. observed all along the northern drop of the plateau stops suddenly just south of *Offensee* and not to continue to the west.

Capping either *Raibl* Lys. or laying directly on the *Wetterstein* Fm., the so-called **Hauptdolomit**, or “main dolomite” in translation, forms a thick formation of between a few hundred metres (Lobitzer, 2012; Mandl et al., 2012) up to 1500 m (Egger, 2007). Forming from the Upper Carnian to the Norian on the Triassic carbonate platform, but at a distance from the reef, it often shows interfingering with the **Dachstein Lst.**, whose time of formation also starts in the Upper Carnian but reaches until the Rhaetian. In some areas, an intermediary layer of **Platten Lst.**, or dolomitised *Dachstein* Lst., can be seen, i.e. in the area of *Hohe Schrott* on map sheet 96 (Mandl et al., 2012). The mapped outcrops of *Dachstein* Lst. include both well-banked, lagoonal limestone with light beige dolomite and marl intercalations, as well as massive, unstratified white reef and reef debris limestone. Regarding this formation’s thickness, varying estimates abound: according to the geological part of the soil map of the area drawn by BFL Bundesamt und Forschungszentrum für Landwirtschaft (1998), the *Hauptdolomit* and the *Dachsteinkalk* together reach up to 1500 m of thickness. Adding to this the analysis by Piller (1976), who found that toward the north of *Totes Gebirge*, *Dachstein* Lst. loses thickness in favour of *Hauptdolomit*, as the facies zones change from the former to the latter, an idea of its total thickness begins to emerge. Mandl et al. (2012) estimates at least 800 m of *Dachstein* Lst. Schwingenschlögl (1986) drew up to a thousand metres of *Dachsteinkalk* in his western geological section. However, concerning this author’s fault tectonic map, the regions of banked and massive *Dachstein* Lst. are not identical with same classification in map sheets 96 and 97 by Mandl et al. (2012) and Moser (2019). Additionally, areas seemingly declared as Triassic *Dachstein* Lst. in the fault tectonic map by Schwingenschlögl (1986) at Loser and Trisselwand, with the attached plateau to the NE, are defined as Jurassic *Tressenstein* or *Plassen* Lst., both in the geological section 1 in Schwingenschlögl (1986) and on map sheets 96 and 97 (Mandl et al., 2012; Moser, 2019).

The characteristic fossils to be found in *Dachstein* Lst. are the Megalodontoidea, easily

discernible by their heart-shaped profile which resemble a cow's hoof print (Mandl et al., 2012) or a stag's tracks (G. Geyer, 1916). As large parts of the *Totes Gebirge* plateau is made up of denuded and karstified *Dachstein* limestone, the fossils can be spotted occasionally.

To continue along the massif's stack, the **Kössen** Lys. represent the last part of the Triassic sedimentational strata, although in the main part of the massif, and this thesis' scope of interest, they have all but disappeared by erosion (Mandl et al., 2012). Lithologically, they consist of gray-brown marl, claystone and marly limestone strata from between the Norian and Rhaetian. They represent the beginning of increasing terrigenous siliciclastic sedimentation in the Upper Triassic, as the supercontinent of Pangaea was in the process of breaking up. This marks the end of the Triassic sedimentary rock in the *Totes Gebirge*.

The Jurassic cover in the area of interest of *Totes Gebirge* shows two forms: in the areas of otherwise denuded *Dachstein* Lst., it is constrained to very local occurrences of a variety of Lower to Middle Jurassic **Buntkalke**, or "colourful limestones" with marly or sandy qualities, which have such small individual outcrops that they are amalgamated into larger units. Unfortunately, the precise combinations in each of the map sheets in question are different in extent; for instance, while 96 merges early Jurassic marly limestones of the *Adnet*, *Hierlatz* and *Klaus* Fms. (Mandl et al., 2012; Schäffer, 1982), 97 includes the *Hierlatz*, *Crinoid* and Liassic *Spatkalk* Fms. into an older group, followed by another which comprises the *Adnet* Fm., red and colourful Liassic Lst., and colourful Cephalopod Lst. (Moser, 2019). Egger and van Husen (2007) follows a similar method in map sheet 67 to Schäffer (1982) by including all the various formations into a class of *Bunte Jurakalke*, which means colourful Jurassic limestones in general. Irrespective of precise delineation, they are united by being made up of mainly carbonates of a lower sedimentary milieu than the purer limestone of the Triassic platforms. As such, they were formed as syntectonic fault fills on the submarine, but higher ridges of gravitative transport sheets that were formed by Jurassic tectonism (Mandl et al., 2012; Piller, 1976).

In the associated basins between the colourful limestone ridges, the majority of available carbonate mud came to deposition as marly limestone down to siliceous depths, combined as the **Allgäu Fm.** on all map sheets of interest. Because of ever-increasing depths of even the ridges, *Allgäu* layers also formed over the fault-filling red limestones. This continued until the Oxfordian Age of the Upper Jurassic, with the more siliceous examples of the *Allgäu* Fm. being younger (Mandl et al., 2012). In fact, the assertion was made by the same author that in actual fact, the siliceous limestone of the *Allgäu* Fm. are actually part of the radiolarite and siliceous limestone group that are part of unit number 49, "**Radiolarit, Kieselkalk**". This unit's lithology comprises well-banked radiolarite of dark grey to red colouring and siliceous

limestone with marly intercalations (Mandl et al., 2012). It can be found on the eastern slope of the Loser with a varying thickness. Mandl et al. (2012) say that these layers represent the deep depositional milieu into which gravitatively sliding sheets, like the *Höllengebirge* or the *Totes Gebirge*, moved in the early Upper Jurassic. Alternative interpretations involving salt tectonic diapirism à la Fernández et al. (2021) or similar usually focus on the Juvavic nappe stack, whose interactions with Tirolic sliding sheets remain unclear to the author.

The other form of Jurassic cover of Triassic carbonates is represented by the thick layers of the Upper Jurassic formations drawn in the map sheets of concern. The **Oberalm Fm.**, **Tressenstein Lst.** and **Plassen Lst.** all represent different facies of the *Plassen* carbonate platform that formed during the Kimmeridgian to the early Tithonian, shallowing upward toward the end of the Jurassic, and drowning during the Cretaceous Berriasian. In the area of *Trisselwand*, south of Lake Altaussee, the earliest clastic deposition appears to have only started in the Tithonian, with the *Oberalm* Lys. from the Valanginian marking the end of the platform. Mandl et al. (2012) also say, however, that the map sheet 96, drawn decades earlier than the description (Schäffer, 1982), makes little sense in the distribution and tectonic delineation of Upper Jurassic (/Lower Cretaceous) carbonates in that area.

To describe the formations mentioned before lithologically, the *Oberalm* Fm., usually drawn as underlying the other two (cf. Schwingenschlögl, 1986, section 1 in supplement 6), is made up of undulating cm-thick beds of grey, marly limestone that intercalate with thin silt layers (Mandl et al., 2012; Moser, 2019). *Tressenstein* and *Plassen* Lst., on the other hand, are purer in carbonate content. The former is massive or thickly bedded limestone of light grey colour and made up of fine breccia down to calcitic turbidite. The latter is massive throughout and mainly white with occasional yellowish to brown colouring. Its depositional milieu is seen as that of a shallow-water carbonate platform (Mandl et al., 2012).

No younger formations than the ones described have been observed in the part of *Totes Gebirge* under scrutiny. An exception to this are the so-called *Augensteine*, or “eye stones”, relicts of the Oligocene fluviatile S-N drainage system that transported material from the higher hills to the south toward the molasse ocean in the north, during the early days of Alpine uplift. On a range of carbonate plateaus in the NCA, i.e. the *Dachstein*, the *Hochschwab*, the *Rax* or the *Totes Gebirge*, these relicts can be found on the massifs or inside their caves (Schuster and Stüwe, 2010). These caves follow the mainly NE-SW- or NNE-SSW-directed faults which formed tectonically in the fabric of the plateau in the course of its post-Jurassic movement into its current emplacement, and during the following uplift (G. Geyer, 1916; Mandl et al., 2012; Schwingenschlögl, 1986). The karstification across the whole *Totes Gebirge* was, of course, encouraged by the deep fault systems and, coupled with the bedding

planes in various carbonate sedimentary strata, developed systems of caves that count among the longest and deepest in all of Austria and even the European Union (E. Geyer et al., 2016; Pfarr et al., 2023; Schuster et al., 2014).

A major feature of western *Totes Gebirge* fracture tectonics is the so-called Altaussee-Wildensee-Line, already described by G. Geyer (1878, 1915) and further investigated photogrammetrically and mechanically by Schwingenschlögl (1986). Just from the outcropping formations on either side of the southern part of the fault (Upper Triassic on northwestern side, Upper Jurassic on southeastern side), it is clear that relative movement must have taken place. Schwingenschlögl (1986) could not detect any indications for lateral movement from either the photogrammetric approach or the following field observations. However, based on a mechanical view, the side fractures joining the main system under angles of 40° to 60° could be seen as “Riedel surfaces” (Riedel, 1929), whose orientation and distribution would lead to a model of mixed dextral and vertical displacement. G. Geyer (1915), in the northern part of the fault along Rinnerboden and Wildensee, saw the sheet generally dipping toward Offensee in the north on the west of the fault, while the strata to the east of the fault would be dipping toward the south. A visual verification of the structure data points by the author could not replicate this impression, with bedding dips on both sides of the fracture system being directed both north and south. In ?? this becomes clear.

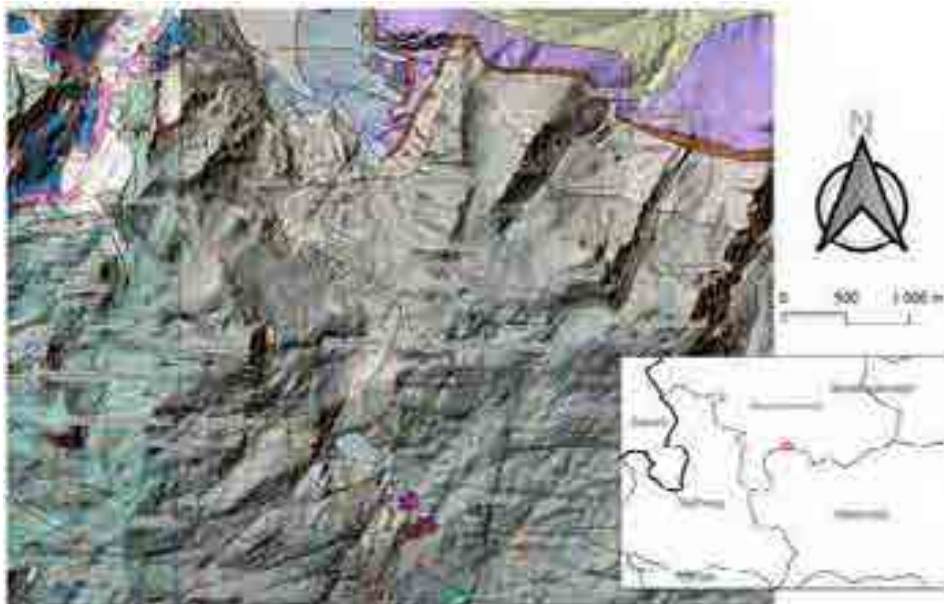



Figure 1.12: Map showing Rinnerboden, Wildensee and their and environs, with structural geological data points in Clar notation with given dip ranges, 100 m contour lines in orange, and planar geological unit outcrops from map sheets 96 and 97 blended with a hillshaded DEM of 10 m resolution, smoothed cubically.

1.2.2 Hydrogeology and its application in karst

Water is a necessity for all life on Earth to exist and thrive. Humans are about 70 % water by weight. Logically, water resources have always been vital, especially so in otherwise arid environments. There, springs have played even more of a role than in humid or temperate climates, where surface water bodies are more likely to persist year-round. However, in dry periods, even those springs might have become unreliable, leading the peoples of Persia to be one of the first to utilise groundwater as early as 3000 years ago. They dug so-called qanats or alfaj which appear all over the arid band reaching from Morocco to Afghanistan and whose communal use as an irrigation water distribution system was and is central to local cultures (Young, 2002 quoted in Hiscock, 2005, p. 3). In ancient Rome, vast networks of aqueducts ensured that the centre of the empire would be supplied with ample fresh water from the surrounding springs, totalling at that time about $6 \text{ m}^3 \text{ s}^{-1}$ (Hiscock, 2005).

Only much later, an understanding of groundwater should form: where it comes from, how it behaves physically and chemically underground and how its users can be protected from potential pollution carried through the soil and rock. Up to the 17th century, no connection between above- and underground hydrological processes was drawn, under the assumption that earth was too impervious and rainfall too sparse to feed the large volumes discharged from springs. A long list of famous scientists was necessary to understand the entire hydrological cycle and empirically as well as theoretically describe the processes governing water underneath the surface: Pierre Perrault (1611–1680) and Edme Mariotte (c. 1620–1684) from France and the Englishman Edmond Halley (1656–1742) compared rainfall, runoff and evaporation from the sea and found that these all fit together. The geologist William Smith (1769–1839) applied his knowledge of rocks to find groundwater to tap – incidentally, he also drew the first modern geological map, his Map of England, in 1815 (Hiscock, 2005). In the 1870s, British polymath Joseph Lucas first defined the term “hydrogeology”, drew the first maps of groundwater resources and gave instructions on how to perform hydrogeological surveys (Mather et al., 2004). A few years later, the water supply of a town was reported systematically for the first time for Sussex in England, by Whitaker and Reid (1899). 

Some of the fundamental equations were also developed in this time period. Henry Darcy (1803–1858) was a French hydraulic engineer whose groundwater flow equation appears in the first few slides of any class on hydraulics or hydrogeology as “Darcy’s law”. Soon after, Arsène Dupuit (1804–1866) found the eponymous equation to describe the flow of water through a porous aquifer towards a well with axial symmetry. The Austrian Philip Forchheimer (1852–1933) was then the first to apply the advanced mathematical approaches of his time to hydraulic problems in the groundwater realm. Following the solutions to heat flow questions,

he developed an application of Laplace's second-order partial differential equation to steady groundwater flow. For porous media he expanded on Darcy's law by adding a term for the head loss stemming from water turbulence, the result bearing the eponym "Forchheimer's law". Another innovation in hydrogeology at the time, the mirror image method, was also pioneered by Forchheimer to address situations like wells located next to rivers. Transient groundwater flow states, previously only to be estimated, became calculable in 1940 thanks to C. E. Jacob (Hiscock, 2005; Jacob, 1940). Based on these and other scientific discoveries in the first half of the 20th century, any and all computer-based modelling of groundwater resources developed until the present became possible.

In the ensuing decades, the issue of groundwater quality became more pressing with increased contamination problems of hitherto potable water becoming polluted. Another host of scientists invested their knowledge and capacity for reasoning in applicable solutions, among others A.M. Piper and H.A. Stiff with graphical interpretation methods for water quality, I. Chebotarev with groundwater's chemical evolution along its path of travel, and J.D. Hem, whose work aided in the study of natural water's chemical characteristics (Hiscock, 2005). Because both physical and chemical aspects of hydrogeology are necessary to work on groundwater contaminant transport, these two previously separated branches of groundwater hydrology merged toward the end of the 20th century to form the interdisciplinary field of modern hydrogeology. To quote Hiscock (2005, p. 7): "[...] and students who aim to become hydrogeologists require a firm foundation in Earth sciences, physics, chemistry, biology, mathematics, statistics and computer science, together with an adequate understanding of environmental economics and law, and government policy."

Because of this wide field of disciplines that intersect with one another to form hydrogeology in all its facets, the definitions for the field tend to be rather general. According to the International Association of Hydrogeologists (IAH), hydrogeology is the "study of groundwater – it is sometimes referred to as geohydrology or groundwater hydrology. [It] deals with how water gets into the ground (recharge), how it flows in the subsurface (through aquifers) and how groundwater interacts with the surrounding soil and rock (the geology)." (IAH, 2024) All aspects of this definition find their application in karst hydrogeology too. However, karst aquifers have certain differentiating characteristics that demand specialised or adapted methods of research, and an interdisciplinary approach (see Figure 1.13). (Goldscheider et al., 2007) give the following overview:

1. **Aquifer evolution:** Because of the dissolution of ~~the rock encompassing~~ a karst aquifer by the CO₂ within it, certain fractures are enlarged ever further, as long as water flows through them. Depending on a long list of inner and outer influences (e.g. cave collapses

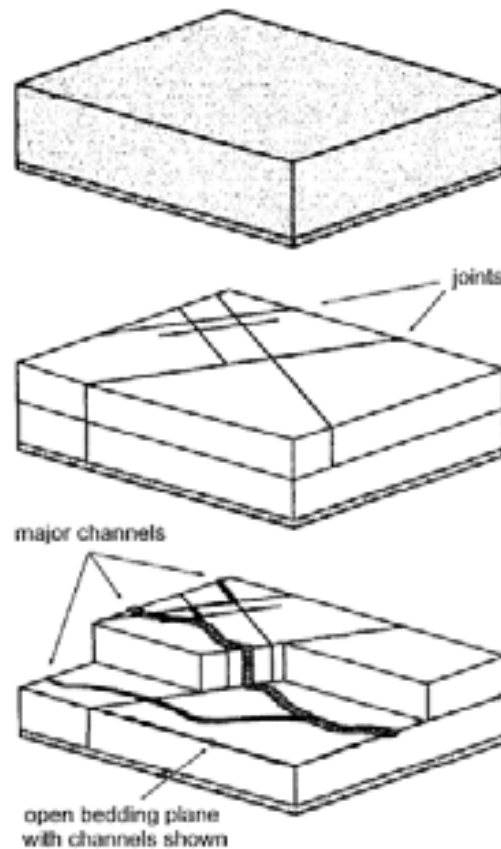




Figure 1.13: Block diagram of the three basic aquifer types, porous, fracture and karstified, conduit aquifers, from Worthington (1999) in Ford and Williams (2007, p. 106)

or sediment infill, change in climate or regional hydrological system, glaciation, shift of active spring level, etc.), the way a karst system functions may change ~~unpredictably~~.

2. **Spatial heterogeneity:** In contrast to the predictable occurrence of groundwater in a porous medium, and therefore the relative ease with which a borehole might be sited, karst aquifers are often made up mostly of low-porosity, low-permeability limestone matrix and occasional high-porosity, turbulent-flow conduits at, in general, random points. Choosing the correct site for, e.g., a well, is therefore a task requiring very high precision and good knowledge of the system. Additionally, “all types of interpolation and extrapolation are problematical if not impossible in karst.” (Goldscheider et al., 2007, p. 2) Except if a large number of water level measurements are already given from which to derive a system-wide water level or direction of flow, it is often more useful to employ other methods such as tracer tests (more about this below).

3. **Hydraulic conductivity-scale effect:** Where laboratory analyses of rock samples and well-based pumping or packer tests can give representative values for conductivity in porous or well-understood faulted aquifers, karst systems are very dependent on their conduit network, which in total will have a higher conductivity than those measurable by the methods mentioned. Thus, should these methods be applied, their results must be treated with care and checked for plausibility by other means.
4. **Dualities of recharge, infiltration, porosity, flow and storage:** Karst aquifers may be recharged both auto- and allogenicly, meaning either from precipitation that has fallen directly on karstified rock, or from stream or subsurface flow originating from adjacent, non-karstified catchments. These inputs can infiltrate into the carbonate subsurface through discrete points (ponors, dolines, etc.) or diffusely, again either through small fractures in the rock itself or through covering soil and the underlaying epikarst layer. Once inside the aquifer, water can percolate quickly (up to thousands of metres per day (Kresic, 2007)) through solutionally enlarged fractures and large conduits, or enters the rock matrix pores, where it creeps through often very low-primary-porosity limestones (see also Ford and Williams, 2007, p. 114, Tables 5.5, 5.6). That also already explains the duality of storage: short-term, karst water is stored in the conduits which are dwarfed in terms of total volume by the matrix storage, whose much slower discharge contributes much of the base flow of karst springs during low flow periods (see also Ford and Williams, 2007, p. 107, Table 5.2).
5. **Temporal variability:** As previously stated, hydrological events cause a fast and dramatic reaction in karst systems, with epiphreatic water table increase up to  hundred metres and more and fast, turbulent conduit discharge. In numerical modelling, this can require the application of both open-channel and pipe equations, depending on the degree to which the conduits are filled (Bögli, 1980). Should spring hydrographs or physico-chemographs be of interest, instrumentation should be installed which enables high-frequency data logging during hydrological events, as all parameters associated with karst system response can vary wildly (Goldscheider et al., 2007).

In  2.1, both a sectional and a block diagram view of a typical karst system is shown, with most of the relevant terminology regarding geomorphology and hydrogeological zones. From Ford and Williams (2007) and Jeannin (2014), respectively, they give supplementary overviews as it does not seem useful to cram all aspects into one illustration. Seeing as every karst system is defined by individual circumstances and specific characteristics, detailed classification

schemes have been developed. These delineate systems based on the following (Stevanovic, 2015):

- **Dominant lithology:** Limestone, dolostone, gypsum, anhydrite, halite, chalk or marble are the sedimentary or evaporitic lithologies in which karst can develop.
- **Productivity:** Based on conductivity and storativity, high, moderate or low productivity-aquifers can be distinguished.
- **Spatial setting with regards to impermeable layers:** Karst aquifers occur in unconfined, confined and semi-confined settings. The former are not overlain by impermeable rocks, meaning they have a free water table. The second are continually under pressure underneath an aquiclude, with their potentiometric surfaces rising above the upper limits of karstified strata; in a borehole, water would thus rise higher than the lower border of the aquiclude. Semi-confined karst aquifers are a hybrid form, with unconfined and confined parts each constituting a part of the whole. A special form is the perched aquifer: it “perches” on an aquiclude lens, either inside this impermeable layer or above the water table of the main aquifer.
- **Bottom boundary:** While the top boundary of a karst system is relatively easy to determine - either the surface or, in the confined case, the bottom of the overlaying impermeable layer - the same often cannot be said of the bottom boundary. In cases such as *Totes Gebirge*, with carbonate layers being hundreds of metres or up to 2 km thick, the bottom of the phreatic zone is either an aquiclude at large depths, or a karstification base. This is a zone of quickly decreasing levels of karstification, transitioning from well- to non-karstified carbonate rock (or whichever lithology dominates).

1.2.2.1 Karst genesis and development

But how do these conduits come to be in the first place, and how do they evolve with time? And how are surface-level geomorphological elements of a karst landscape linked to the subsurface conduit system? Karst, by definition, is both a landscape characterised by a variety of hollow forms in limestone (i.e. dolines, ponors, karren, poljes, etc.) and a catchment which is drained almost entirely underground, along faults, fractures and bedding planes enlarged into conduits that stretch throughout the carbonate rock mass (Jeannin, 2014). The former and the latter of these aspects are, generally speaking, results of exogenic erosion, which any other type of rock is also afflicted by. However, carbonate rock is additionally especially

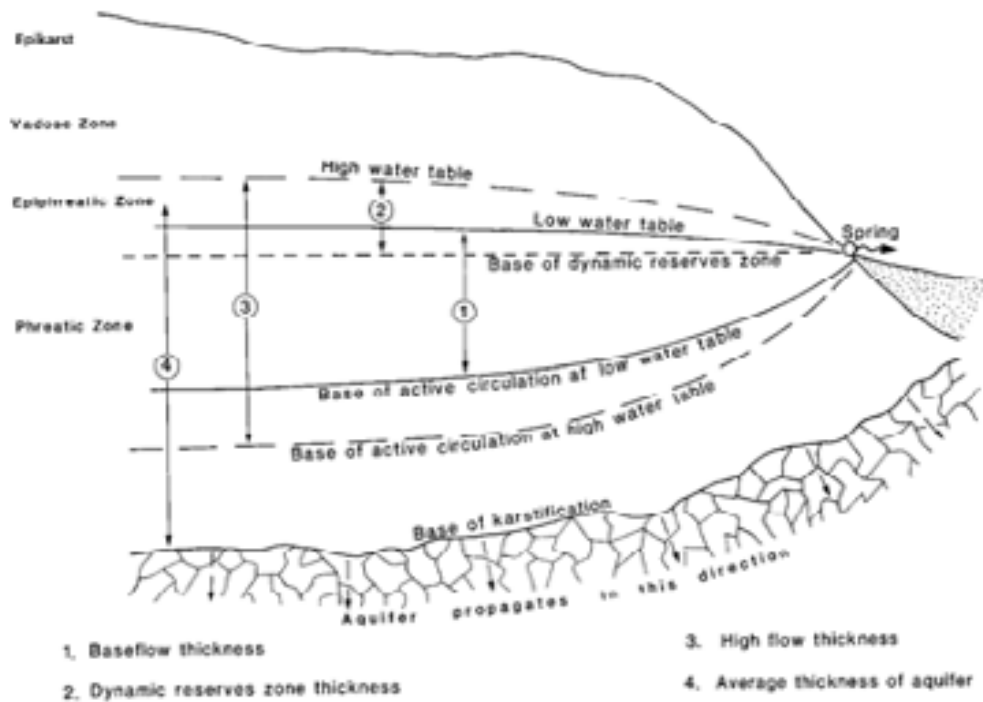


Figure 1.14: Sectional diagram of a typical karst system's hydrogeological zones, from Ford and Williams (2007, p. 115).

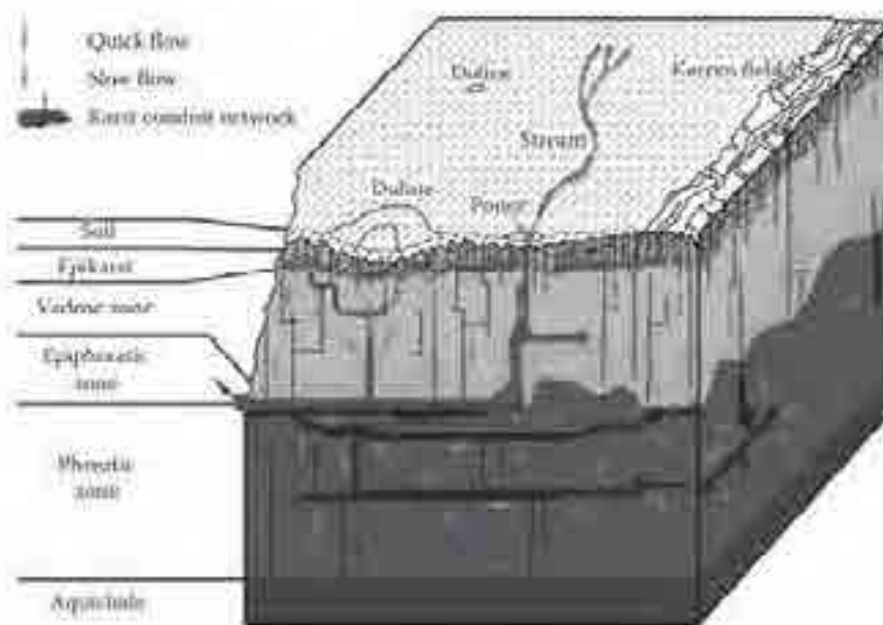
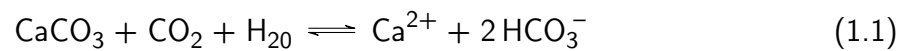


Figure 1.15: Block diagram of a typical karst system's hydrogeological zones, inputs and flows, from Jeannin (2014, p. 382).

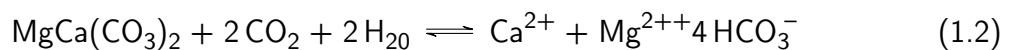
vulnerable to chemical dissolution by the CO_2 present in water it comes into contact with. To quote Bögli (1980):

"The dissolution of limestone and dolomite is the central problem of superficial and underground karstification. It takes place in a system of substances of the type $\text{CO}_2 - \text{H}_2\text{O} - \text{MeCO}_3$ (Me: Ca or else Mg). It comprises numerous physical and chemical processes, in which all three aggregate states – gas, liquid, and solid – participate. This causes a mass transfer through the interfaces air/water and water/rock. " Bögli (1980, p. 15)

In stoichiometric form, the effect of these mass transfers on the carbonate rock is summarised by the dissolution equation of limestone, in which the left side represents the solid limestone in contact with water containing CO_2 , and the right side is made up by the dissolution products:



For dolomite ($\text{MgCa}(\text{CO}_3)_2$), the dissolution equation runs parallel:



When limestone or dolomite are dissolved by contacting water, the magnesium and calcium ions going into solution decrease the solution's aggressivity, making it ever less capable of further dissolution of the rock. Once the water reaches saturation (or even supersaturation, given the right conditions), no further ions can be dissolved (see Figure 3.3 in Ford and Williams (2007, p. 44)).

However, many complementary factors concerning each of the participating elements of this system affect the dissolution process. For instance, the rate of dissolution is governed by, e.g., the diffusion coefficient of Ca^{2+} -ions in the contacting water, the current concentration of ions in the vicinity of the interface, the saturation concentration of the water, which in turn is inversely related on the system's temperature and is affected differently by other ions in solution too (Jennings, 1985), and the rock's surface area. Further, a higher speed of water flow increases ion removal rates in very small fissures with laminar flow, but especially once turbulent flow sets in (Worthington et al., 2017). This is the beginning of a spiral of increasing dissolution: higher flow means more corrosion, which means wider conduits, which again means higher flow, starting the cycle anew Bögli (1980).

Regarding the rock itself, its lithology, structure, position in its stratigraphic neighbourhood, bedding and tectonic history have important roles to play. The purer the limestone (>70 %


carbonate), the finer its grain, the larger its specific surface, the better its solubility. How the carbonates were sedimented, where and from which source is also important (Ford and Williams, 2007). Mechanical compressive strength of carbonate rock is generally quite high, enabling them to support cliff faces or cave walls for long periods of time. With thinner bedding and more intense fracturing this strength decreases though.

The zonation of karst systems also has an impact on karst development, especially the existence of an epikarst layer with soil cover. Rain water falling on soil-covered karst areas first infiltrates through said soil into the epikarst zone. Having been enriched in CO_2 from the biological processes taking place there, it quickly loses its additional aggressivity and saturates with calcite upon first contact with the carbonate rocks. This leads to the characteristic water storage and distribution in systems with an epikarst layer, as the well-karstified depth directly underneath the soil can hold water which only relatively slowly percolates through thinner fissures into the vadose zone Harlacher (2003).

Two implications arise from this: First, in karst aquifers with an epikarst, the vadose zone mainly experiences dissolution enlargement during storms, when the rainwater infiltrates quickly, flushes the stored water and remains aggressive until reaching vadose fractures and fissures. Organic particles that are carried along into the vadose zone decay there, acting as another source of CO_2 in the conduits and caves, causing concentrations in cave air of 1.6(8) % or even up to 6 %. From this source, percolating water can regain some aggressiveness against limestone for further dissolution in the vadose zone (Ford and Williams, 2007). Second, once the water has reached the phreatic zone, further karstification would be extremely slow underneath the water table, especially in as deep a system as the *Totes Gebirge* represents. Where the requisite solution capacity comes from for further-reaching dissolution will be explained below.

On this topic, the difference between open and closed systems must be elucidated. An open system is one where of the three aggregate states, liquid, solid, and gaseous, all of them can react together, participating in establishing system equilibria. Closed systems, on the contrary, involve only two phases, either atmosphere and liquid, or liquid and solid. Applied to karst environments, the open system is exemplified by “an open air pool on limestone” (Ford and Williams, 2007, p. 52). Any carbon dioxide “used up” by limestone dissolution in the water can be replenished by further CO_2 from the air until a dynamic balance is established. Should the water flow into tight fractures or filled conduits, however, no more free atmosphere is in contact with the water. This means that once the dissolvers present have been associated with calcium carbonate, no further dissolution can occur, ~~capping the calcite saturation of the water at 40 % of the open system equivalent~~ (Ford and Williams, 2007). During the

genesis and early evolution of karst conduits, dissolution “will almost always occur under closed conditions.” (Ford and Williams, 2007, p. 53)

A long list of physico-chemical effects that affect water solution capacity have been described by, e.g., Bögli (1980) or Ford and Williams (2007). Some of the more important ones, namely mixing, cooling and thermal corrosion, will be elucidated on here. Mixing corrosion happens when water from two or more sources mixes. Although both bodies of water are originally saturated with regard to calcite, due to the mixing aggressiveness  limestone can be reactivated. The chemical reason for this is the non-linear relationship between the partial pressure of dissolved CO₂ and calcite in water. When each of the water sources is saturated at different concentrations due to different conditions under which saturation occurred, the combined water body has new solvent capacity (see Figure 3.13 in Ford and Williams (2007, p. 60) or Figure 2.29 in Bögli (1980, p. 36)). Originally proposed by A. Bögli (e.g. Bögli (1980)), the phenomenon has been confirmed by others, although its significance has been diminished by the discovery of higher-order solution kinetics at higher calcite saturation levels (Ford and Williams, 2007).

Cooling corrosion occurs due to the inverse relationship between water temperature and its saturation concentration for calcite. When infiltrating water cools down upon entering a karst system, it becomes increasingly aggressive toward the limestone with decreasing water temperature. Especially in regions with large daily or clear seasonal temperature variations, this effect can greatly enhance the dissolution of the rock in the first metres of the vadose zone, where the air temperature stays around the yearly average. The higher temperature of water during the day in the former case and in the warm season in the latter decreases in contact with the colder vadose zone air, causing cooling corrosion. In very mature karst regions, which the *Totes Gebirge* can be counted amongst, air circulation reaching deep into the rock mass is very active, the resulting cooling more than making up for the geothermal gradient (Bögli, 1980). Here, cooling corrosion will have less of an effect, the lower temperature causing a larger base solution capacity in meteoric waters. What does have an effect in deep karst are pressure effects involving air trapped underground, with hydrostatic pressure rising around it. In such circumstances, any CO₂ bubbles forced into solution will strongly increase the resulting water's aggressiveness toward the rock (Ford and Williams, 2007).

Should the circulating waters be sourced from deep below, cooling steadily and decompressing as they rise through the crust, however, strong solutional effects can be observed; Bögli (1980) cites the structures underneath the thermal springs in Bratislava as an example of cooling corrosion-dissolved thermal water caves. Klimchouk (2009) designates this type of karst development from below as hypogenic speleogenesis. In Austria, with 70 discovered

caves that are designated as such, there are only comparatively few examples (Plan et al., 2009a), located mainly in the south of the Vienna basin, on the south-eastern rim of the NCA.

Once the initial dissolution has taken place in freshly exposed karstifiable rock and fracture and bedding planes are slowly starting to be enlarged, speleogenesis in the narrower sense begins. The definition of this narrower sense is difficult due to the overwhelming variability in karst systems in existence. Due to the many factors that can affect the initiation and evolution, the most general phrase “in karst interstices and joints are widened to form caves by the dissolution of rocks” has been criticised by a number of authors for verging on irrelevance by unspecificity (Bögli, 1980). To gain a basic understanding of the processes at play in further conduit evolution and cave creation, the governing factors will be elucidated further here.

First, dissolution of carbonate rock cannot appear out of nothing in the middle of massive rock, structures are necessary for water to come into contact with it and to transport away the solute, keeping upright a necessary concentration gradient. These structures are most often bedding planes and joint interstices in the widest sense. They, however, differ in effect on cave development, the explanations for which will follow those given by Bögli (1980, pp. 200 ff.). First, the hydraulic environment of effect must be considered: bedding planes are, unless tectonically altered, subcapillary and relatively constant in width. Only water under pressure will move through such tight constraints, which implies phreatic conditions. Joints, and especially tension joints, on the other hand, are often much wider - up to decimetres - and as such water can flow through them freely, i.e. under vadose conditions.

Second, the spatial extents of the features under consideration. Bedding planes are usually planar structures stretching in all directions for up to many kilometres. Joints, however, often terminate after at most a few hundred metres, with faults reaching up to a few kilometres. Nappe overthrust planes, such as, in this thesis' area of interest, that of the *Totes Gebirge* on its western and far northern border (see Fernández et al. (2024) and Schäffer (1982)), usually do not allow for crossing speleogenesis, probably due to mylonitisation during overthrusting. An exception for this can be post-overthrust tectonic faulting across that plane, in which case the usual rules apply again.


To show the hierarchical, competitive structure of cave development in karst systems with meteoric recharge, a simple example will be used here (Ford and Williams, 2007). Water introduced from a single input point into a bedding plane dipping quite gently in one direction seeks microfeatures allowing it to preferentially follow the hydraulic gradient. How fast these proto-tubes form depends on the parameters of each system. Once one of the possible proto-

tubes has gained an advantage over the others, the latter are hindered in their development by the change in equipotential field induced by the former. At some point, this winning tube reaches the output end of the fissure, in the general sense, relatively quickly triggering effects that enhance dissolution along the fissure and, a little later, introduce turbulent flow, increasing the rate of enlargement even further. Additionally, the thus increased flow changes the hydraulic gradient for the subsidiary tubes, making them tributaries to the primary conduit (Ford and Williams, 2007). Thus, over time periods spanning several tens of thousands of years or more, hierarchical cave networks develop.

1.2.2.2 Analysis and modelling in karst (hydro-)geology

Seeing as karst systems are characterised by comparatively very high heterogeneity located underground and additionally are each very different from one another, analysis of the parameters of each system and successive use of those characteristics in models is a challenging endeavour. Methods and approaches that are applied or adapted to karst thus come from different fields of research, some “from surface hydrology, [...] and others from classical hydrogeology.” (Jeannin et al., 2013, p. 1001) While the former will be explained further in Section 1.2.3.1, the latter have their place in the following paragraphs.

1.2.2.2.1 Analysis

A karst system's spring is often the only point at which the water that has traversed the subsurface can be monitored and its physicochemistry measured. As the resulting values incorporate all the processes that had been at play in the aquifer, any derived assertions to these processes must be system-global in nature, without much spatial resolution beyond, e.g. covered or uncovered infiltration or elevation bands of recharge (from chemograph analysis and stable water isotope methods, respectively). The hydrogeological methods come into their own in answering more specific questions about e.g. possible *a priori* distributions of the conduit network through speleogenetic modelling, or modelling of the relationship between the geological situation and observed karst phenomena. For the observation of ~~said~~ phenomena, clearly hydrogeological methods like borehole piezometric surface measurement are options, but also approaches at the intersection of the hydrological and hydrogeological fields, for example tracer tests. Hugely important in karst field research, they are signed to either the former or the latter depending on which field the respective author hails from originally (e.g. (Bögli, 1980; Ford and Williams, 2007; Groves, 2007; Zötl, 1974)). For this thesis, they will be designated hydrogeological in nature and explained here.

Having been used since antiquity, tracer tests have a long history in karst research to link system input points with output points (springs), and “are the most powerful method to delineate the catchment areas” (Goldscheider et al., 2008) of those springs. Some of the earliest tracing employed salts and dyes, but also dyed eels are recorded as having been used once (Zötl, 1974). In the 1870s, green fluorescein was used in the proof of the Danube’s spring (Ford and Williams, 2007). In general, following the classification by Benischke (2021), they can be subdivided into natural and artificial tracers, and physical and chemical parameters of the investigated medium, e.g. temperature or conductivity. Each of the former two can further be classified as (1) ideal, or conservative, or (2) reactive, or nonconservative (Benischke, 2021).

Ford and Williams (2007) gives a slightly different view of this classification, dividing any phenomenon or substance that can be measured at the spring into (1) artificial labels: dyes and salts, (2) particulates: spores, fluorescent microspheres and bacteriophages, (3) natural labels: microorganisms, ions in solution and environmental isotopes, and (4) pulses: natural pulses of discharge, solutes and sediment, and artificially generated pulses. The (non-)conservatism of each class is not further expounded, possibly under the assumption that a truly conservative tracer does not exist, and that instead the reactivity of any applied tracer must be taken into account for each case and circumstance (Benischke, 2021). As pulses in the broadest sense will be covered in the hydrological section on spring hydrograph analysis, the following description will follow the first classification given and combine the first and second classes of Ford and Williams (2007).


Natural tracers already occur in the system that is being researched and do not need to be introduced. That is the case for artificial tracers: Even if they are of natural, or biological, origin, their purposeful addition into the system makes them artificial. Examples for the former are stable water isotopes, organic and inorganic compounds (Benischke, 2021), and representatives of groundwater biota (Hilberg, 2016). The stable water isotopes usually used for tracing, ^{18}O and deuterium (^2H), vary in their occurrence in water bodies depending on the elevation and season of recharge owing to their sensitivity to temperature. In karst applications, the mean elevation of a spring’s catchment can be estimated, and, using that information, areas of drainage across boundaries can be determined (Benischke et al., 2018; Harum et al., 2014). Due to the large amount of nuclear warhead tests following World War II, the radioactive hydrogen isotope tritium (^3H) content in water rose sharply and was used for residence time studies. Nowadays, tritium levels have been dropping due to the international ban on nuclear testing, and research has adapted, focusing instead on the relationship of tritium to its decay product, helium-3 (^3He) (Benischke, 2021).

As an example for organic compounds used as a natural tracer, carbon content of spring water can be linked to the infiltration processes at play, including the differences as to which of these are active during different flow conditions. On the inorganic side, the behaviour of trace metals, e.g. copper or nickel, also varies in its binding activity from low to high flow periods (Benischke, 2021).

Artificial tracers include a wide variety of possible tracers: *Lycopodium* spores, sometimes dyed (Maurin and Zötl, 1964; Zötl, 1974), and fluorescent dyes F. Bauer and Völkl (1989). Furthermore, “particle, microbial, inorganic and organic chemical tracers [...], stable isotopes, activated and radioactive tracers.” (Benischke, 2021) Of all these, Ford and Williams (2007) sees fluorescent dye tracing with continuous fluorometry measurements as the most useful for quantitative purposes, coupled with analysis of the tracer breakthrough curve.

Goldscheider et al. (2008, p. 28, Table 1) presents a list of fluorescent dye, salt and particle tracers, details of their detection and problems they might exhibit in their use. Missing in this list, and important for the history of hydrogeological research in *Totes Gebirge* (Maurin and Zötl, 1960, 1964; Zötl, 1974), spore tracing will be explained in more detail here. First developed in the first half of the 20th century, it really gained popularity when the chemist M. Dechant managed to dye the spores while retaining their tracer-qualifying properties. This allowed injections at up to six inputs into the same karst simultaneously, greatly increasing the applicability of the method (Zötl, 1974). Of the species *Lycopodium clavatum*, the spores have an average size of 33 µm. Due to their density that is slightly higher than that of water (1.10), they do not float, which would leave them bobbing on the water surface in siphons, rendering them useless, instead they drift along the conduits in their medium. This already gives a hint as to the limit of this method: a spore needs an opening larger than itself so as to not get stuck. Consequently, porous or thinly fissured aquifers are not passable for spores (Zötl, 1974). Because of their miniscule size, they can easily and unobservedly cling to the equipment and personnel used to inject them into the system. If there is not a very strict delineation between people and materiel involved in injection and sample collection, spores can easily end up in the plancton nets used to filter them from the water at springs or in caves (F. Bauer and Völkl, 1989; Zötl, 1974). Further below, the spore tracing tests carried out by Maurin and Zötl (1964) in *Totes Gebirge* in the 1960s will be described in detail, along with their indirect repudiation by F. Bauer and Völkl (1989).

To not go beyond the scope of this thesis, only one more method of tracing, with fluorescent dyes, will be explained here. For more in-depth review and description of natural and artificial tracers, see e.g. Benischke (2021), Goldscheider et al. (2008), and Hilberg (2016) or the classic karst hydrogeology sources like Bögli (1980) and Ford and Williams (2007).

Tracing with fluorescent dyes is seen as the most important type of solute tracing by Goldscheider et al. (2008), and, as stated above, Ford and Williams (2007) is of the same opinion when it comes to quantitative analysis on the basis of tracer tests. There are a number of reasons for this claim: first, the very nature of fluorescent dyes. As the name says, when they are subjected to natural light or spectrum-selective artificial light sources they emit fluorescent light in certain, specific spectra, different for each dye. That is why different dyes can be injected into one system at the same time and still be told apart, and why they have very small detection limits (e.g. uranine: $1 \times 10^{-3} \mu\text{g L}^{-1}$  second, many dyes are toxicologically safe, making their use ethically unproblematic. The low cost of the more widely used dyes (e.g. uranine) is also an advantage. Care must be taken, however, in the selection of appropriate tracers for each injection point in multi-tracer tests, as each dye has different interaction kinetics with water as such, and additionally depending on the specific chemical properties prevalent in a system (Goldscheider et al., 2008). During the test preparation, an estimation regarding the necessary amount of the tracer must be made which is a compromise between the least necessary to still exceed the detection limit after dilution in the system, and the maximum possible before negative effects for the environment or different user groups become limiting. A range of different equations are available for this estimation, most of them empirical in nature (Goldscheider et al., 2008).

As with any other tracer, fluorescent dyes are preferentially injected into ponors or sinking streams that are active. Should this be impossible, flushing water can also be used, although then care must be taken to not exceed usual flow conditions due to the danger of influencing the flow paths taken. Slightly before or once the dye has been injected into the system, strictly separated personnel can start sampling the cave or spring water in three different fashions: integratively, discretely or continuously. Integrative sampling can only really give qualitative data (if a tracer reached that point or not) because the entire time of sampling is accumulated into one sample, for example of activated charcoal (F. Bauer and Völkl, 1989). Discrete sampling involves the automatic or manual collection of water samples at certain moments in time, which are then taken to a laboratory for analysis. Continuous sampling, in the fluorescent dye case with fluorimeters, gives temporally very high-resolution tracer concentration curves, with concurrent measurement of multiple dyes in one instrument and coupled with other water properties (e.g. temperature or conductivity). The concentration curves can then be analysed and interpreted for estimations of not only general flow paths, as in the qualitative case, but also with regard to different velocities of flow, dispersion, conduit volume and other system properties (Goldscheider et al., 2008).

In the *Totes Gebirge* massif, some tracer experiments have been conducted: Maurin and

Zötl (1964) used the method of coloured *Lycopodium* spores inserted into ponors near lakes to investigate the karst connectivities in the area of Tauplitzalm, to the southeast of Grundlsee, originally for water supply purposes. However, they interpreted their results (see ????), as conclusive evidence that karst water drainage happened radially inside the main plateau of *Totes Gebirge*: their coloured spores were found, amongst others, in the two small surface springs (30 and 31) beside Lake Altaussee. A second, larger spore tracing experiment with inputs at *Elmsee* and *Steirersee*, themselves located directly on the main plateau, reinforced this view, as, again, the Lake Altaussee springs contained them. As can be seen in Dinçer et al. (1972), radial karst drainage was believed to be the mechanism at play in this, the largest karst plateau in the NCA. However, as cited in Mandl et al. (2012), F. Bauer and Völkl (1989) gathered results gained by a similar methodology in the Dachstein massif, and compared them to spore tracing done by J. Zötl in the '50s in the same place, that put into question these far-flung connectivities. Based on this new interpretation, a S-N-directed karst drainage along fault systems and bedding planes in *Dachsteinkalk* was modelled which also fit much better to the geological situation (Herlicska and Lorbeer, 1994; Scheidleder, 2001). For this reason, F. Bauer and Völkl (1989) also doubted the results of the *Totes Gebirge* spore tracing tests, as they suspected that on the one hand, the division between injecting material and personnel and sampling material and personnel had not been upheld sufficiently, and on the other hand that the detection limit applied was lower than advisable. Based on a few spores found in any spring, connectivity was seen as proven, while these few spores could have reached that place by being carried there by personnel (F. Bauer and Völkl, 1989; Schriebl et al., 2024; Winkler, 2004).

Remote sensing can also play a role in geological and karst studies: Radulovic and Sekulic (2015) used satellite thermal data to determine the approximate location of sublacustrine karst springs at up to 70 m water depth, and analysed the regional and local fault lines with stereoscopic satellite and airborne imagery with regard to their control on these springs. Earlier, Kresic (1995) had already developed a variety of different methods and data sources for the investigation of the fault tectonics in Dinaric karst, which are tightly connected to groundwater flow directions. Schwingenschlögl (1980, 1986) used stereoscopic photogeological lineament drawing coupled with field campaigns to map the fault tectonics of *Totes Gebirge*, an effort which has helped the author a great deal and reached quite a high level of accuracy, despite the instrumentation which, compared with today's technological possibilities, seem rudimentary. To pre-empt the upcoming section on hydrology, various elements of the hydrologic cycle, such as evapotranspiration (Ollivier et al., 2021) and snow cover resp. snow melt (Çallı et al., 2022; He et al., 2014) can be estimated and modelled from satellite-acquired data, increasing

the accuracy of regular hydrological models.

1.2.2.2.2 Modelling

Generally, a region's geology is first documented by geologists that can see and measure surface-level, 2D observations from outcrops, borehole profiles, tunnel galleries or, in the karst case, cave walls. These measurements often already have a 3D aspect, as e.g. dip direction and dip of a bedding plane often points out of the plane they are measured in. Combined with the topography, an idea of the 3D structure of the subsurface geology can start to form. Drawing geological cross sections is then already an application of this idea to gain a 2D visualisation of the formations present. To represent the 3D structure, then, is the next step. Having started to develop in the mining sector, the advancement of graphical computing power and according software has made it possible to do so. In principle, it means to intersect where geological formations are situated and their extent (vector data) with their descriptive variables that behave continuously within units, but discontinuously between them (raster data). The 3D spatialisation is carried out with geostatistical interpolation and prediction techniques. That is why, although called "geological modelling" for short, its purpose is "computer representation of geological characterization", reminding the user of the lack of numerical simulation continuous systems present (Houlding, 1994). Of course, once a geological characterisation model is used to calculate e.g. predictions about the evolution of the geology of a region, or to restore pre-folding stratigraphy, the term "modelling" in its usual sense once again applies.

One important differentiating feature between methods of geological characterisation is if they work implicitly or explicitly. The latter denotes a modelling environment in which the necessarily very knowledgeable and trained user inputs separately each geological units boundary and fault, connecting their known points one by one. Examples for this approach are the MOVE suite by Petex (<https://www.petex.com/pe-engineering/move-suite/>) or the GOCAD Mining Suite from Mira Geoscience (<https://www.mirageoscience.com/mining-industry-software/gocad-mining-suite/>). On the other hand, implicit geological subsurface characterisation uses geostatistical interpolation and best-fit calculation to automatically produce 3D meshes representing different strata. Here, examples include GeoModeller from Intrepid Geophysics (<https://www.intrepid-geophysics.com/products/geomodeller/>) or GemPy, a Python-based geological modelling library (La Varga et al., 2019). The geological side of the VisualKARSYS approach falls into the latter category, as will be explained further below.

In contrast to this, most hydrogeological models, interested in describing the temporal

evolution of the state of water flow through a medium, do conform to the traditional sense of the word model: they use numerical representations of physical processes to simulate their behaviour and predict outcomes. A classification for them is thus given in Section 1.2.3.1, as many of these methods also reflect different levels of spatio-temporal resolution and varying grades of adherence to physical reality in applied equations. Here, a quick overview of typically applied hydrogeological models is given.

The absolute classic of these is MODFLOW, developed by the United States Geological Survey (USGS, <https://www.usgs.gov/mission-areas/water-resources/science/modflow-and-related-programs#software>). It was developed for porous or fissured media, in which piezometric surface measurements can reliably be used for prediction and interpolation, and Darcy's equation is applicable without issues. Reflecting this latter element's problem in karst representation, an extension package called MODFLOW-CFP (Conduit Flow Process and karst aquifer simulation, <https://www.usgs.gov/software/conduit-flow-process-cfp-program-simulate-turbulent-or-laminar-groundwater-flow-conditions>) was developed until around 2011. As the name says, it allows the user to integrate tertiary-porosity elements into a porous surroundings, with flow linking between the two and turbulent open-channel to pipe flow in conduits. Recently, a re-integrative release of the base platform with a range of already published extensions has been itself published, called MODFLOW-OWHM (One-Water Hydrologic Flow Model, <https://www.usgs.gov/software/modflow-one-water-hydrologic-flow-model-mf-owhm>). As it's predecessors, it is free and open-source and includes the conduit flow package. It's latest version was published in January of 2024, underlining the ongoing development by the USGS of their product. A third-party extension, iMOD by Deltares (<https://www.deltares.nl/en/software-and-data/products/imod-groundwater-modelling>) is equally open-source and free and provides an interface for the production of especially large MODFLOW models with fast, efficient computation.

The private sector is of course also active in offering optimised, well-supported software packages to paying customers interested in hydrogeological modelling. As an example for this category, DHI has developed FEFLOW (<https://www.mikepoweredbydhi.com/products/feflow>), which, among other selling points, offers integration with the MIKE surface flow programmes, allowing for the modelling of the complete surface-subsurface system.

1.2.2.3 3D-modelling with VisualKARSYS

As has been previously mentioned, the three-dimensional geological and hydrogeological modelling for this thesis was performed using the freely available platform VisualKARSYS, developed by the Swiss Institute of Speleology and Karst Research (~~SISKA~~) (SISKA, 2023).

Originally developed for an estimation of Swiss karst groundwater resources (Jeannin et al., 2013), it has generated international interest, being applied in projects in countries like Argentina, Brasil, Canada, China, Greece, Italy, Norway, and others (see Figure 1.16).



Figure 1.16: Screenshot from 12/01/2024 of visualkarsys.com showing worldwide distribution (top) and distribution of projects in VisualKARSYS in Europe and the Mediterranean region (bottom).

The platform is open-access, free and browser-based, so anyone with an interest in modelling geology and hydrogeology in general, and karst specifically, can easily use it by simply registering on the website. Its backend geological processing is handled by a C++ and Python-based library called GmLib (Lopez et al., 2018), but modules and extensions for the KARSYS

approach are constantly being developed and implemented, a programming effort led by Arnauld Malard. Relatively recently, a flow animation module (FAM) was released and is available upon request that is especially useful for end-user communications, and even more so should the end-user group be laypersons. It can visualise very intuitively how water falls on a karstified system, infiltrates and percolates, to then be discharged from the spring. Participatory groundwater management can thus become more inclusive toward the average population affected by the results of any management decisions (Malard et al., 2023).

Because of how GmLib works at its core, VisualKARSYS is an implicit and conceptual hydrogeological modeling platform. As described above, an implicit 3D geomodeller takes geological information as input, like bedding dip and dip direction, faults, etc., and interpolates between them to create meshes representing strata. In VisualKARSYS, additionally, the hydrogeological characteristics of the stratigraphy and springs are used to generate phreatic groundwater bodies, underlying aquiclude formations are used as such for flow direction mapping and catchment delineation (Malard et al., 2015). From a hydrogeological perspective, a few basic assumptions need to be made to use VisualKARSYS, as elucidated by Malard et al. (2014, p. 239): (1) groundwater flow through formations defined as aquicludes is, as the name implies, negligible. (2) All aquifer volume underneath the elevation of the karst spring can be seen as phreatic, so the EPM porosity given to the karstified unit is filled with water. (3) The hydraulic gradient in low-flow conditions is often very small and, in practice, given a null value for simplicity. (4) Infiltrating recharge water flows vertically through the vadose zone until it hits either the phreatic zone, or (5) the underlying aquiclude, in which case it flows along the unit border until reaching the constant water table. (6) Once in the phreatic zone, water takes the shortest hydraulic path to the system's spring. Due to these simplifications and the abstention from direct flow simulation, VisualKARSYS does not need a more well-distributed representation of porosity than an EPM. The water volume stored in the phreatic zone is mainly in primary porosity, anyway (Ford and Williams, 2007).

On this basis, it is obvious that of the two reasons given by Ford and Williams (2007) to try to model a karst aquifer:

1. "to characterize and understand the system" for groundwater resource management purposes, or
2. for speleogenetic and conduit system evolution simulation,

VisualKARSYS is an appropriate option if the first of these is the aim of a study. However, in contrast to the hydrogeological models explained above, it follows much more of a conceptual approach. Due to its relative simplicity in handling and iteration, and very basic karst

hydrogeological assumptions, it aims to serve more as a framework for all the data and system knowledge already present in a working group. Once a potential subsurface model is visualised and hypothetical catchments are delineated, collaborators of different backgrounds have a central model on which to base a consensus on. In the course of the synthetisation of this common idea, doubts and areas of strong uncertainty as to the system's characteristics and behaviour will crop up. The model can then be used to pinpoint where precisely further research needs to be undertaken, e.g. geological field campaigns, tracer tests, borehole drilling, spring monitoring or other methods (Jeannin et al., 2013).

With increasing amounts and fidelity of data, the original model can then be iterated on further, for the precise delineation of a spring's catchment (Malard et al., 2015), groundwater resource estimation, including at the e.g. Swiss national scale (Jeannin et al., 2013), tunneling hazard prediction in karstified environments (Jeannin et al., 2015) and other applications. Additionally, should the need arise, geological models can be built in GeoModeller (see above) and then imported into VisualKARSYS.

Seeing as VisualKARSYS modelling results are uncertain estimations of real-world conditions, at best, validation from various sources is necessary. Jeannin et al. (2013) suggests comparison of the catchment delineated in VisualKARSYS with one obtained from hydrological water balance modelling (see below), or by taking into account 3D distribution of caves from speleological surveys with their structure, density, form, perched sumps, siphons, vadose/epiphreatic/phreatic borders etc. Existing tracer tests can of course also offer information about flow paths that definitely exist and their flow times.

As G. Völkl is reported to have told R. Winkler personally in 2003, the catchment boundaries in the *Totes Gebirge* are largely unknown (Winkler, 2004). To the author's knowledge, there have been no previous 3D hydrogeological investigations of karst aquifers in the *Totes Gebirge*, but a relatively large amount of geological, hydrological and cave data has been gathered. Just how little is known about this karst system is also shown by the fact that even very large, global-scale dataset on karst spring hydrographs that include the nearby Rettenbach spring does not feature Lake Altaussee in its incredibly long list (Olarinoye et al., 2020). This thesis is then also an effort to synthesise the existing body of knowledge into one place, to be further discussed and form the basis for concentrated efforts to clear up any uncertainties, just as Jeannin et al. (2013) proposed originally. As such, this is an ideal use case for the KARSYS approach.

1.2.3 Karst hydrology

As a branch of Earth Sciences in general, hydrology is defined by the Encyclopedia Britannica as the

"scientific discipline concerned with the waters of the Earth, including their occurrence, distribution, and circulation via the hydrologic cycle and interactions with living things." Encyclopedia Britannica (2024a)

Different subdisciplines of hydrology have formed to gain a deeper understanding: hydrometry for surface water measurement, hydrography for larger surface water body research, and groundwater hydrology for that part of the water cycle that takes place in the saturated zone underground (Encyclopedia Britannica, 2024a). Speaking of the water cycle, it describes the various processes by which Earth's water constantly moves between storage volumes, fundamentally powered by the Sun's energy. Broadly, between the reservoirs (oceans, atmosphere, land water bodies like lakes, rivers and aquifers) water moves by evapotranspiration, precipitation, flow and sublimation. Figure 1.17 shows the global water fluxes between the different reservoirs and their volumes.

In karstified regions, to some extent or another, all parts of the hydrologic cycle play a role. Often, karst systems are fed autogenically by meteoric waters, meaning rainfall. Once the rain reaches the karstified surface, a part of it either returns directly to the atmosphere via evaporation, or is taken up by the often sparse vegetation to be transpired. The rest of the precipitation infiltrates into the subsurface, the epikarst. This rest is often a higher percentage in karst systems than in regular areas, because of the previously mentioned dissolutionally enlarged channels (Linsley et al., 1949).

Allogenic recharge, however, also occurs when karstified formations are situated underneath the headwaters of streams and rivers that form on less permeable geology. In this case, these flowing water bodies disappear into the subsurface at discrete forms called *ponors* (or swallets or swallow holes (Groves, 2007)), or more diffusely along the stream bed, diminishing in size until the channel runs dry.

On its way through any covering soil, the water's CO_2 saturation is increased by the biological activity in that medium, which then serves to dissolve the limestone of the epikarst, near the surface (Hunkeler and Mudry, 2007). Because this water is then quite quickly saturated with calcium (Harlacher, 2003, p. 32), the border between epikarst and the following vadose zone can be characterised by a decrease in permeability. This gives the epikarst a water storage capacity, making it an important factor in aquifer recharge and contaminant transport (Groves, 2007; Jeannin, 2014). Further vertical movement propels the water through the

vadose, or unsaturated, zone, until it reaches the phreatic, or saturated, zone. ~~Owing to a variety of hydrochemical processes (see e.g. Bögli (1980, pp. 35-45)), limestone dissolutional capacity can be reactivated on this journey and far in the depths of the phreatic zone, leading to ever increasing depths of the aquifer.~~ In any case, comparatively few springs discharge the water again at some point, usually forming streams and rivers, but sometimes, like in the case of Lake Altaussee, being situated underneath lakes (sublacustrine) or salt water bodies like an ocean (submarine, or “vrulja”) (Bögli, 1980).

Remaining underground longer-term is water stored in conduits in the deep phreatic zone on the one hand, and slow-flowing matrix and subcapillary-width joint-stored water on the other hand. Especially the latter source is emptied in times of little or no rainfall, and thus low to no conduit flow, and constitutes the baseflow of karst springs (Hartmann et al., 2014). It is this duality of storage time span, inverse to the throughput speed, which give karst springs their unique hydrographical signature. This feature also extends to the hydrophysicochemistry of karst springs, which can reveal a lot about the karst aquifer beneath and the catchment area above (Borsato, 2001).

On the difference between the hydrogeologic view of a karst system given in the preceding section and the hydrologic concept explained here, Jeannin (2014) gives an intuitive explanation in Figure 1.19. It shows how karst system boundary delineation cannot be done sufficiently based on topography alone, on the one hand, and on the other explains why a mixture of

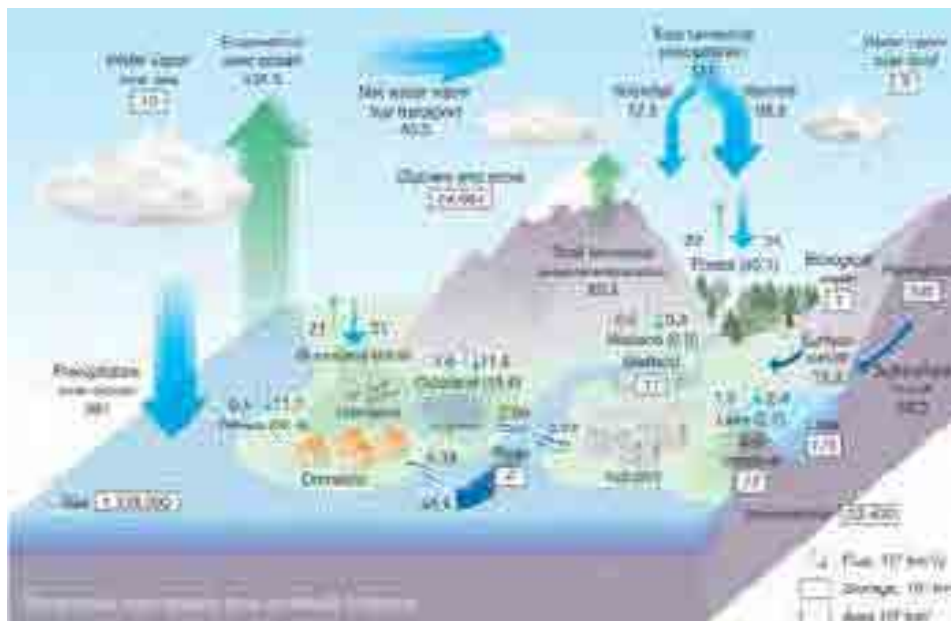


Figure 1.17: Diagram of the hydrological water cycle with global water fluxes from Oki and Kanae (2006).

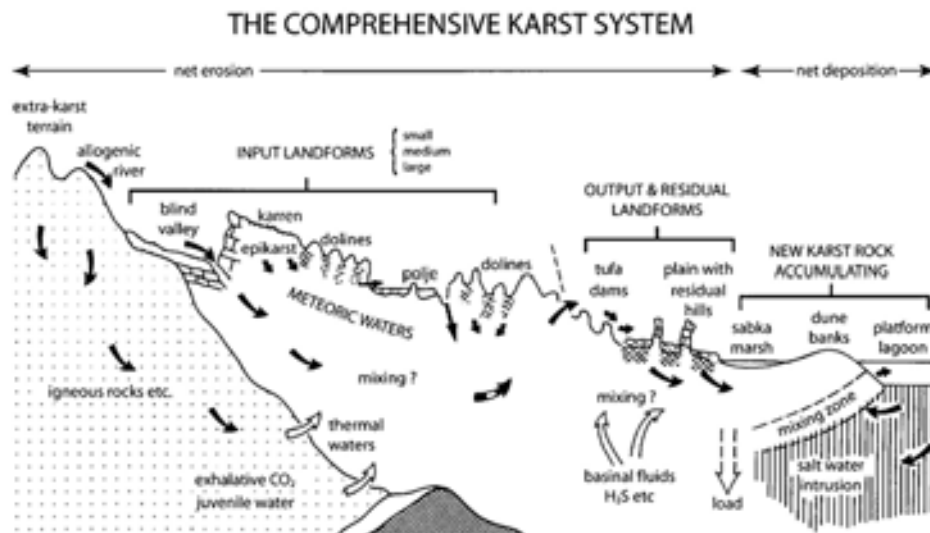


Figure 1.18: Diagram of the entire karst hydrologic system drawn by Ford and Williams (2007, p. 3). Both surface and subsurface karst characteristics are shown, along with output features and the interplay with non-karstifiable geology.

hydrological and hydrogeological approaches is often helpful in describing karst systems, as an understanding of the geological intricacies can explain flow regime-dependent catchment intersection.

1.2.3.1 Analysis and modelling in karst hydrology

1.2.3.1.1 Analysis

As has already been established in Section 1.2.2, karst systems are characterised by strong heterogeneity, anisotropy and duality of flow, making them significantly different compared to the “usual” porous or faulted aquifers. Due to this, not only do the hydrogeological methods employed differ significantly, the hydrological approaches to analysis and modelling, too, must be adapted to the specific requirements (Groves, 2007).

First, the basic concept of water balancing: Being the most basic hydrological concept, it also finds application in karst hydrology, as the idea of “what comes in (P), minus what comes out Q_{out} and evapotranspiration (ET), is the change in storage (ΔS)” (formulated in Equation (1.3)) must continue to be valid. Of course, depending on the actual situation, additional terms might be necessary, describing e.g. groundwater storage tapping for human use, or leakage from one groundwater body to one lower, or to other springs, depending on current flow regime (Groves, 2007).

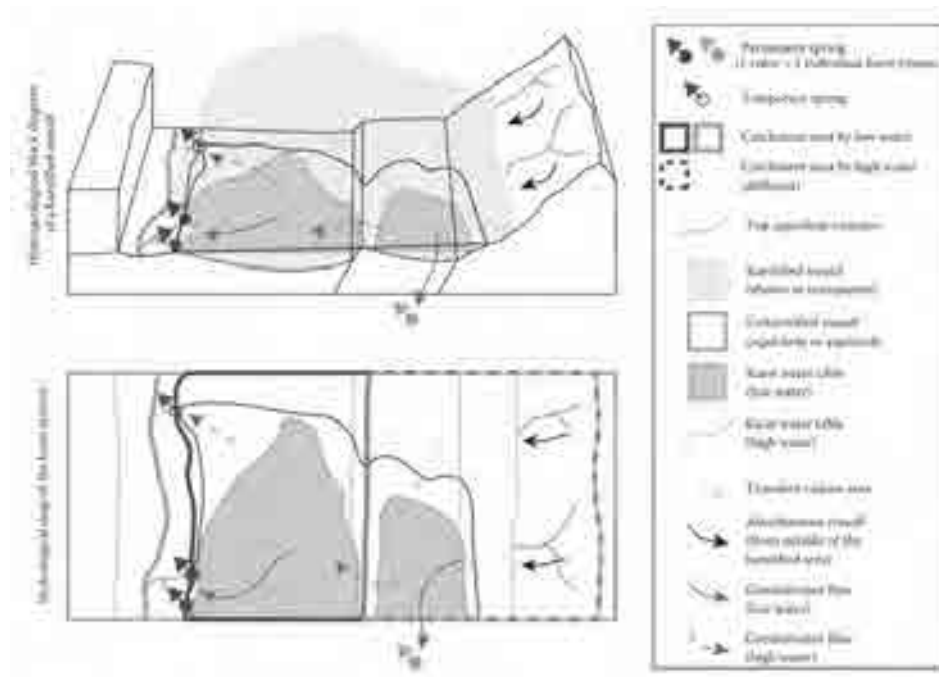


Figure 1.19: Diagram showing the difference in perception of a karst system between the hydrogeological (above) and the hydrological (below) view, from Jeannin (2014, p. 384).

$$\Delta S = P - (Q_{out} + ET) \quad (1.3)$$

The biggest problem of this approach in a karst environment, is that even if ΔS is seen as negligible, as it often is over long time spans, the precise recharge area cannot be delineated based only on topography, as mentioned above. This makes it very difficult to model the water balance, as evapotranspiration (ET) is spatially distributed, especially in karst areas with soil-covered and denuded surfaces, and the precipitation is too, of course. If ET is estimated and the observed system discharge assumed to be known, i.e. no leakage or unknown springs in the system, the above equation can only be transformed for either catchment area or spatially resolved precipitation, the latter of which can be more easily estimated from meteorological data. Thus, in the absence of other data regarding a karst spring's recharge area, it can only be guesstimated from rough precipitation and ET values Groves (2007).


These other data points might come from a range of other methodological approaches. Groves (2007, p. 48) lists “tracer tests, cave exploration and survey, and potentiometric surface mapping” as examples, the first two of which have been explained here already in the hydrogeological section above Section 1.2.2. Potentiometric surface mapping involves first


drilling representative boreholes into the phreatic zone and then measuring the potentiometric surface over time, observing the change in the values during precipitation events and the following decline of discharge until baseflow. The difficulty of this method is finding conduits to precisely drill into, as the cave system must be well known already for that. Attempting to use the triplet well method easily applied in regular aquifers would result in different measurements in karst, depending on the precise position of each of the three wells (Kresic, 2007). Mapped to the area, this method can provide insights into the inner workings of the system, but the danger of gathering senseless data due to previously undiscovered hydraulic connectivities exists, resulting in even more questions by the end of the research. Because of these problems connected with the very high cost of borehole drilling, other, more easily measured approaches would be preferable.

Another method of gaining insight into a karst body is the analysis of the spring hydrograph and the associated chemo- and physicograph. Measured values of e.g. discharge, water temperature, turbidity, dissolved organic carbon (DOC), stable water isotopes, electrical conductivity and other characteristics are analysed vis-a-vis their change over time during and after precipitation high-flow events, and seasonal and annual trends can be read from hydrographs with a long enough time series. These measurements can also be gathered from cave flow paths (see e.g. Harlacher (2003)), but this involves cost and danger in the transport and installation of the instrumentation, as well as extra effort in gathering data: data loggers usually cannot wirelessly transfer their findings through hundreds of metres of solid rock. Therefore, the surface access to springs is a lot easier to exploit and additionally the data gathered there integrates all processes and inputs of the entire system (Groves, 2007).


Aquiring spring hydrograph data can involve the use of weirs or flumes and water level measurement, similar to surface water hydrology in streams. Also similar is the difficulty in accurately measuring high-flow or even flood events, which are so important in hydrograph analysis. Especially with karst systems, whichever system is used should offer the highest temporal resolution possible, as especially storm rainfall is transported in a matter of hours to the spring, dependent on storm and karst system size: the larger the storm and the smaller the system, the faster its signal will arrive at the spring. Technical options available for water level and discharge measurement are expounded upon by Groves (2007, p. 52). For daily and hourly timestep spring hydrographs there are software packages available that make recession curve analysis and karst system classification easily accessible. Recently, two new contenders were released: for R, Bailly-Comte et al. (2023) developed KarstID, and for Microsoft Excel, Cinkus et al. (2023) programmed XLKarst. Each of these offer a range of statistical analysis methods and indices with which karst aquifers can be classified and

compared with one another, as well as provide information about their peakflow-baseflow-ratio and other characteristics that impact their behaviour. The former has already been applied to the hundreds of spring hydrographs included in the WoKaS dataset (Olarinoye et al., 2020), enabling comparison of the user's system with a large number of other karst aquifers globally. The latter, being programmed for Microsoft Excel, is intuitive and easy to use in almost any context, provided basic computational capacity is available. Both software packages include a strong representation of ideas and approaches developed or adapted to karst by Mangin (1975, 1984). Their detailed array of implemented methods can be found in the respective technical instruction manuals online.

On the topic of hydrochemical analysis, Hunkeler and Mudry (2007) give a good introduction and overview of the topic. They also emphasise that although a spring's hydrochemistry can be analysed for the purposes of vulnerability studies of an already understood karst system, the chemical signal can itself assist in understanding in the first place. Laimer (2005) would warn, however, not to confuse intrinsic and extrinsic vulnerability: While the former describes how a karst system's hydrogeology can be vulnerable to contamination because of its structure, the latter includes the interactions between the specific contaminants and said hydrogeology. However, when accounting for a substance's environmental impact and behaviour, it "can sometimes also provide information about the characteristics of karst aquifers." (Hunkeler and Mudry, 2007) 

In a multitude of studies all over the world (e.g. Baedke S. J. and Krothe N. C. (2001), Birk et al. (2006), T. Geyer et al. (2008), Harlacher (2003), and Krainer et al. (2021)), spring hydro-, physico- and chemograph analysis was used to estimate a range of hydrological and hydraulic characteristics of karst aquifers. In their study of a karst system in Indiana, U.S.A, using spring hydrographs and stable water isotopes, Baedke S. J. and Krothe N. C. (2001) introduce the possibility of a third storage reservoir - they suggest small fractures - that is activated after a precipitation event, between fast conduit flow and slow matrix water release. Birk et al. (2006) find that the analysis of temperature and solute concentration curves in spring discharge reflect different processes from one another through their reproduction with software modelling based on physical processes. Thus, observing each of these factors is independently helpful in the characterisation of a karst aquifer. T. Geyer et al. (2008) apply a conceptual two-reservoir model to karst spring hydrographs from two recharge events and, using recession coefficients estimated from tracer tests and spring hydrograph analysis, split up the aquifer recharge between short-term conduit discharge and long-term fissure and matrix storage. They show that the usage of time derivatives of the discharge, as well as inflection points and extrema of the curve can provide insight into the inner workings of a karst aquifer. 

Krainer et al. (2021), meanwhile, use stable oxygen isotope and electrical conductivity data to delineate three recharge areas for a Tyrolian karst spring, as well as observe seasonal variations in hydrological origin of recharge (rainfall, snowmelt or long-term groundwater storage).

In an area of the *Totes Gebirge* plateau intersecting with this thesis' area of interest in the east, Harlacher (2003) gathered spring and cave channel discharge and hydro-physico-chemical data (temperature, electrical conductivity, pH-value and ion concentrations) as well as meteorological information. While the meteorological data had a temporal resolution of one hour, the data loggers saved data points approx. every 20 minutes under normal conditions, and on  minute when a flood was detected. From this spatially distributed information, he found that area to be well-karstified, with very fast reaction times to hydrological events. The summer groundwater recharge in the *Totes Gebirge* and the catchment area of one spring could be roughly estimated, as well as a karst denudation rate that fell into those in the literature. Borsato (2001) characterised an alpine karst aquifer in the northern Italian Dolomites with respect to its hydrological behaviour throughout the year, reaction to different recharge types and mean flow velocity (170 m h^{-1} to 230 m h^{-1}).

1.2.3.1.2 Modelling

In these and other hydrological studies of karst systems, the applied modelling approaches fall into certain classifications that will be explained here, following the technical reference manual for HEC-HMS (Hydrologic Engineering Center - Hydrological Modeling System), a hydrological modelling platform developed by the U.S Army Corps of Engineers (USACE Hydrologic Engineering Center, 2024). Approaches can be part of a number of different classes, depending on their exact implementation, and individual parts of a model can be implemented in ways that fall into different classifications (USACE Hydrologic Engineering Center, 2024, pp. 12-14). Whichever approach is chosen, that choice depends on available data, previous knowledge of the system to be modelled, and the fidelity and robustness of the results necessary. It must also be stated that many classic hydrological techniques were first developed for above-surface stream hydrology, and only later were adapted to karst aquifers.

First, a hydrological model can attempt to either simulate real conditions over a longer period of time (continuous) or for shorter periods centred on hydrologic events like rainfall or snowmelt. Many of the previously mentioned studies of karst spring hydrographs were examples of the latter type of model: due to the duality of flow and storage in karst aquifers, the processes behind peakflow conditions (mainly conduit flow) are different than those influencing baseflow conditions or the transition (small conduit/fissure/matrix flow) (Harlacher, 2003; Hartmann et al., 2014). Investigations into e.g. active conduit volume must therefore focus

on storm event hydrographs and recession curves. For more general, global water balancing, a long-term continuous approach is more appropriate, especially if the temporal resolution of available data is too low in the fast-reaction karst domain, precluding the application of event-based modelling.

Second, the spatial distribution of a model's constituent parts can be classified into lumped, semi-distributed and distributed. In lumped models, the system is treated as a single, integrated entity, with model parameters representing their corresponding real system components - reservoirs and fluxes - without respecting spatially distributed differences. For example, a lumped model will assume as valid one variable value for the entire area's epikarst reservoir, averaging out covered and denuded surfaces that are governed by different processes in reality. While this approach makes broad assumption necessary, it is a lot easier to gain e.g. one average epikarst data point for a large area than tens or hundreds of data points needed for (semi-) distributed models. An example for the lumped approach is KarstMod (Mazzilli et al., 2017), an application of the classic hydrological idea to karst aquifer modelling. The price for this simplicity in application, however, is an inability of the model to reproduce the system behaviour completely (Hartmann et al., 2014).

Compared to the relative simplicity of lumped models, surface stream hydrologists also developed semi-distributed and distributed modelling. They both share a discretisation of the catchment area of an arbitrary point along a stream; the difference lies in the method of discretisation: semi-distributed catchments are divided into parts often called hydrologic response units (HRUs) that share similar characteristics in a certain area. Distributed models, on the other hand, work on a grid basis, applying model parameters and process equations to the grid nodes. One can see that although these approaches resolve the catchment under investigation more clearly, there is still spatial averaging at play (USACE Hydrologic Engineering Center, 2024). Citing Hartmann et al. (2014), distributed models are very seldom useful in a karst context, as the strong three-dimensional heterogeneity of a karst aquifer would require a spatial data resolution not feasibly achievable on the grid scales usually employed (0.01 km^2 to 1 km^2), irrespective of the actual model used. Furthermore, as Beven and Binley (1992) point out, distributed models depend on an often large set of model parameters, only slight variations of whose values can produce widely variable results with the same likelihood function. Coupled with often poor knowledge of the actual conditions inside a karst network, significant hurdles must be overcome to successfully apply a (semi-)distributed hydrological model to a karst system. If this is managed, though, the reward is a very accurate representation of a karst system's response (Hartmann et al., 2014).

The third model classification concerns the random variability of input values: while

deterministic models assume that measured input data is precise and not subject to natural, random variability, stochastic models do not make this assumption and calculate the results based on input with statistical means, deviations and biases. Taking into account the difficulty in accurately describing the probability functions of all inputs necessary for karst modelling, stochastic modelling is rare and challenging. An example in recent literature is Gouy et al. (2024): they developed the KarstNSim algorithm, to simulate a range of potential karst conduit networks from geological data and stochastically interpreted recharge input points, in effect showing the control of recharge distribution over conduit development. The application to a real system shows general overlap of the simulated with the real network. This is also an example showing that this classification of models can also be applied to hydrogeological models of karst systems.

Lastly, models can differ in the “realism” of the implemented equations with which they obtain their results. Empirical equations are only interested in transforming input into output based on previous observations, without necessarily following actual physical processes. That is why they are often seen as “black boxes”, as it is not really possible to check the plausibility of results based on the formulas at play. In contrast, conceptual, or physical, models do aim to mathematicise the processes happening on (or in) the ground. The more abstract version of this is a model ‘based on “first principles”’ (USACE Hydrologic Engineering Center, 2024, p. 6), in which conservation of mass and energy or momentum are applied to control volumes to arrive at a model of the processes involved. A mechanistic approach, on the other hand, seeks to precisely reflect the physical processes affecting e.g. water in its travel through soil (USACE Hydrologic Engineering Center, 2024).

To give an overview over the many different methods that have been developed to model karst systems based on their spring hydrographs, Jeannin et al. (2021) relatively recently challenged thirteen scientist teams to compete against one another. Each used their own discharge prediction models, trained on the same basic 4.5 years’ discharge data from the Milandre karst system in France, to forecast one year’s hydrograph which was validated with observed data. The results showed that the global approaches with few, automatically calibratable parameters performed best, and that the largest sources for simulation errors pertained to baseflow, indicating an over-emphasis on peakflow replication.

1.2.3.2 Hydrological modelling of *Totes Gebirge* karst

As sparse as (hydro-)geological data is on the *Totes Gebirge* plateau and its vicinity (see above), the same must be said for hydrological data useful for modelling purposes. Beginning with precipitation data, there has been no collection on the plateau itself with the exception



Figure 1.20: Map of meteorological stations (red points) collecting precipitation data around *Totes Gebirge*. Screenshot from www.ehyd.gv.at with terrain relief and water bodies with flow directions.

of 4 years (1954-1958, Dinçer et al. (1972)) at Albert-Appel-Haus. On the official website of the Austrian Hydrographic Service, www.ehyd.gv.at, the neighbourhood of *Totes Gebirge* is covered by some weather stations in valleys, but practically none in higher elevation ranges (see Figure 1.20).

Bullmann (2018, Tab. 4, pp. 40-41) lists a few sources that don't seem available anymore, or only by communicating directly with the institutions collecting the data. As an example, there appears to have been a weather station on Lichtersberg north of the town of Altaussee (point number 2 in Figure 1.21) that was closed in the year 2000, to be replaced by a station at the local saline. Neither of these are given as options on the ehyd web-map.

Although (Mandl et al., 2012, p. 9) writes that no orographic precipitation gradient for rainfall can be observed in the area, results from Bullmann (2018) (see Figure 1.21) clearly show this to be an overly simplistic assumption. Very locally (around Altaussee and the far northwestern edge of *Totes Gebirge*) northwesterly weather formations bring large amounts of rain ~~even in to valley~~, making the corrected monthly average precipitation for July in Altaussee, at 760 m a.s.l. 248.4 mm, almost as high as that on the mountain Krippenstein, at 2050 m a.s.l. 265.9 mm. Even so, Bullmann (2018) puts forward 3 different precipitation enhancement gradients, depending on the up- or downwind position around the mountains in the area of the involved weather stations. For the core zone of *Salzkammergut*, in which *Totes Gebirge* is emplaced, the gradient is 88 mm per 100 m elevation. Figure 1.21 also shows the strong lee effect around Grundlsee, as it is protected from the dominating weather



direction by *Totes Gebirge*.

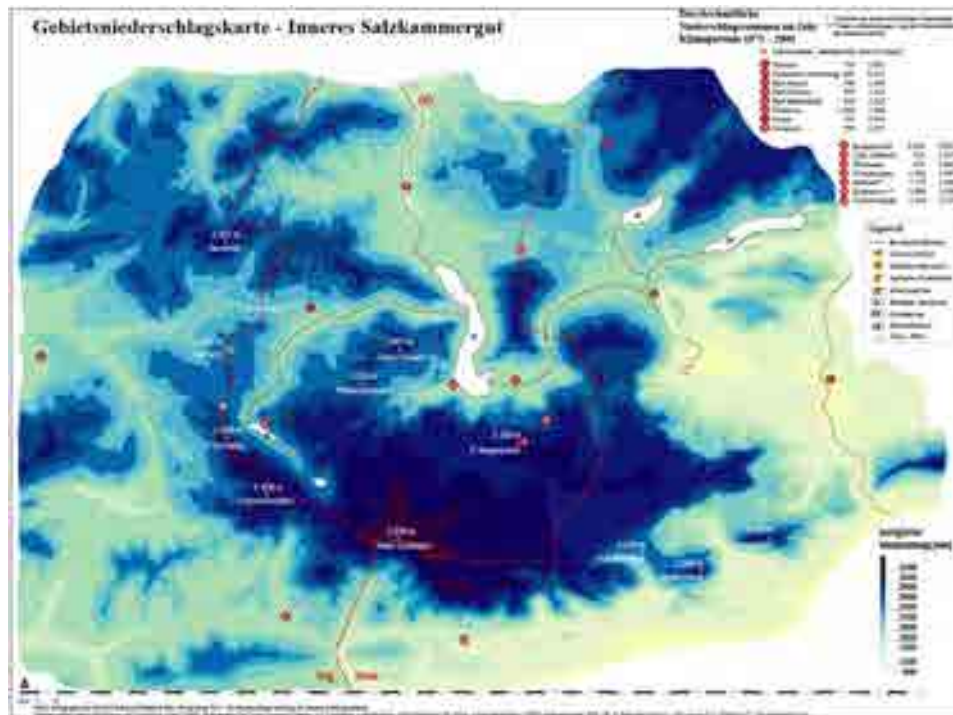


Figure 1.21: Precipitation distribution map of *Salzkammergut*, from Bullmann (2018). Part of *Totes Gebirge* in the northeast corner, showing high rainfall in valley elevations in northwestern aspects and strong lee effect around Grundlsee.

Concerning discharge measurement, the *Totes Gebirge* shows a sort of duality of data collection: most larger streams coming from *Totes Gebirge* that feed either the Traun or the Steyr catchment area (Altausseer and Grundlseer Traun, Augstbach, Rettenbach in the west, and Weissenbach, Steyr, Krumme Steyr and Steyring in the northeast) have discharge or water stage stations in their courses. However, of all the springs identified by Maurin and Zötl (1960) (see Figure 1.22), none are or have been monitored over a longer time. As mentioned above, Harlacher (2003) logged data concerning the Zimitzbach spring in the south and the Nesseltalbach and Weisseneckbach springs as well as the artesian spring at Almsee in the north, but only for a maximum of 3 months in the summer of 1996, making any potential data only valuable as qualitative points of comparison. Seeing as these springs are not mentioned in the map by Maurin and Zötl (1960), it remains unclear if all points of discharge from *Totes Gebirge*, the largest karst plateau of the NCA, are even known, making it even more difficult to assess potential regional water resource management issues.

As will be explained in more detail in the following chapter, any data that might be available in the precipitation or discharge domain is only given in daily sums (precipitation) or averages

(discharge), making many of the previously mentioned spring hydrograph analysis approaches impossible in karst terrain, where, as Harlacher (2003) reported for the vadose zone and the northern and southern springs investigated by him, rainfall and snowmelt event reaction times are in the range of minutes to hours, respectively.

For these reasons, both Harlacher (2003) and Winkler (2004) resorted to basic, global water balancing to gain at least a basic understanding of the catchment areas of their points of interest, the former for Zimitzbach spring, the latter for the Altaussee Traun after the Augstbach feeds into this stream. Their methodological approaches will be explained briefly in order to provide a precedence case basis for the water balancing method performed for this thesis (more on that in the following chapter).

Harlacher (2003) limited his estimation to the time period from mid July to mid September of 1996, when his monitoring was under way. After splitting up baseflow and peakflow, which already was based on conjecture because the high frequency of storms never allowed the hydrograph to truly recede, each was summed up and the former was subtracted from total flow to obtain the latter. Two values were gained for each, because a range was decided on



Figure 1.22: Map showing all springs around *Totes Gebirge* identified and mapped by Maurin and Zötl (1960), with size of spring signature denoting discharge and colour the electrical conductivity; rhombi indicate flood overflow springs. Photograph of original map by author.

for the baseflow to mitigate the assumptions. Then, an estimated evapotranspirative loss was taken off the total precipitation that had fallen in the time period, based on an empirical formula by Haude that requires only air temperature and relative humidity by 2 p.m. and gives the potential evapotranspiration (ET_{pot}). Due to the resulting, unrealistically high infiltration values, a flat 10 mm were added, and the peakflows were divided by these recharge values to gain approximate catchment areas. This was then compared to another method, explained in the following equations:

$$\frac{peakflowVolumePlateau}{areaPlateau} = \frac{peakflowVolumeZimitzbach}{catchmentAreaZimitzbach} \quad (1.4)$$

$$catchmentAreaZimitzbach = \frac{peakflowVolumeZimitzbach * areaPlateau}{peakflowVolumePlateau} \quad (1.5)$$

Despite the sweeping assumptions made about evapotranspirative losses, precipitation, baseflow-peakflow division etc., the results of both methods were quite comparable and in a range of 1 km² to 3 km².

Winkler (2004), in comparison, focused on Lake Altaussee, or, to be precise, the Altaussee Traun fed by the Augstbach. Starting from the daily average discharge (Q) over a time period of 36 years (1977-2003), a synthetic average precipitation (P) was calculated inversely from the discharge with an infiltration rate of 80 %: $Q/0.8 = P$. Then, he broke down the average yearly precipitation (in mm a⁻¹) to L s⁻¹. Dividing the synthetic P by this average precipitation per second, he obtained a catchment area of approx. 61 km². Of course, both of the methodologies described can only give order-of-magnitude values because of their rudimentary nature. They can (and will) serve as inspiration and validation for methodology employed and results obtained for this thesis.



1.3 Research Questions


Based on the information above and the originating proposal for this Master thesis, the following lines of focused inquiry are put forth:

- Using a water balance model of the Lake Altaussee and it's area, what must be the approximate size and location of the lake's karst catchment area?
- After modeling the geological and hydrogeological situation of the relevant part of Totes Gebirge using SISKAs platform VisualKARSYS, what is the hydrogeologically estimated size and geometry of the catchment area of the Lake Altaussee?

2 Methods and Materials

2.1 Data

A large amount of data is necessary to attempt to answer the research questions addressed above. The first step of hydrological water balancing requires precipitation, discharge and evapotranspiration data or estimations. Step two, a three-dimensional geological and hydrological model, further needs geological information concerning stratigraphy, tectonics, fractures, faults and folds, and porosity or permeability for hydrogeological application.  Seeing  as a karstified area is studied, data concerning the caves is also applied. In the following subsections, the used data is presented in all detail.

Any data (pre-)processing, calculations or visualisations were carried out using Microsoft Excel (Microsoft Corporation, 2022) or R (R Core Team, 2023) using RStudio (Posit team, 2023). Geoinformation visualisation and (pre-)processing was carried out either in ArcGIS Pro  Inc. (2023) or QGIS QGIS Development Team (2023). The construction of geological sections involved the use of Inkscape (Inkscape Developer Community, 2024) and AutoCAD (Autodesk, 2023). Geological and hydrogeological modelling was performed on the online software platform VisualKARSYS (SISKA, 2023). Cave data was visualised using Survox, “an open-source software package for cave surveyors” (CUCC, 2018).

As an integral part of any hydrological or geological research, the Digital Elevation Model (DEM) used was created by the ArcGIS Living Atlas World Elevation Terrain service by collating sources from all over the world. For the Austrian territory, the service uses the 1 m pixel resolution DEM published by the Austrian Federal Office of Metrology and Surveying (*Bundesamt für Eich- und Vermessungswesen* in German). For the purposes of the thesis, a 5 m pixel resolution DEM was deemed sufficient and within the allowed fidelity for raster download from the Living Atlas service. The download of data took place on December 4, 2023.

2.1.1 Hydrological data

As will be explained later, in the methodology section below, the water balancing approach taken requires data of the most important hydrological processes taking place on *Totes Gebirge*, these being precipitation (P), evapotranspiration (ET) and discharge (Q). The sources for and information about the data on these elements will be described below.

2.1.1.1 Precipitation in the region

As can be seen in Figure 2.1, the measurement stations ~~for meteorological data like precipitation~~ whose data is freely available are unfortunately not situated directly in the area of interest. Instead, 3 stations in the wider vicinity were chosen to cover a wide range of elevations (see Table 2.1). Data in the time span of ~~1971-01-01 to 2018-12-31~~ was used. This time period fit best with the rest of the necessary data and avoided a necessary correction of the raw data which was sent by direct request, going from ~~2019-01-01 to 2023-01-01~~. The chosen time span was applied because instrument and continuity corrections had already been carried out by the provider, the Austrian Hydrographic Service, a department of the Federal Ministry for Agriculture, Forestry, Regions and Water Management (data platform: www.ehyd.gv.at). All types of precipitation are included in the downloadable data, and no distinction was made before further calculation.



Table 2.1: Overview of the meteorological stations in the region chosen for a wide range of elevation. The average annual precipitation is calculated from www.ehyd.gv.at, the official hydrographical data source in Austria, before wind-error correction following Bullmann (2018), described below.

Station	Elevation (m a.s.l.)	Coordinates (Bessel 1841)		Distance to Q station (km)	Average annual precipitation (mm)
		Longitude	Latitude		
Gößl	710	13°53'34"	47°38'29"	9.36	1582
Pötschen	1000	13°41'44"	47°37'25"	5.67	1639
Krippenstein	2050	13°41'39"	47°31'24"	13.7	2019

The precipitation data from each of these stations was given as daily sums in mm, measured mainly using ombrometers, although since 2016 an ombrograph is employed additionally at Gößl station. Temperature, snow level and snow fall data would also be available for all weather stations. In Figure 2.2, an overview of the precipitation data per station is given, with the respective summary statistics presented in Table 2.2. These two representations

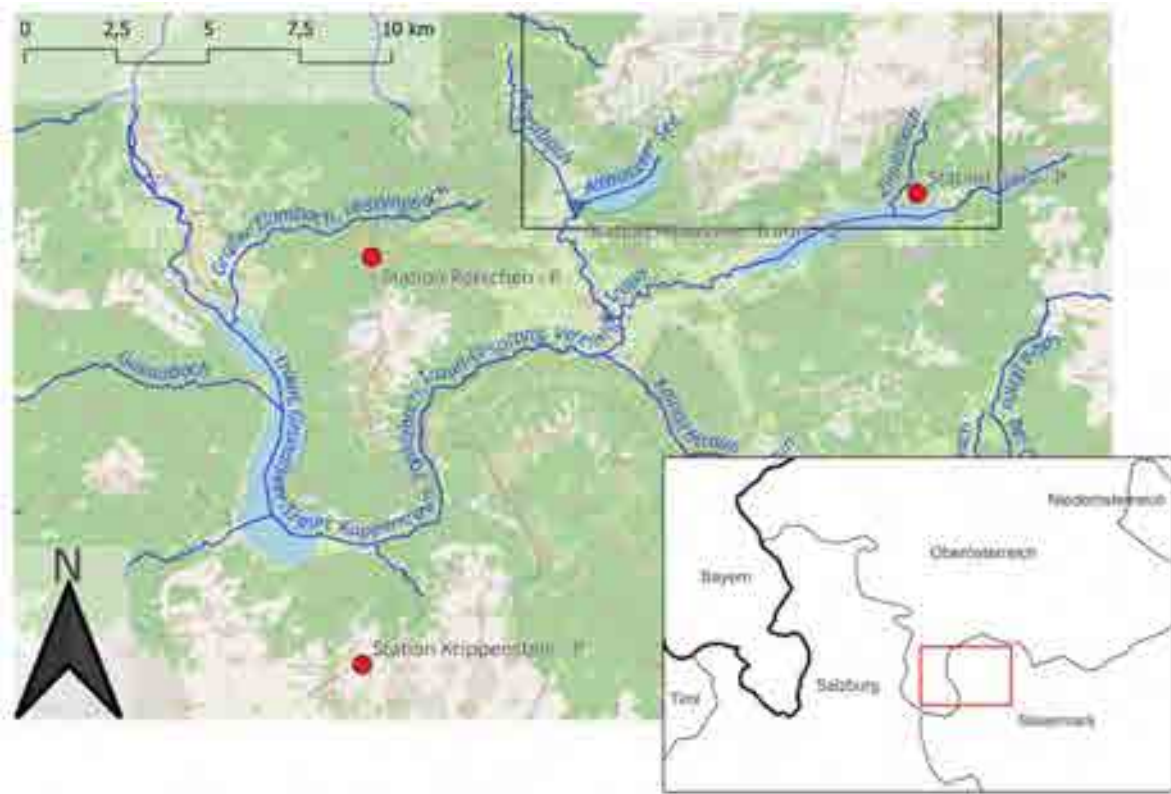


Figure 2.1: Map showing the regional hydrological points of interest and sources of the data used in thesis: streams and lakes (source: Umweltbundesamt, <https://docs.umweltbundesamt.at/s/8rYyRjFDse8Za4D>), discharge measurement in Altausseer Traun, precipitation measurement at Gößl, Pötschen and Krippenstein.

show a clear bias of all P measurements that are larger than zero toward small values, the maximum values being about ten times larger than the 75th percentile. As the mean value is significantly higher than the median, it must be assumed that the outlier rainfall events are distorting this mean, which means that precedence must be given to the median P when describing normal conditions. Regarding the elevation-based differences, a slight increase of P with elevation is noticeable, especially in the core percentile box of Krippenstein, which, reflecting the summary statistics, does cover a higher range of P values. However, the station in Pötschen has the three highest daily P sums in the time series.

2.1.1.2 Evapotranspiration on the *Totes Gebirge* plateau


Because no direct evapotranspiration (ET) data was available for *Totes Gebirge*, a flat value of 500 mm per year was assumed based on personal communication with Philipp Häuselmann


Table 2.2: Summary statistics of precipitation data (in mm) from the three stations selected. Data with wind-error correction following Bullmann (2018), described below, and without “0” values.

Station	N != 0	Mean	Std. Dev.	Min	Pctl. 25	Pctl. 50	Pctl. 75	Max
Gößl	8869	10	13	0.12	2.2	5.8	14	143
Pötschen	8250	12	14	0.13	3	8.2	17	170
Krippenstein	8701	19	18	0.17	5	13	27	145

and Pierre-Yves Jeannin. Their decades of experience in alpine karst catchments led to this recommendation that includes direct evaporation from bare rock, transpiration from any soil cover and vegetation, and interception by vegetation.

2.1.1.3 Discharge from Lake Altaussee

As mentioned above, Lake Altaussee discharges into the river Traun via a short tributary section called the Altausseer Traun, which is joined by the Augstbach before merging with other Traun tributaries (see Figure 2.1). The lake discharge has been derived from water height continuously since 1950, with automatic measurement from 1998 onwards. Data with different time scale averaging is also available from www.ehyd.gv.at. For the purposes of this thesis, the smallest available time scale, daily average discharge as m^3s^{-1} , was used in the same range as above, of 1971-01-01 to 2018-12-31. ~~This time period fit best with the rest of the necessary data and avoided a necessary correction of the raw data which was sent by direct request, going from 2019-01-01 to 2023-01-01. ??-??~~  an overview of the discharge observed from Lake Altaussee, and Table 2.3 presents the summary statistics of the daily average discharge.

As can be seen from Table 2.3, the median and mean discharge values, $1.7\text{ m}^3\text{s}^{-1}$ and $3.7\text{ m}^3\text{s}^{-1}$ respectively, are quite different. This and the form of the histogram in Figure 2.3 suggest that the outliers are statistically quite significant in increasing the mean discharge value, and that the median  value is more representative of the usual outflow regime from Lake Altaussee. The monthly average discharge (Figure 2.4), meanwhile, shows the typical monomodal hydrological regime of an alpine catchment, with the main peak being caused by snowmelt in May and June. A slight uptick can be observed in September when autumn rainfalls are prevalent. Figure 2.5 gives quite a clear picture about the development of the karst system's annual discharge averages: the linear regression model's 95 % confidence level interval covers the long-time average discharge, making the slight upwards trend given by the

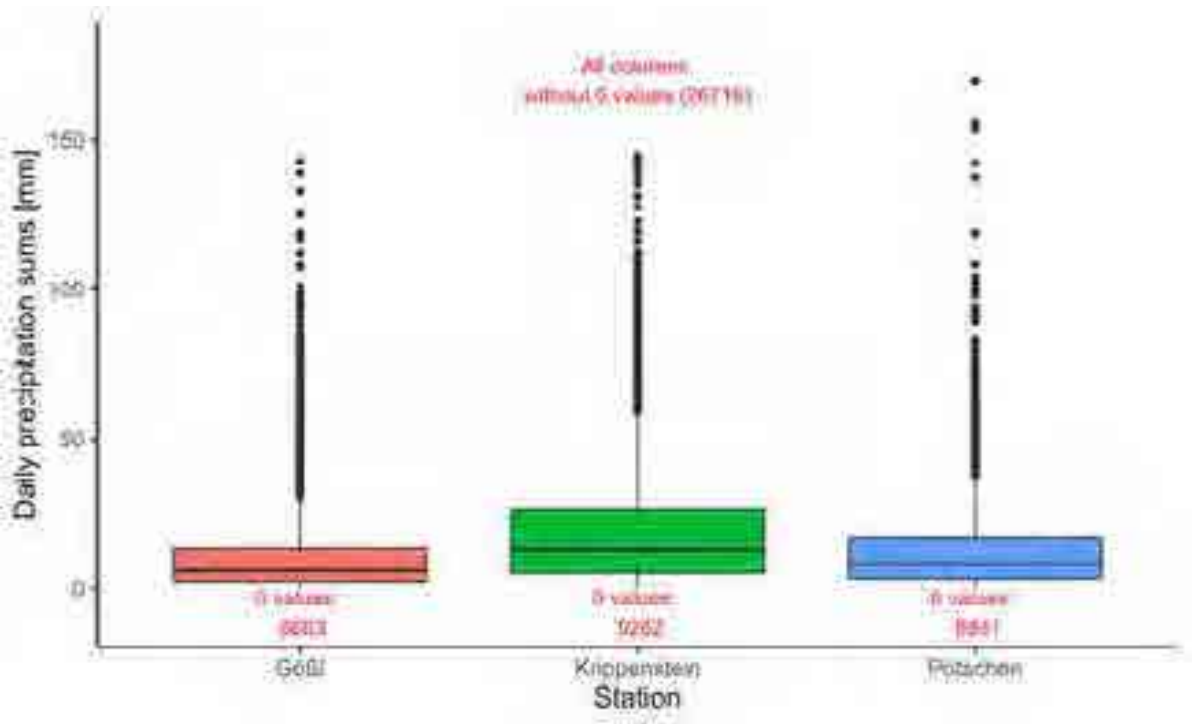


Figure 2.2: Boxplot overview of the precipitation data for each of the stations considered. Data corrected following the method described below, following Bullmann (2018), and “0” values removed from boxplot.

line itself questionable.

Table 2.3: Summary statistics of discharge from Lake Altaussee in given time range.

	N	Mean	Std. Dev.	Min	Pctl. 25	Pctl. 50	Pctl. 75	Max
Q	17532	3.7	4.5	0.14	0.80	1.7	4.8	46

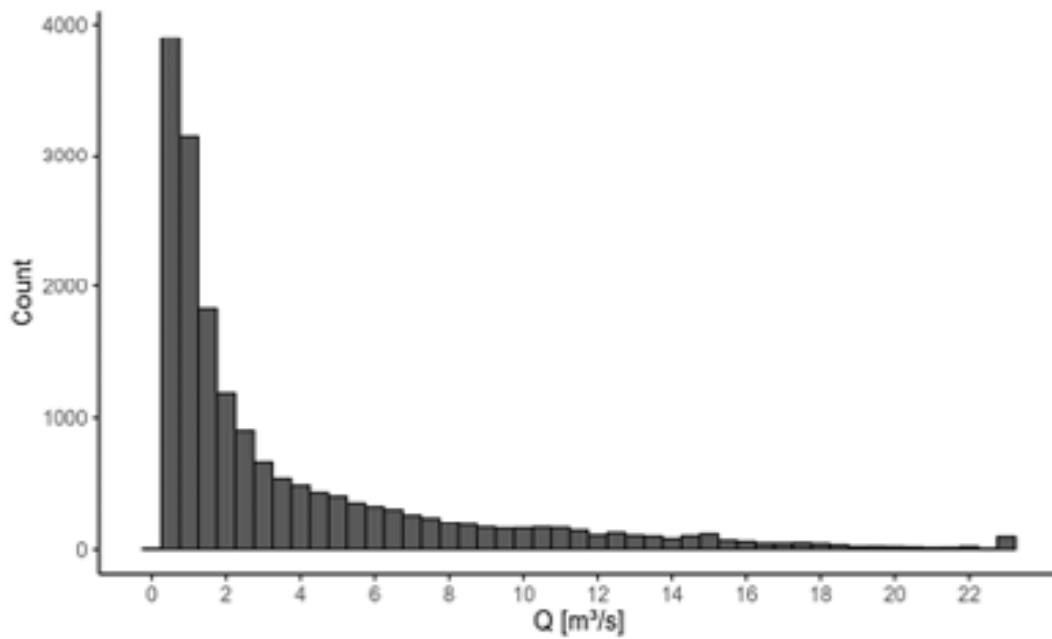


Figure 2.3: Histogram of daily average discharge from Lake Altaussee, with outliers binned at $23 \text{ m}^3 \text{ s}^{-1}$.

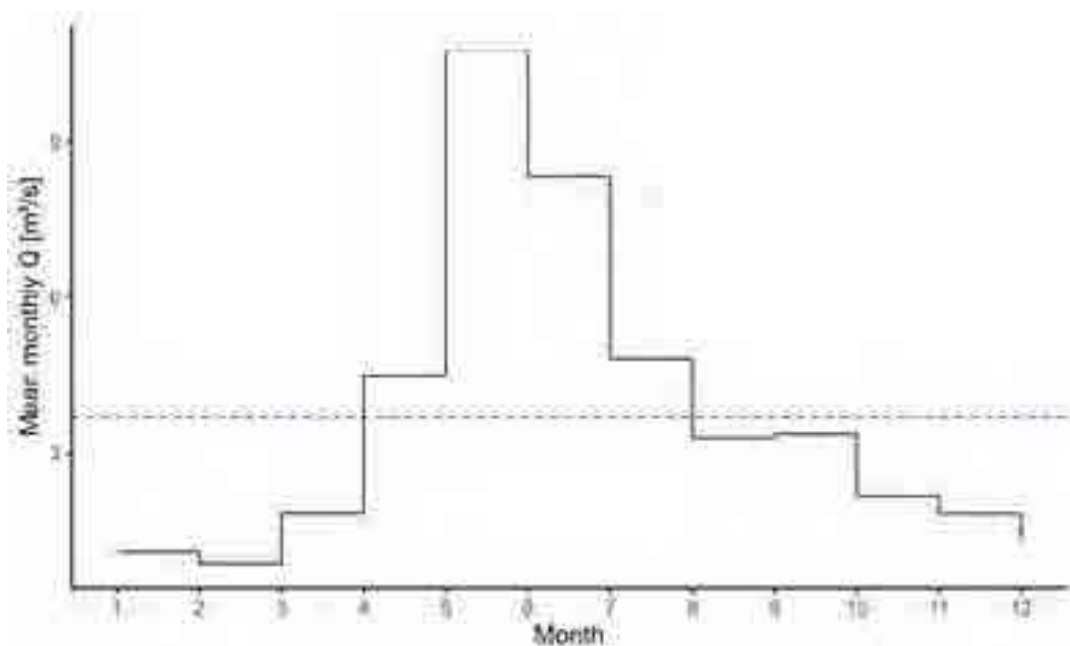


Figure 2.4: Graph of long-term averaged monthly mean discharge from Lake Altaussee, with annual average discharge overlaid in blue dashed line.

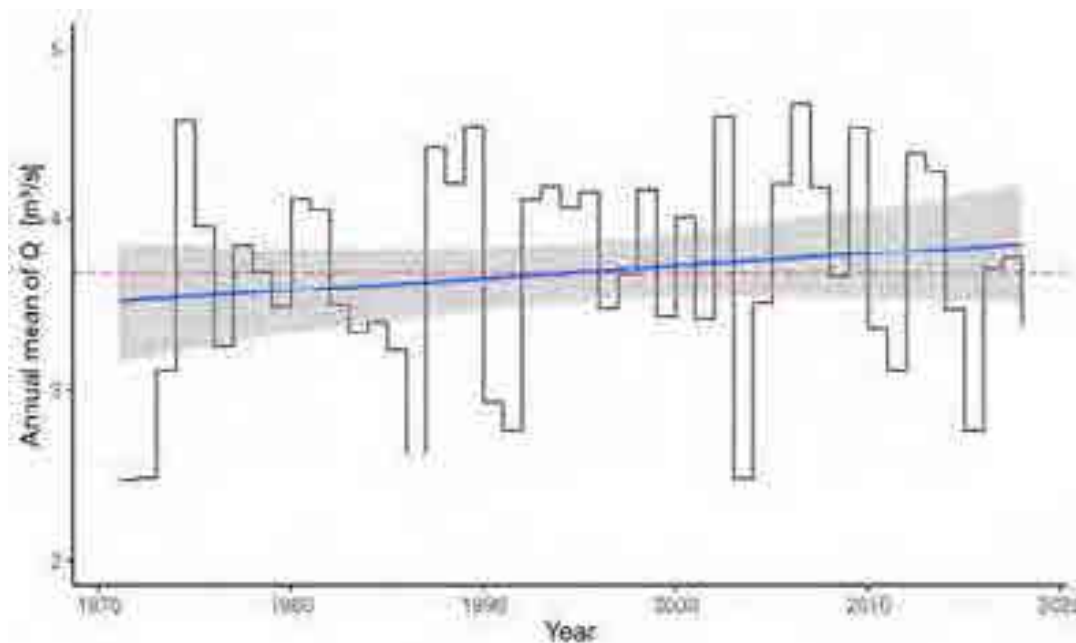


Figure 2.5: Graph of the development of the yearly averages of average daily discharge from Lake Altaussee. Overall average discharge in dashed red line, linear trendline in blue with grey 95 % confidence level interval.

2.1.2 (Hydro-)Geological Data

Different types of geological data are necessary to construct a three-dimensional hydrogeological model of a region. In the following sections, their variety and respective sources will be shown.

2.1.2.1 Geological maps

The definitive geological maps in Austria are made by what is now a part of the so-called Geosphere Austria, formally known as the *Geologische Bundesanstalt* (GBA, Geological Survey of Austria). Their long-term mapping project *Geologische Karte Österreichs 1:50.000*, GÖK 50 in short, aims to deliver a country-wide geological map in the scale of 1:50000, divided into the map sheets of the ÖK 50, the topographical map of Austria in the same scale, which is published by the Austrian Federal Office of Metrology and Surveying. Because the GÖK 50 maps take a lot of work hours and effort to complete each one, only about one third of the country has been covered so far. To provide planners, engineers and officials with geological data in the rest of the country, the GEOFAST project was launched. In its course, archive maps and materials were compiled to cover the hitherto empty map sheets, but no field surveying campaigns were undertaken. The resulting maps, therefore, offer an imperfect, interim solution until ~~such a time that~~ the Geological Survey of Austria can dedicate itself to whichever new geological map. Of course, this has the side effect of borders between neighbouring map sheets of the former and latter type showing inconsistencies in their content. A good example pertaining to this thesis can be seen in Figure 2.6, where the sheet border also seems to constitute a sudden change in outcropping strata.

Along with the mainly lithographic GÖK 50 maps, a geological map focusing on fault tectonics of the plateau of *Totes Gebirge* was used. Drawn by Schwingenschlögl (1986), it is based on extraction of lineaments from aerial photographs and topographic maps and their inspection in the field. For this thesis, the field measurements of bedding planes and notes on local lithology were especially helpful during the construction of geological sections and the data input into VisualKARSYS.

2.1.2.2 Geological sections

In his 1878 monography on the *Totes Gebirge*, Georg Geyer already complained about the scarcity of geological data available for the massif (G. Geyer, 1878). Even now, this problem persists: a thorough literature search revealed geological cross-sections of the area in question from only 4 sources. First, 4 sections were drawn by Dr. Rudolf Schwingenschlögl and



Figure 2.6: Example of the geological map sheet border inconsistencies resulting from difference in map creation process: On the left, map sheet 96 as official map product from the Geological Survey of Austria, on the right map sheet 97, a map of the GEOFAST series, compiled from archive material by the same institution. Background map in the top right overview map from <https://basemap.at>, and extent indicator in red.

published in two parts, once in a report to the Austrian petrol company OMV (*Österreichische Mineralölverwaltung*) in the course of a feasibility study for fossil fuel extraction from *Totes Gebirge* (Schwingenschlögl, 1980), and once in the follow-up paper described above (Schwingenschlögl, 1986). From the 3 sections included in the former, only sections 1 and 3 were used, roughly N-S and W-E, respectively. Section 2, unfortunately, does not intersect with the VisualKARSYS modelling area (see Figure 2.7 for section traces). Of the two cross-sections included in the latter paper, only the first lies within the area of interest for this thesis.

The second source for geological cross-sections is an investigation of the geology of the western *Totes Gebirge* by Ortwin Ganss, the 10 sections of which overlap rather well with the scope for the author's own section construction, and slightly less well with the VisualKARSYS project scope (see Figure 2.7 and Ganss (1937)).

Thirdly, Mandl (2013) performed a study of the geology of the Sandling-Alm – Blaa-Alm region, sections 5 and 7 of which also reached into the area the VisualKARSYS project, if only partly. At least a clearer picture was made available of the geological situation of the

Loser and its surrounding peaks, as well as through the valley of Lake Altaussee toward the Trisselwand.

Lastly, Georg Geyer himself also published some geological sections through the surroundings of Grundlsee (G. Geyer, 1915) in the course of research for the first iteration of a geological map for map sheet 97 (Vacek 1915). It is striking how similar this very early idea of the geological situation of *Totes Gebirge* is to the sections drawn later. The section of interest is one of four, Figure 2 on Panel II.

Because of the low density of available geological sections, the author was obliged to construct his own so that a suitable three-dimensional (hydro-)geological model can be constructed (see below).



Figure 2.7: Traces of existing geological sections used for VisualKARSYS model creation. Labels starting with “80” from Schwingenschlögl (1980), the one starting with “86” from Schwingenschlögl (1986), numbering with Roman numerals indicative of Ganss (1937), purple traces with arabic labeling from Mandl (2013) and red trace is labeled as being from G. Geyer (1915). The spatial extent of VisualKARSYS model shown as smaller rectangle, the larger one being the scope for author’s construction of cross-sections. Background map: OpenStreetMap.

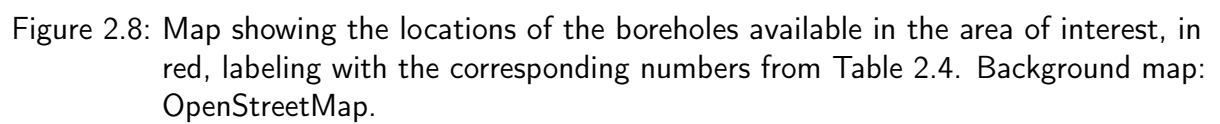
2.1.2.3 Boreholes

Although there are 18 boreholes available for the area of interest, none of these was used directly for modelling in VisualKARSYS because the drilling depth did not suffice to reach

aquiclude depths, and the shallow quaternary data was not of interest for this thesis. The following Table 2.4 gives details about the available boreholes, and Figure 2.8 shows their locations in the Altaussee and Grundlsee valleys. The source for this data is the GIS-Steiermark (2023), available over the “Geotechnik” layer.

Table 2.4: List of available boreholes with drilling profile data in the area of interest of this thesis (GIS-Steiermark, 2023).

Nr.	Longitude EPSG: 32633	Latitude	Surface elevation (m a.s.l.)	Depth (m)	Method
153869	413568.8	5276014.3	708.22	17.1	Borehole
153870	413571.0	5276008.7	708.22	17.4	Borehole
156271	407167.8	5277010.1	725.7	10	Borehole
163289	406521.3	5276402.6	744.11	105	Percussion Drilling
163290	407310.2	5277365.3	754.7	105	Percussion Drilling
163356	407655.3	5276017.1	751	93	Percussion Drilling
163389	407400.3	5276675.5	716.11	75	Percussion Drilling
163390	407513.8	5276813.0	714.98	88	Percussion Drilling
163391	407253.4	5276815.1	720.57	100	Percussion Drilling
163392	407730.6	5276041.2	758.17	100	Borehole
163437	407543.4	5277081.0	720.62	95	Percussion Drilling
163438	406526.0	5276397.0	743.98	105	Percussion Drilling
163439	407305.0	5277370.8	755.84	105	Percussion Drilling
164288	407295.0	5276587.5	713.3	105	Borehole
164298	407546.1	5276297.9	727.4	90	Borehole
168404	407174.6	5276495.6	715.83	105	Borehole
168946	407748.9	5277414.0	747.7	86	Other Method
168947	406626.4	5276162.4	756.82	90	Percussion Drilling

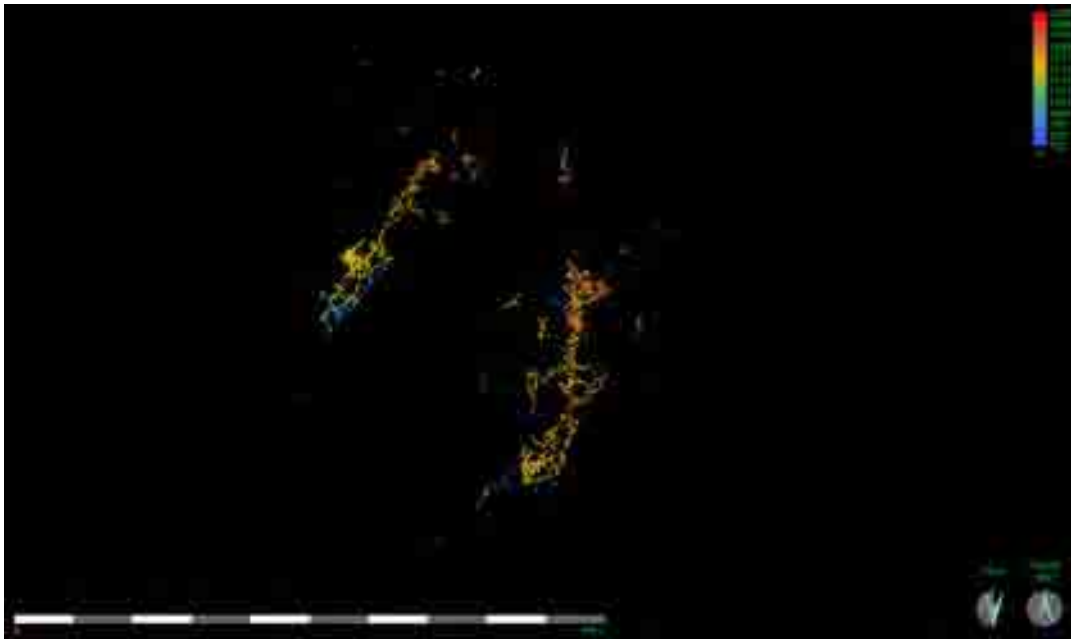


2.1.2.4 Other data

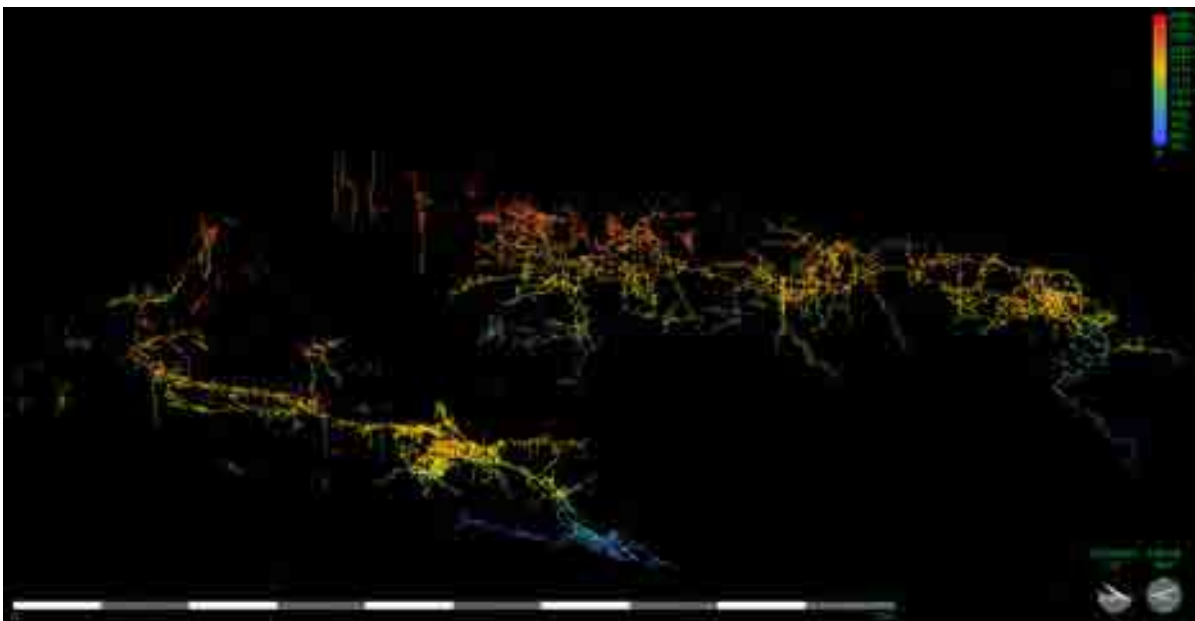
As mentioned previously, next to other, smaller ones, there are two massive cave systems in the *Totes Gebirge* plateau, called the *Schwarzmooskogel* (SMK) and the *Schönberg* caves, respectively. In the system of the *Österreichisches Höhlenverzeichnis* (Austrian cave index), they are given the localising numbers 1623 and 1626, respectively. They have been surveyed extensively, but not exhaustively yet, over the last decades by a variety of caving groups. Using the three-dimensional visualisation programme for cave surveying data in Survox format, Aven, the production of Figure 2.9 was possible. With a terrain file provided by the CUCC, the SMK cave system could be shown in the context of the topography of *Totes Gebirge* (Figure 2.10). The locations of all the cave systems in the *Totes Gebirge* can be seen on pages 602 to 604 of E. Geyer et al. (2016). To pre-empt a detail of the methodology section, the cave survey logs unfortunately could not be used directly in VisualKARSYS, although the platform does support tunnel gallery data. Each single leg of the entire cave system would have had to have been input by itself, manually, as no import capability ~~for this use case~~ has been implemented. Additionally, even if this had been done, the only data that could have been entered for each cave was that the walls were made of limestone or loferite, both of which would have been subsumed in the karstified unit in the end, rendering the whole exercise pointless.

To get more of a feeling for the area and the cave systems, the author visited the August 2023 expedition of the Cambridge University Caving Club (CUCC) and informally interviewed the caver Robert Watson, who was kind enough to discuss the past, present and future cave surveying conducted by the CUCC and the other caving clubs in the 1623 and 1626 caves. From him, experiential information concerning, for example, depth of the phreatic zone, drainage directions, siphons and perched sumps could be gleaned, along with practical help in interfacing Survox with QGIS.

As listed by E. Geyer et al. (2016), the other, albeit smaller, cave systems in the area of interest of this thesis are the *Woising*, *Hüttstatt* and *Almberg* cave systems, from NE to SW (see E. Geyer et al. (2016, pp. 602 to 604). These are each smaller than the previously described cave systems, but can still boast one of the largest cave rooms in the *Totes Gebirge* with *Hallwalla* which covers about 6000 m² and which is located in the Hüttstatt area. This is also the area in which the caves Harlacher (2003) visited for sampling are situated (Altherrenhöhle, Dellerklapfhöhle). Unfortunately, although the process to gain access to the cave survey data platform was already underway, it was not possible to be completed before this thesis was handed in. Therefore, no actual speleological data from these smaller systems could be used for validation of the VisualKARSYS model, only the characteristics reported in



(a) Schönberg (western) and SMK (eastern) cave systems in plan view.



(b) Schönberg (lower left) and SMK (upper right) cave systems, facing east with an elevation angle of -14° .

Figure 2.9: Visualisation of *Schwarzmooskogel* (1623) and *Schönberg* (1626) cave system surveys in Aven, facing east and with a viewing angle of -14° . Survey legs coloured by increasing depth in red-blue gradient.

the literature.

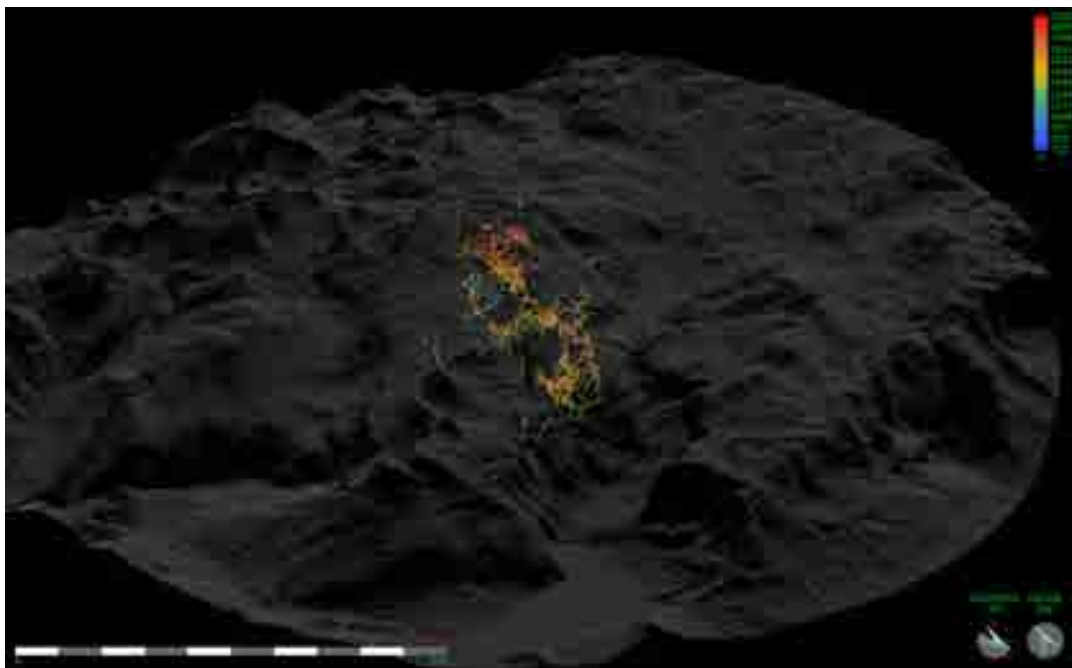


Figure 2.10: Visualisation of the *Schwarzmooskogel* (1623) cave system in Aven, facing 31° and with a viewing angle of -29° . Survey legs coloured by increasing depth in red-blue gradient, with topography of the *Totes Gebirge* included, Lake Altaussee visible as a flat surface at the bottom edge.

2.2 Methodology

As outlined in the introduction (Chapter 1), this master thesis' aims were approached in two steps. At first, an estimation of the catchment area of Lake Altaussee was made by modelling the water balance of the region. Because the resulting estimate was supposed to be rough and the time spent on it be kept in a tight scope, a discontinuous, e.g. event-based, lumped model was chosen at first (pers. comm. Häuselmann and ~~Jeannin, 2023a~~). However, once that approach failed due to the coarse data available, another was developed, based on yearly precipitation (P), evapotranspiration (ET) and discharge (Q) sums (pers. comm. Häuselmann and ~~Jeannin, 2023b~~). In the next section, the water balance modelling will be described in further detail.

The next step was to gather all available geological data and knowledge of the area (see above) and build a three-dimensional (3D) geological model of a part of the western *Totes Gebirge* plateau, using the VisualKARSYS platform developed in Switzerland by the *Swiss Institute of Speleology and Karst Research* (SISKA). See Section 2.2.2 for more detail.

2.2.1 Water balance modelling

The water balance model for estimation of the catchment basin of Lake Altaussee was ~~only ever~~ meant to give a rough idea of its dimension. That is why, as introduced in Section 1.2.3, the approach was a very broad, continuous one, so as to stay in this thesis' scope and devote more time to the main, hydrogeological part. It follows a very straightforward path, described below.

At first, the daily P sums from the three meteorological stations mentioned above (*Göbl*, *Pötschen* and *Krippenstein*) were obtained for each year (Equation (2.1)). Then, the elevation-dependent wind-error correction factors given in Bullmann (2018) were applied. It must be mentioned that these factors are given directly for the stations *Pötschen* and *Krippenstein*, but for *Göbl*, which was not included in that study, the factor for Abtenau (714 m a.s.l.) was used as the elevation of their stations only differ by 4 m. The factors were also only calculated based on elevation of the station and without actual wind direction or speed data, as these were not available (see Bullmann (2018, p. 47)). Table 2.5 shows the factors applied to each station, as well as the raw and corrected average yearly P.

Then, based on the decades of karst study experience of the SISKA Häuselmann and Jeannin (pers.comm. 2023b), a flat value of 500 mm of ET and other losses were subtracted per year from each P sum. This may seem too simple at first sight; however, it is a fast and easy empirical simplification where more detailed analysis and modelling based on, for

Table 2.5: Raw and corrected average annual P for each station, together with elevation-dependent wind correction factor from Bullmann (2018).

Station	Elevation (m a.s.l.)	Raw P (mm)	Corrected P (mm)	Wind correction factor
Göbl (from Abtenau)	710	1582	1914	1.21
Pötschen	1000	1639	2131	1.3
Krippenstein	2050	2019	3392	1.68

instance, soil cover, vegetation, radiation, wind, snow sublimation and melting or other factors would add a great bulk of work for relatively little gains in precision, and would go beyond the purpose of the water balancing. The percentage that this flat value represented of each year's P sum was also calculated and is presented with the other results, and discussed in comparison to the literature.

On the discharge (Q) side of the water balance, the daily averages were summed up for each year, effectively giving the volume of water flowing out of Lake Altaussee over each year (Equation (2.2)). These Q sums were then used as the denominator for the corresponding yearly P sums for each station, resulting in an approximate catchment size for each year (Equation (2.3)). To gain a range of plausible results, these operations were done on both the raw and the corrected annual sums of P. The unit conversions that took place can be followed in the list below, with the equations being referenced in the text at the appropriate points.

1.
$$\frac{\text{mm}}{\text{d}} \Rightarrow \frac{\text{L}}{\text{m}^2 \text{ a}} = 10^{-3} \frac{\text{m}^3}{\text{m}^2 \text{ a}} \quad (2.1)$$

2.
$$\text{m}^3 \text{ s}^{-1} \Rightarrow \text{m}^3 \text{ a}^{-1} \quad (2.2)$$

3.
$$\frac{\text{m}^3 \text{ a}^{-1}}{\frac{\text{m}^3}{\text{m}^2 \text{ a}}} = \text{m}^2 = 10^{-6} \text{ km}^2 \quad (2.3)$$

Following the advice of Pierre-Yves Jeannin again, an alternative approach was also applied: in his experience, a karstic catchment's minimum specific discharge (discharge relative to the catchment size) never falls below $3 \text{ L s}^{-1} \text{ km}^{-2}$, irrespective of the size of the catchment. So,

he and Philipp Häuselmann suggested a method whereby the minimum discharge of Lake Altaussee could be divided by this value to obtain a different estimation of catchment size.

Purely visually, a flat minimum discharge value of $0.3 \text{ m}^3 \text{ s}^{-1}$, or 300 L s^{-1} , was chosen (see Figure 2.11). This represents the 1st percentile of all discharge values which seems like a good fit. As Philipp Häuselmann observed, the time series line sometimes suddenly dips from around 400 L s^{-1} down to 100 L s^{-1} , a phenomenon that he attributed to lake freezing, impacting outflow and instrument accuracy, and a minimum value that thus cannot be seen as representative for the whole. In the figure, the zoomed in discharge time series section shows one of these instances of the discharge very quickly dipping to 143 L s^{-1} on the 31st of December 1984 before quickly recovering above minimum flow. Seeing as in that same January, most of the lakes at which bird populations were counted in Upper Austria were frozen (Winding, 1985) and the Upper Austrian cold record was established at -33.2°C in Aspach (Salmen, 2012), it does not seem far-fetched that the lake outlet would be frozen.

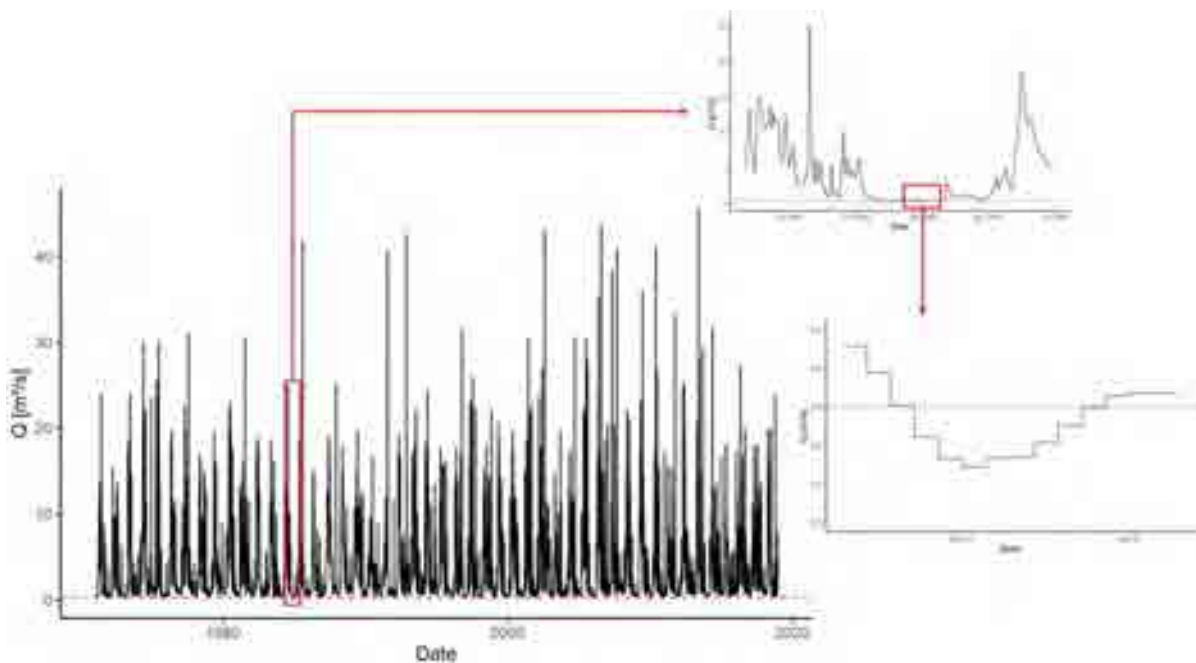


Figure 2.11: Discharge graph from Lake Altaussee over entire time series with flat minimum flow line (dashed red) from visual estimation at $0.3 \text{ m}^3 \text{ s}^{-1}$. Included as callout is the discharge time series from 01/05/1984 to 01/07/1985 showing a very fast dip to even lower flow, due to freezing of the lake and consequent mismeasurement.

2.2.2 Hydrogeological modelling with VisualKARSYS

To answer the second research question (see Section 1.3), a three-dimensional geological and hydrogeological model was built in VisualKARSYS (SISKA, 2023). The workflow necessary for a successful model can be seen in Figure 2.12 and is comprised of the following steps:

1. A hydrostratigraphic model, based on available geological data of the area and existing geological sections, is input into the system. This hydrostratigraphy's hierarchy is as follows: A series comprises all geological formations that were deposited in conformable beds. A unit, then, is made up of neighbouring formations grouped by their permeability: Either into karstified, porous-permeable, non-permeable or undefined. If a unit is declared as karstified, an equivalent porous media (EPM) porosity value must be given, between 0 and 1. For porous-permeable unit, a hydraulic conductivity value is necessary, from 1 ms^{-1} to $1 \times 10^{-10} \text{ ms}^{-1}$. Hydrostratigraphic units defined in this way do not have to strictly follow the geological formations observed in the field or given in geological maps or sections, they only serve the purpose of practical delineation of karstified strata. These units come to the fore during the data input phase, see below.
2. Contacts between units, dip angles of the units and faults are “drawn” onto the geological sections and maps, boreholes and galleries. A lot of care must be given in this step to patiently input little by little, iteratively, so that the geometric mesh generation does not go haywire, as the meshes cannot be directly manipulated on VisualKARSYS itself.
3. The platform generates three-dimensional meshes of the hydrostratigraphic units. Depending on the currently necessary model fidelity, three different quality settings are available, where a higher mesh quality needs more time to process. This step needs to be repeated every so often in the course of data input, in the coarse quality, to be certain that no large mistakes are being generated by the user's choice of input data. Once the user is satisfied with the geological quality of the 3D model, the next step can be attempted.
4. So-called points of interest can be entered into the model. Cave entrances, cracks, dolines, trenches, sinks and aboveground waterbodies are the options, beside the most important, springs. Each spring's entry must contain the following information: Is it at ground surface, within a gallery or undefined, what are its XYZ coordinates (elevation, so Z, can also be derived from the DEM in the system), what is its hydrologic regime (permanent, temporary, dried-up or undefined), its discharge rate in ranges of Ls^{-1} :
 - $<1 \text{ Ls}^{-1}$,

- 1 Ls^{-1} to 10 Ls^{-1} ,
- 10 Ls^{-1} to 100 Ls^{-1} ,
- 100 Ls^{-1} to 1000 Ls^{-1} ,
- 1000 Ls^{-1} to 10000 Ls^{-1} ,
- $>10000 \text{ Ls}^{-1}$,

and its status regarding human use of its water (tapped, not tapped, abandoned, undefined).

5. Each spring is assigned to a potential groundwater body, one of which is assumed to be present in each hydrostratigraphic unit with either karstic or porous permeability values assigned. Once the button “Compute groundwater bodies” is pressed and the aquifers to be processed are chosen, all aquifer volume under the respective system’s spring is assumed to be phreatic (=saturated) and shown as light blue (see step 3 in Figure 2.12).
6. Based on the topography of the meshes of impermeable and permeable/karstified units (aquicludes/relative aquitards and aquifers, respectively), karst groundwater flow paths in the vadose and phreatic zone are drawn and phreatic groundwater volumes can be calculated. This is done for low, medium and high flow regimes to discover overflow conduit relationships between different catchments and springs. To account for these connections, karst spring catchment borders are drawn for each regime.
7. Depending on the current quality of the model, there are two options:
 - Another iteration of the modelling process can be started, beginning once again at the hydrostratigraphic model step and aiming for results more consistent within themselves and with available literature on the hydrogeology or hydrology of the area in question.
 - The iteration cycle is interrupted once the model quality necessary for the output or possible with the input is reached. Maps, sections and 3D-visualisations can be generated that show the modelling results in the respective application, which can be one or various of the following: karst catchment delineation, flood hazards, waste deposit site search, hydroelectricity, etc.

The basic setup information for this model was a height range of -1000 m to 3000 m a.s.l. , and the spatial scope was chosen to be of a reasonably manageable size, east of the western



Figure 2.12: Schematic diagramme of the VisualKARSYS workflow (from end-user course held by Arnaud Malard of SISKa (Malard and Jeannin, 2022)).

and south of the northern border of *Totes Gebirge*, including the Jurassic limestone plateau behind Trisselwand, and include Lake Altaussee itself. This resulted in the smaller rectangle visible in Figure 2.7, with longitudinal and latitudinal extents of 13000 km and 10000 km, respectively. The project coordinate reference system (CRS) used was “WGS 84 / UTM zone 33N”, with the EPSG code 36233. This CRS was also used in ArcGIS and QGIS for the preparation of maps, section traces etc. to make ex- and import as seamless as possible.

For the present application of VisualKARSYS, some assumptions and simplifications were necessary. First, as can be seen in Figure 2.13, the main spring funnels are on the bottom of Lake Altaussee (also visible in Figure 1.2). If input into VisualKARSYS directly, they would only reflect real world conditions in VisualKARSYS if the platform was able to work with lake bathymetry and had the possibility to input a standing water level higher than a karst spring. However, because this is not an option, the individual springs were combined into one “synthetic” spring. Given its perennial nature and the total discharge being $3.5 \text{ m}^3 \text{ s}^{-1}$ on average, in VisualKARSYS it was assigned the regime “permanent” and the discharge rate class 1000 L s^{-1} to 10000 L s^{-1} . The synthetic spring location was fixed at mean lake surface elevation, along the lake shore, at the place with the smallest normal distance to the weighted geometric centre of the karst funnels found by Wagner (2021) (see Figure 2.13).

The weights of each funnel were assigned by the author based on relative size and depth in order to reflect the probable discharge volumes. At first, the idea was to take into account three different lake water levels, minimum, mean and maximum, which depend on water regime (low, medium and high outflow). This was attempted by generating three points on a line from the aforementioned weighted geometric centre to the shore, one for each water table height (see Table 2.6). However, because the DEM in VisualKARSYS has a resolution of 10 m, this approach was abandoned, instead placing the synthetic spring on the water surface, so that the lake elevation of 711 m a.s.l. would at least reflect the usual water table.

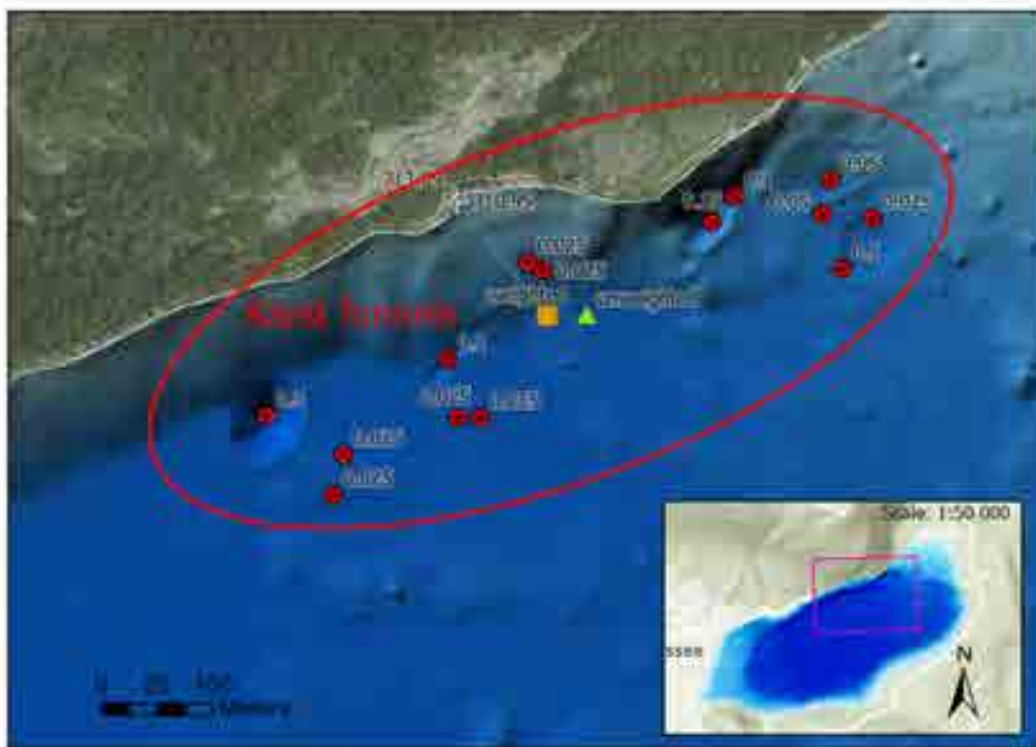


Figure 2.13: Visualisation of the bathymetry of Lake Altaussee assembled by Wagner (2021). Two geographic mean points are also marked: The unweighted mean (green triangle) and the weighted mean (orange square). The funnel weights were assigned by the author based on funnel depths and surface areas, and the comments made by Wagner (2021, pp.67–68). Marked as crosses are the intersections of a line from the weighted geometric centre with the lake shore at different lake water table elevations. Orthophoto of lake shore's source: GIS-Steiermark (2023).

Table 2.6: Elevations above sea level of the minimum, mean and maximum height of the Lake Altaussee water table. Data from 1976 to 2018, from www.ehyd.gv.at.

Water table height	Elevation (m a.s.l.)
Maximum	713.52
Mean	711.62
Minimum	710.84

2.2.2.1 Hydrostratigraphic model

Using the geological literature available for the Alps, the NCA, and the region in question (especially Mandl et al. (2012)), as well as the basic concept of karstification - “the purer the limestone, the more likely to be karstified” (Ford and Williams, 2007), a hydrostratigraphic model for use in VisualKARSYS was developed. As mentioned above, two map sheets of the 1:50 000 scale Austrian geological maps cover the area, 96 and 97. For convenience, better visualisation and processing efficiency, they were clipped to the rectangular scope in which the geological sections constructed by the author are contained (larger rectangle in Figure 2.16). The relevant stratigraphic formations present inside this scope are shown in Figure 2.14, divided up by the respective map sheet.

In the spirit of how to use VisualKARSYS as set forth by Jeannin et al. (2013), namely starting slow and iterating a lot, the hydrostratigraphic model also changed over time. At first, the model illustrated in Figure 2.15 was created, strictly defining as aquicludes all formations that weren’t more or less pure limestone, e.g. the Oberalm Fm. and any dolomitic strata. Then, with further study of the available literature, a radically different model was tested too: seeing as “actual” definite aquicludes like the Permo-Triassic Haselgebirge or Werfen shales seemed to be only depths greater than the base elevation of the model (Fernández et al., 2024), another solution for a bottom aquifer boundary had to be found for a model in VisualKARSYS to even give any results at all.

A relatively straight-forward answer seemed to present itself: given that even at surface level, dolostones do not tend to karstify as easily or well as limestones, and even pure limestone karst aquifers, at great depth, transition into a zone of decreasing phreatic karstification (Stevanovic, 2015), dolomite layers may present such a low degree of karstic dissolution as to act as an aquitard, if not an aquiclude. Occuring at useful depths in the area of interest are two dolomite formations: for one, the Wetterstein dolomite that crops out all along the northern border of *Totes Gebirge* and dips south-west. The other is its covering formation, Hauptdolomit, which in turn is covered directly by Dachstein limestone (although in places, a

transition and lateral intercalation with dolomitised Dachstein limestone, loferite, has been reported (G. Geyer, 1915; Mandl et al., 2012)).

The sandstone and marl Raibl Grp. that quite reliably crops out directly above the Wetterstein dolomite in the northern faces of *Totes Gebirge* would make immediate sense as an aquiclude. Unfortunately, however, it does not crop out in the south of the plateau at all, allowing only the assumption that its sedimentary region was not continuous toward the south, or that the less competent, more plastically deformable layers were squeezed out toward the north by the dolomite and limestone load above (Grottenthaler, 1978).

Concerning the Triassic-Jurassic contact between Dachstein Lst. and either colourful Jurassic limestones or directly Oberalm Fm. with the purer Plassen Lst. above that, the following reasoning was formed during modelling. Based on literature reporting that faulting and corresponding cave systems traverse the Tressenstein Lst. - Oberalm Fm. - Dachstein Lst. boundaries along vertical solution-enlarged fracture planes in the area of Albert-Appel-Haus (E. Geyer et al., 2016; Harlacher, 2003) and the Plassen Lst. plateau (Schneider, 2013), and the assumption that the Plassen Lst. plateau drains at least partially into Lake Altaussee, the hydrostratigraphic borders between these units were removed. Kuffner (1998, p. 15) confirms that both Oberalm Fm. and Tressenstein Lst. is well karstifiable. Consequently, only one karstified unit remained that included everything from Plassen Lst. down to either Hauptdolomit or Wetterstein dolomite, depending on the hydrostratigraphic model.

As with the Raibl Grp. above so there are at this level a few relatively thin formations that were previously agglomerated as “colourful Jurassic limestones”. They form the border between the Oberalm Fm. and Dachstein Lst. at the former's northeastern boundary, presenting in an intriguing stair-like shape resulting from tectonic activity and already awakening interest in the early days of *Totes Gebirge* geological research (G. Geyer, 1915). As such, these strata contain a lot more siliciclastic material than their neighbours and would also work well as an aquiclude. However, again, they do not crop out at all in the southwest of the Jurassic plateau, around Trisselwand and Tressenstein. Lacking any data, this makes it impossible to know until where they remain a continuous aquiclude. This is why, for the sake of a simple but understandable model, these strata are ignored entirely. In the VisualKARSYS hydrostratigraphy, they are assigned a porosity of 2 % as a whole, as Jeannin et al. (2013) did for Swiss Jurassic karst systems.

Another aspect of the modelling hydrostratigraphy is that no quaternary cover is included, although in reality it is present, especially in the valley troughs as glacial and erosional sediments. This was decided on for modelling reasons; on the one hand, VisualKARSYS expects normally deposited units and does not know to constrain the quaternary to the valleys.

On the other hand, the exclusion of young sedimentary cover of minor spatial importance does not impact the results of a model focusing on relatively much more thick and well-karstified older rock masses. In the original example of VisualKARSYS application, Jeannin et al. (2013), this simplification is also allowed.

Toward the Hallstatt zone of Bad Aussee and Altaussee in the west and southwest, and the *Höllengebirge* in the northwest and north, the base of the *Totes Gebirge* overthrust crops out and was mapped as a Jurassic gravitational sliding nappe by Schäffer (1982). Following Bögli (1980, p. 201), this feature is assumed to include mylonitised and thus impermeable rock along its planar extension for the sake of a modelable aquiclude between these areas. If this truly is the case could be verifiable with a borehole campaign or a trained eye inspecting suitable outcrops. Should this assumption prove faulty, however, there still remains the Brunnkogel-Ahornkogel synclinal system beyond it whose south-eastern fold flank could provide an aquiclude or, at the least, an aquitard too.



Figure 2.14: Relevant stratigraphic formations present per map sheet of geological map of Austria inside scope for section drawing.

2.2.2.2 Construction of own geological sections

Because the amount and density of existing geological cross-sections was not sufficient for robust model construction in VisualKARSYS, the author was forced to draw sections himself. As no field surveying campaign was possible or would have been useful, given the author's inexperience in field geology, the section construction was based solely on the information available in the geological map sheets mentioned above, the commentary report (Mandl et al., 2012) on map sheet 96, the fault-tectonic map and sections by Rudolf Schwingenschlögl (1980, 1986) and the sections drawn by Ganss (1937) and Mandl (2013). This, coupled

with the author's inexperience in cross-section construction, resulted in, at best, imprecise characterisations of the geological subsurface of the area. Thankfully, the author could attend a course on engineering geology with a focus on the construction of geological sections held by Rudolf Schwingenschlögl and Reinhard Gerstner, of the Institute of Applied Geology at BOKU, which was very helpful.

At first, the section traces had to be situated. As can be seen in Figure 2.16, they form a rectangular pattern to regularly cover the entire area of the smaller black rectangle, the spatial scope of the VisualKARSYS project. Their nomenclature follows a simple system: The NW-SE-striking sections are named alphabetically from west to east (A, B, C and D), while the NE-SW-striking sections are given numbers increasing from west to east (1 to 3). This system can be seen in Figure 2.17. Based on communication with Philipp Häuselmann, a larger scope was then drawn that covered more area to the north, including the northern face of the *Totes Gebirge* plateau. This had the effect of including the outcrops of a few important formations (i.e. Hauptdolomit, Raibl Grp, Wetterstein dolomite) and thus gave more insight into the structure of the plateau.

The topographic profiles of the sections were generated using the qProf plugin (Alberti and Zanieri, 2023) in QGIS. They were then exported as Scalable Vector Graphics (SVGs) and edited and scaled correctly (1:50.000) in Inkscape (Inkscape Developer Community, 2024) to allow for easier drawing. The topographical sections were printed physically, along with the clipped extents of map sheets 96 and 97 and the fault tectonic map by Schwingenschlögl (1986). The next step was the selection of surface data to include in the sections. Inside a 500 m buffer to each side of a section's trace, all structural data, i.e. strata dip direction and dip, intersecting fractures, fold axes, etc., was numbered. For those data points to which it applied, an outcrop line was constructed manually, using contour lines generated from a smoothed version of the DEM (5x5 pixels, nearest neighbour method) in 25 m intervals. However, because of the large scale of the map (1:50000), 100 m intervals were applied for outcrop line construction. At the intersections of either the data points or their outcrop lines with the section trace, they were drawn onto the topographic profile of the section. For the data with dip directions and dip values, the apparent dip was calculated from dip direction, true dip angle and section strike using the following formula:

$$\gamma = 360 + \sigma - \delta \quad (2.4)$$

$$\beta = \arctan(\tan(\alpha) * \cos(\gamma)) \quad (2.5)$$

where γ is the angle between a section trace's strike (σ) and the dip direction of a bed

(δ), β is the apparent dip and α is the true dip of a plane. In Appendix A (Page 144), the Table A.1 is shown which is a precise list of the data points applied to each section. Also in Appendix A, the locations and numbers of these points can be seen in Figures A.1 to A.7. Seeing as the dip values on the geological map sheets are only given in ranges, these range borders were also converted to apparent dip for the table.

In drawing and subsequent digitalisation of the sections, care was taken to give precedence in thickness, folding and other aspects to those geological sections from the literature (Ganss, 1937; Mandl, 2013; Schwingenschlögl, 1980, 1986), as they were drawn by trained professionals based on data gathered in the field. An exception to that was made when units that were drawn outcropping on a certain part of a section obviously contradicted the geological maps by Moser (2019) and Schäffer (1982). As an example, geological section 1 from Schwingenschlögl (1980) has Wetterstein limestone and, underneath, dolomite, breaching the surface from the Offensee valley floor until an elevation of approx. 1350 masl, when, on the geological map, the section's trace crosses Hauptdolomit from 850 masl until the crest of the plateau's northern edge.

Given that, the author also let the sections drawn for this thesis influence one another, for example, including the Hauptdolomit formation, self-evident in outcrops along the traces of sections 1, 2 and D, into sections 3, A, B and C that do not cross that formation.

Although the boreholes listed above were not used in VisualKARSYS, they did give evidence for the occurrence of limestone underneath the quaternary cover around Altaussee: in boreholes 168946, 163437, 163438, 163439, 163289 and 163290, limestone was breached at depths of between 35 m to 60 m under the surface, continuing down until the end of the drilling profile.

In constructing the sections across the Jurassic plateau, the underlying Triassic Dachstein limestone and Hauptdolomit were drawn in based on a few points of data: First, dextral and vertical relative movement seems to have occurred along the Altaussee-Wildensee-line (G. Geyer, 1916; Schwingenschlögl, 1986), and outcrops of Dachstein limestone appear at the northeastern shore of Grundlsee. Furthermore, there are areas of direct contact of Jurassic colourful limestones under Oberalm Fm. limestone with Dachstein limestone in northeast of the Jurassic plateau. Harlacher (2003) confirms that Dachstein Lst. indeed lies underneath Jurassic carbonates on the south side of *Totes Gebirge*. The continuation of Dachstein Lst. and Hauptdolomit, although discontinuous across the Altaussee-Wildensee line, under the Jurassic strata, can also be seen in the respective parts of the sections from G. Geyer (1915), Mandl (2013), and Schwingenschlögl (1980, 1986).

After having drawn the sections by hand, they were scanned and digitised in Inkscape again. The style of drawing was heavily influenced by Mandl (2013). The so produced sections were

then also input into VisualKARSYS.



(a) First, very detailed hydrostratigraphic model.



(b) Second, conceptual, applied hydrostratigraphic model.

Figure 2.15: Iteration on applied hydrostratigraphy for VisualKARSYS model, each as exported directly from the platform.



Figure 2.16: Traces of existing and newly constructed geological sections used for VisualKARSYS model creation. Labels starting with “80” from Schwingenschlögl (1980), the one starting with “86” from Schwingenschlögl (1986); Roman numerals for sections drawn by Ganss (1937), purple traces with arabic labeling from Mandl (2013) and red trace is labeled as being from G. Geyer (1915). The spatial extent of VisualKARSYS model as the smaller rectangle, the larger one being the scope for sections constructed by the author, their traces as orange lines. Background map: OSM



Figure 2.17: Traces of constructed geological sections with their assigned numbering following the system explained above. A black rectangle shows the spatial extent for sections constructed by the author, their traces as red lines with names in red. Background map: <https://basemap.at>

2.2.2.3 Data input and model calculation

Data input into VisualKARSYS is quite intuitive. Each visual source of geological data (cross-sections, boreholes, tunnel galleries, maps) can be selected to be shown by itself on the screen. The geological unit or fault that the user wishes to enter data for can then also be selected by drop-down menu, and contact data or dip data can be entered. For the former, it is important to ascertain the settings beforehand, as both the option exists to enter top contact data or bottom. However, once an option is selected, it cannot be changed without deleting all previously input data points. As the project was concerned with contacts relatively deep in the subsurface, the bottom option was chosen. Contact points between formations are given by clicking once on the appropriate line of the e.g. section and, following the line of choice, clicking again shortly afterwards, forming relatively short contact point lines. As explained by Arnauld Malard during the course (Malard and Jeannin, 2022), long contact lines limit the flexibility of the implicit interpolation, more easily resulting in strange forms being computed.

Dip data can also be entered very easily: in vertically-oriented 2D data sources, like sections or galleries, the strike of each data source is used to automatically calculate the dip direction, leaving only the dip to be entered. On maps and in boreholes, of course, both elements need to be typed in manually.

Should faults be important for the model, they need to first be created in the platform. They can be defined as either infinite faults, in which case no further information is necessary. Otherwise, the option for finite faults also exists, for which lateral and vertical extent, as well as radius of influence are necessary. In the latter case, the first contact point that is entered is used as the bathycentre, with half the lateral extent reaching in each direction from there. Once a minimum of data for each unit in the hydrostratigraphy and each fault has been given to the system, the geometric intersections can be calculated for visualisation on the sections and maps, and the 3D meshes are computable in three different resolutions, where the higher the desired resolution is, the longer it will take to compute. For this reason, the coarsest setting is usually chosen in the modelling process as it only takes a few seconds and already gives a good understanding of how the meshes are being shaped by the data input. For groundwater body computation and the generation of the finished model product, higher resolutions are possible.

Also in this project, the data input in the geological part was approached iteratively, with re-computing of the intersections and 3D meshes being done quite often to check up on the interactions of unit contact and dip data on sections and maps. During this stage, the model was also manipulated as to reflect the overthrust plane aquiclude characteristic by giving

the nominatively Hauptdolomit aquiclude unit contact data in the southwest of the model, although it is not seen or assumed to occur there, that was just the most straightforward way of simulating the hydrogeological conditions assumed to prevail there.

The comparison of the sections by Ganss (1937) with the other data revealed a large difference in interpretation. As the inclusion of this very divergent data would have made the model nonsensical, the decision was made to forego data input based on these sections in the interest of generating a usable model.

Concerning the data input based on the geological map, it must be reported that no dip data at all was used from it, as the aquiclude formation shows few outcrops and the experience was made that this way of supplying dip data results in very strange forms in the meshes. Rather, it was found advisable to focus on the profile cross-sections for dip data entry. In total, 64 unit contact interfaces and 19 orientations were input, as well as one fault, the Altaussee-Wildensee-lineament. To fill up volume inside the model domain that was not taken up by declared geological units, a dummy mesh was inserted underneath the “Middle Triassic” aquiclude formation.

Once the geological model was in an acceptable state and further improvements based on the present data were not to be expected (see Figure 3.6), a 3D mesh of the highest resolution was produced with which to continue to the next step: hydrological data input and groundwater body computation. ~~As explained above, the sublacustrine springs feeding Lake Altaussee were agglomerated into one synthetic spring, located in VisualKARSYS at the lake shore but on water table elevation at the closest point to the weighted geometric centre of the individual springs (see Figure 2.13).~~ The overflow springs of Liagerhöhle and Kugelmühlhöhle were approximated in their position from E. Geyer et al. (2016, p. 602, Figure 4) and the cave entrance elevation was sampled from the DEM by VisualKARSYS. The reason the elevation of the cave entrance was selected was that in the case the caves become active as overflow springs, it is this height that water exits the subsurface from. VisualKARSYS sampled the elevation above sea level of the two cave exits to be 789 m and 805 m a.s.l. for Liagerhöhle and Kugelmühlhöhle, respectively. Compared to the elevation plan in Seebacher (2015), these values are fairly accurate.

As the karst in this region is purely autogenic in nature, no stream sinks were enterable, and none of the other options for hydrological points of interest were known for Lake Altaussee and its karst, so the groundwater body was computed. At first, only the lake spring was assigned to the groundwater body, to simulate low to normal flow conditions in which the overflow springs are not active. Then the lower Liagerhöhle was used as the spring, followed by Kugelmühlhöhle. Although it is unlikely that the former would be activated while the

latter was inactive, there is still a slight difference in groundwater level between them. Of course the overflow springs are active during very high flow conditions, meaning that the corresponding water table cannot be assumed to be flat in reality.

Catchment delineation is then performed on aquiclude topography and, should the system need it, on varying groundwater connectivities depending on flow regime. In the present case, no such dependency was modelled, meaning that only one catchment boundary was drawn. The results of the hydrogeological modelling done with VisualKARSYS can be seen in the following section.

The previously mentioned flow animation module (FAM) was made available to the author. Unfortunately, up to the point at which this thesis was handed in, it could not be brought to work, apparently failing to update the 3D model recognised by the FAM. Should research on this region continue, it might be interesting to use the FAM to investigate time series-length dependent hydrological effects, although a prior improvement of the model with new and updated data would be advisable (see discussion in Chapter 4).

3 Results

3.1 Water balance modelling

Following the methodology outlined in Section 2.2.1, the resulting data for the hydrological water balance modeling to estimate the catchment size of Lake Altaussee will be presented here. Firstly, Figure 3.1 shows the change over time of the catchment sizes based on the annual precipitation sums from each of the three weather stations chosen. The summary statistics for each of these lines can be seen in Table 3.1, which includes the entire range of catchment sizes, the 25th, 50th and 75th percentiles, as well as the means and standard deviations.

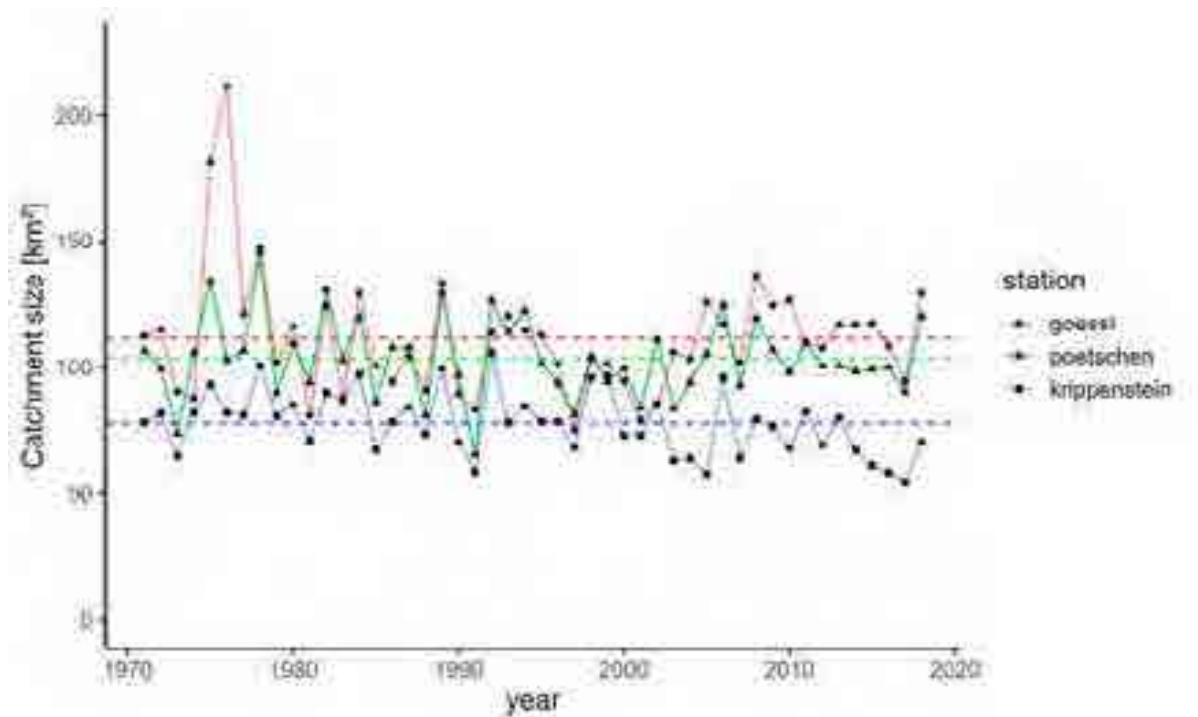


Figure 3.1: Diagram of the results of the water balance estimation. For each P station, its catchment size per year is plotted and connected by lines; using the corresponding colour, that station's mean catchment size is plotted as a horizontal line.

Table 3.1: Summary statistics of the obtained catchment sizes in km^2 for each station and year.

Station	years	Mean	Std. Dev.	Min	Pctl. 25	Pctl. 50	Pctl. 75	Max
Gößl	48	111	24	76	95	109	121	211
Pötschen	48	104	16	66	94	102	110	145
Krippenstein	48	78	12	55	68	79	85	106

Table 3.2: Summary statistics of the percentage of annual precipitation the 500 mm a^{-1} of ET made up for each station and year.

Station	years	Mean	Std. Dev.	Min	Pctl. 25	Pctl. 50	Pctl. 75	Max
Gößl	48	32	5.6	23	28	32	36	51
Pötschen	48	31	4.1	23	28	30	34	41
Krippenstein	48	25	3.8	18	23	25	28	34

All these results are derived from the uncorrected P data. Using the data corrected with the factor given in the preceding section, following Bullmann (2018), the station-year-catchment size diagram (Figure 3.2) differs quite significantly, fitting to the corresponding summary statistics (Table 3.3). The statistics on ET percentage of P have also changed, as can be seen in Table 3.4. Because of the calculation steps used, a higher precipitation value results in lower catchment sizes, which also makes sense: When more water is available per unit of area, less of that area is necessary to accumulate enough P for the same discharge. The unweighted average catchment size across all years and stations, using the mean size per station, is 66 km^2 . However, because the Krippenstein station is so far removed from the *Totes Gebirge*, a weighted average was also calculated, whereby the Gößl and Pötschen station mean values were each assigned a weight $\frac{2}{5}$, leaving $\frac{1}{5}$ for Krippenstein. This resulted in an average catchment size of 71 km^2 . The corresponding range, obtained from the same weight given to the 25th and 75th percentile values for the lower and upper bounds, respectively, came out to 62.8 km^2 to 76.6 km^2 .

To address the last part of the described water balancing methodology, the use of the experientially obtained minimal specific discharge that stays similar across mountainous karst areas: The used 300 L s^{-1} of minimal lake discharge, multiplied by the $3 \text{ L s}^{-1} \text{ km}^{-2}$, results in a drainage basin size estimation of 100 km^2 . In terms of order of magnitude, this result does fit in with the catchment sizes obtained with the other approach, although the approximate

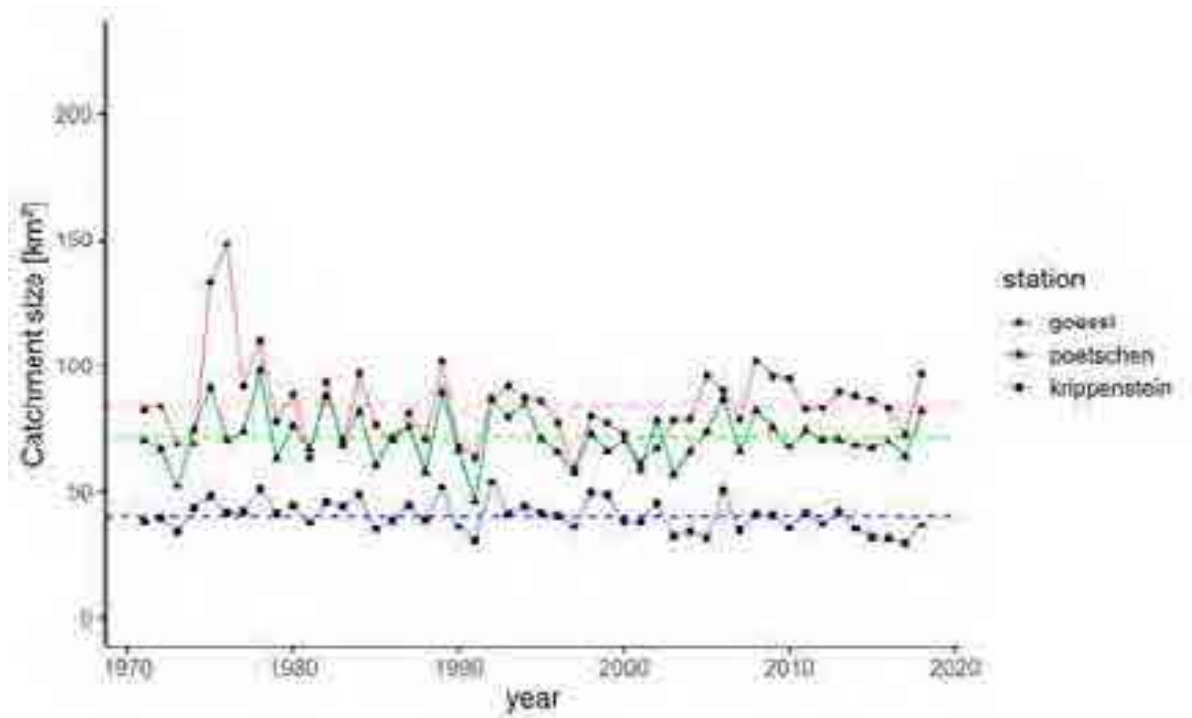


Figure 3.2: Diagram of the results of the water balance estimation, using P data corrected using factors from Bullmann (2018). For each P station, its catchment size per year is plotted and connected by lines; using the corresponding colour, that station's mean catchment size is plotted as a horizontal line.

Table 3.3: Summary statistics of the obtained catchment sizes in km^2 for each station and year, using the corrected P sums.

Station	years	Mean	Std. Dev.	Min	Pctl. 25	Pctl. 50	Pctl. 75	Max
Gößl	48	85	17	59	73	83	92	148
Pötschen	48	72	10	46	66	71	77	98
Krippenstein	48	41	6.1	30	36	41	45	54


average of results from uncorrected P data seems to be a closer fit. Inverting the approach, given the size of the catchment from the first approach as 71 km^2 with the 25th and 75th percentile range being 62.8 km^2 to 76.6 km^2 , the consequent minimal specific discharge would be $4.2 \text{ L s}^{-1} \text{ km}^{-2}$ with a range of $3.9 \text{ L s}^{-1} \text{ km}^{-2}$ to $4.8 \text{ L s}^{-1} \text{ km}^{-2}$. 


Table 3.4: Summary statistics of the percentage of corrected annual precipitation the 500 mm a^{-1} of ET made up for each station and year.

Station	years	Mean	Std. Dev.	Min	Pctl. 25	Pctl. 50	Pctl. 75	Max
Gößl	48	27	4.7	19	24	26	30	42
Pötschen	48	24	3.1	18	21	23	26	31
Krippenstein	48	15	2.3	11	14	15	17	20


3.2 Hydrogeological modelling

In this section, the results obtained from the hydrogeological modelling of the karst aquifer feeding Lake Altaussee will be presented. Before this, though, the geological sections drawn by the author and then used in VisualKARSYS will also be shown.

3.2.1 Geological sections drawn

As was explained in Section 2.2.2.2, the sections necessary for the construction of the 3D model in VisualKARSYS were drawn based on the geological maps available, as well as the geological sections from literature (Ganss, 1937; G. Geyer, 1915; Mandl, 2013; Schwingenschlögl, 1980, 1986). In order to present the cross-sections in this section of the thesis, they have been input in a smaller scale than their original scale of 1:50 000. For the original size, see them printed in Appendix B on Page 160. A scale bar was added to each page to still give an impression of the distances. The sections are not vertically exaggerated. 

3.2.2 Results from VisualKARSYS model

The output page of the VisualKARSYS project can be reached via this URL: <https://www.visualkarsys.com/vk/project/1376/output>. Here, some screenshots of the 3D model are presented (see Figure 3.6), in which the distribution and structure of the model can be seen: In general, a wide-spanning syncline was generated, with a western border roughly along the *Totes Gebirge* overthrust plane towards the Hallstatt zone of the Altaussee basin. The northwestern and northern border face the Hölleengebirge via the Grünbach and Rettenbach syncline behind the Brunnkogel-Ahornkogel anticline, and the north face of the plateau, respectively. Unfortunately, the project domain does not reach far enough north to show this boundary. To the east, no real delineation of the aquifer could be found toward the rest of the *Totes Gebirge* plateau, and considering that Dachstein limestone continues toward the southeast as a mighty topmost formation, a VisualKARSYS model is not likely to show a hard aquicludinal boundary in that direction. At most, a subsurface watershed dividing ridge might occur, but that is literally beyond the scope of this thesis. To the immediate southeast on this project, the Grundlsee fault is  can be seen as the the border from karstified to non-karstified rock. Directly to the south, however, the project domain cuts off earlier the rest of the Jurassic carbonate plateau, intersecting both the aquiclude and the aquifer. The Altaussee-Wildensee-lineament fault that was, as such, input into VisualKARSYS, somehow ceased to show during the modelling process. Potentially, the system was confused by the

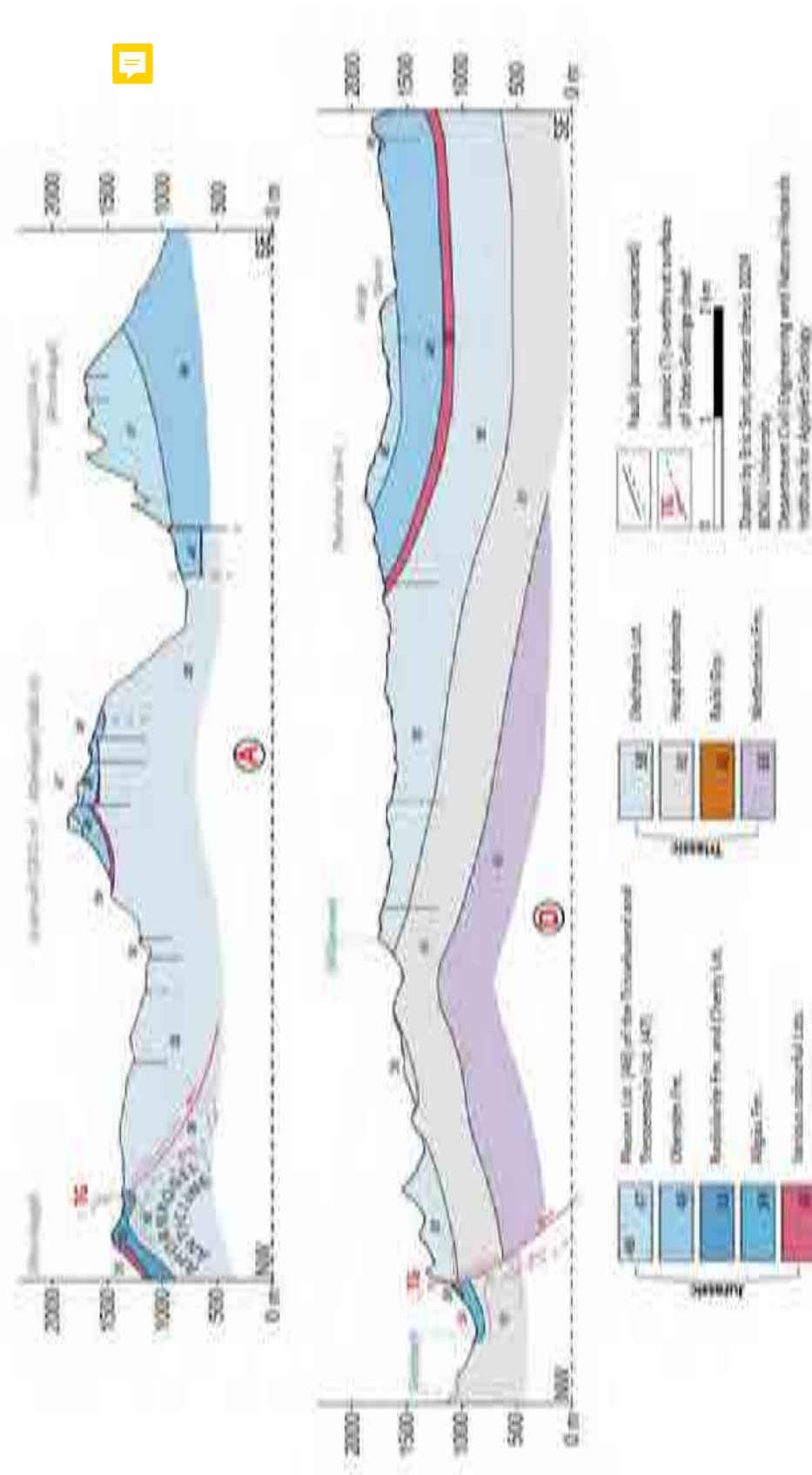


Figure 3.3: Geological sections A and D, drawn by the author. Not to original scale (1:50 000), see full-size prints in Appendix B.

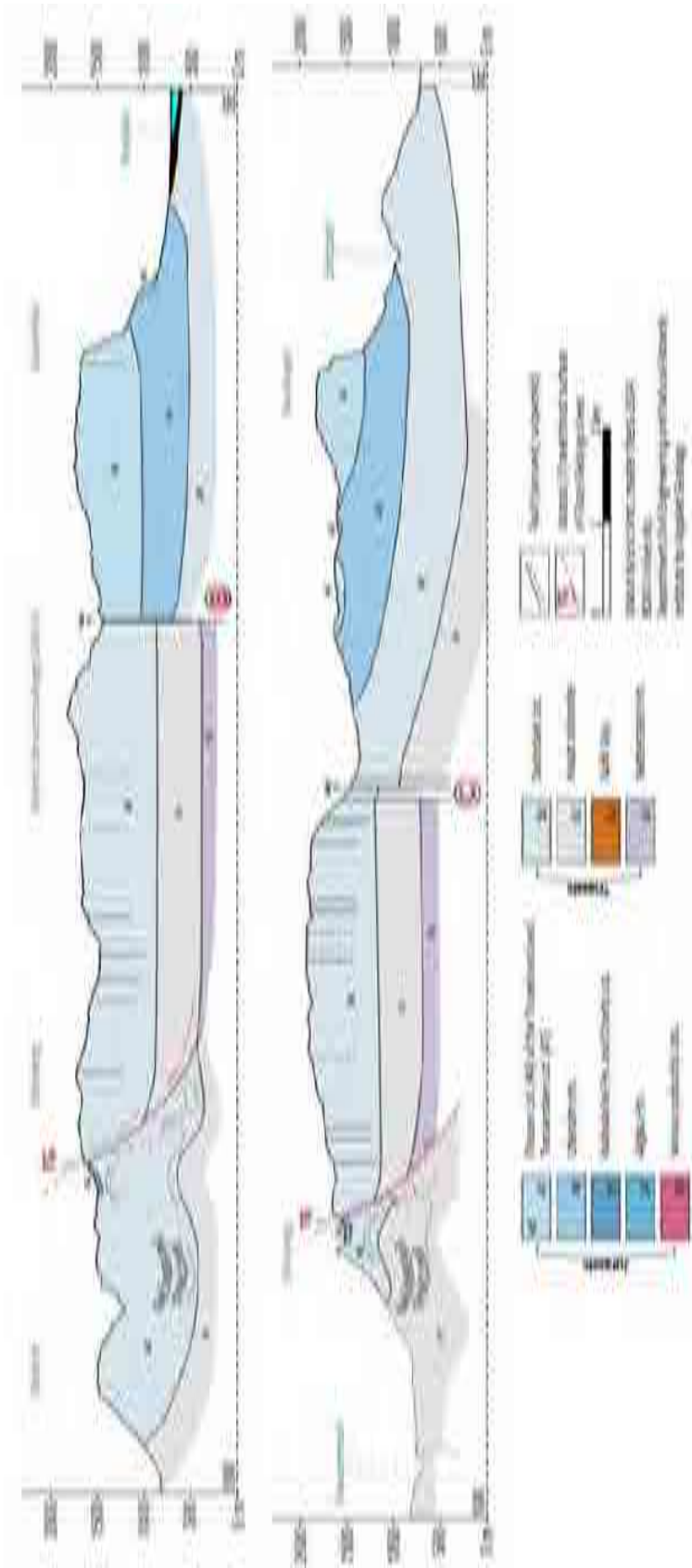


Figure 3.4: Geological sections B and C, drawn by the author. Not to original scale (1:50 000), see full-size prints in Appendix B.

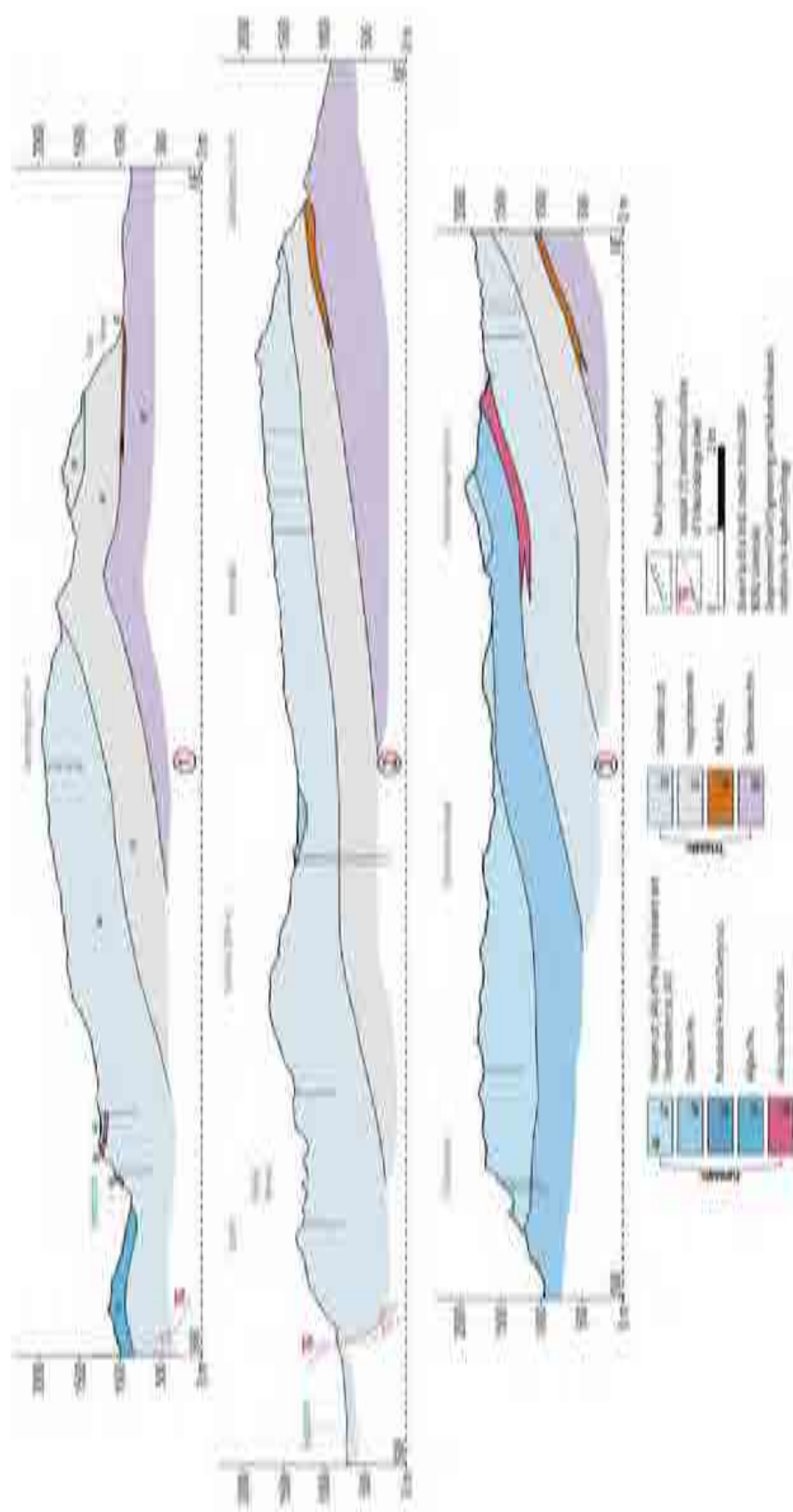



Figure 3.5: Geological sections 1, 2 and 3, drawn by the author. Not to original scale (1:50 000), see full-size prints in Appendix B.

iterative testing with its infinity parameter, the author changing its extents repeatedly.

On the VisualKARSYS output page, cross-sections of the 3D model can be generated, as well as virtual boreholes. To compare the model with the geological sections used as input, the author tried to generate slices following the traces of the input sections; unfortunately, the incredibly slow calculation times for the slices meant that it was not reasonably possible to do so for this thesis. A potential reason for this is the relatively large project volume. The reader is advised to visit the URL given above and to see for themselves. 

In Table 3.5, the volumes that are assumed to represent the phreatic zone are given, depending on which spring was selected as active. Naturally, the higher the spring elevation, the larger the flooded volume. The water storage volume is derived from the 2% porosity value taken from Jeannin et al. (2013) and would change directly depending on whichever percentage of pores is given. The volumes given are calculated assuming low-flow conditions, with a negligible water table gradient in the subsurface. Seeing as this is not the case for situations in which the overflow springs are active, the epiphreatic zone reaches from the average condition water table surface until probably significantly higher than the 805 m a.s.l. as defined by the elevation of the entrance to Kugelmühlhöhle.

Table 3.5: Volumes of VisualKARSYS-derived phreatic zone depending on the active spring.

Spring	Elevation (m a.s.l.)	Total phreatic volume (km ³)	Volume of water stored (km ³)
Lake Altaussee	711	23.0	0.460
Liagerhöhle	789	28.0	0.56
Kugelmühlhöhle	805	29.0	0.58

3.2.2.1 Hydrogeologically modelled delineation of catchment area

Based on the topography of the modelled aquiclude, a karst catchment area was delineated on the VisualKARSYS platform. In Figure 3.7, it is drawn as a dark blue polygon and encloses an area of 138.19 km². As can also be seen in the figure mentioned before, this catchment goes beyond the project boundaries (the black rectangle) and contains a number of cave systems, the approximate locations and extents of which were taken from the map in E. Geyer et al. (2016). The groundwater body included in the figure represents low- to normal flow conditions, when only the springs underneath Lake Altaussee are active. The incongruencies between the aquiclude elevation contours and the project domain boundary rectangle can only

be due to a visualisation bug, as no modelling can take place outside of the project boundary.



(a) View of the 3D model from the SW.



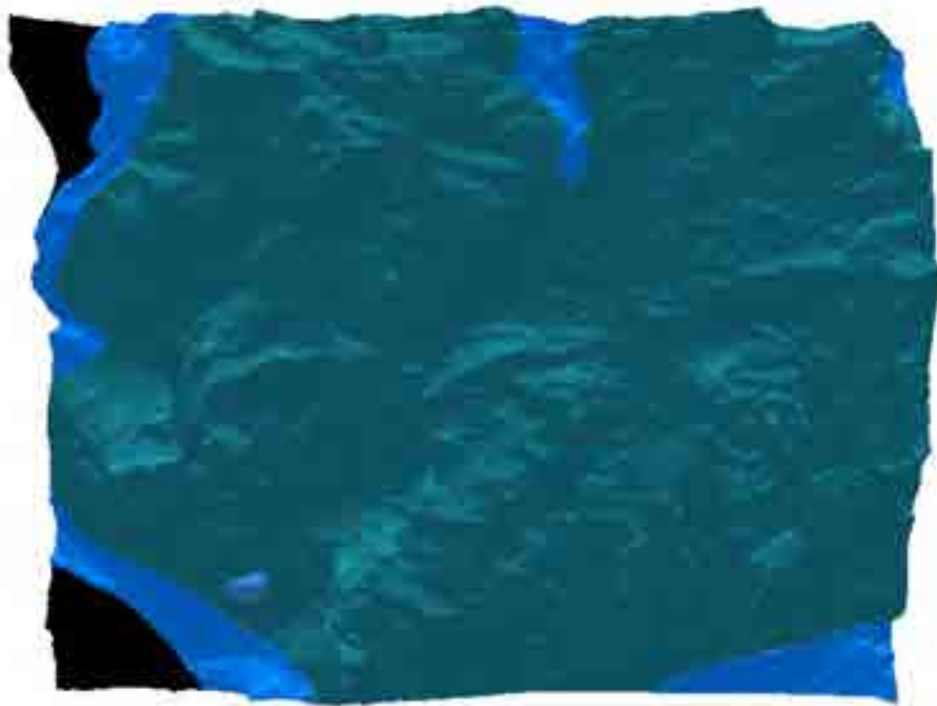
(b) View of the 3D model from the NW.



(c) View of the 3D model from the NE.



(d) View of the 3D model from the SE.



(e) View of the 3D model from above, north toward the top and Lake Altaussee spring in SW as blue sphere.

Figure 3.6: Screenshots of the 3D model in the investigated domain of *Totes Gebirge*. Topmost unit in turquoise: karst aquifer in Triassic and Jurassic carbonate; middle unit in dark blue: aquiclude unit of Middle Triassic Hauptdolomit and *Totes Gebirge* overthrust plane; black mesh at lowest position: automatically inserted dummy mesh to fill model volume.

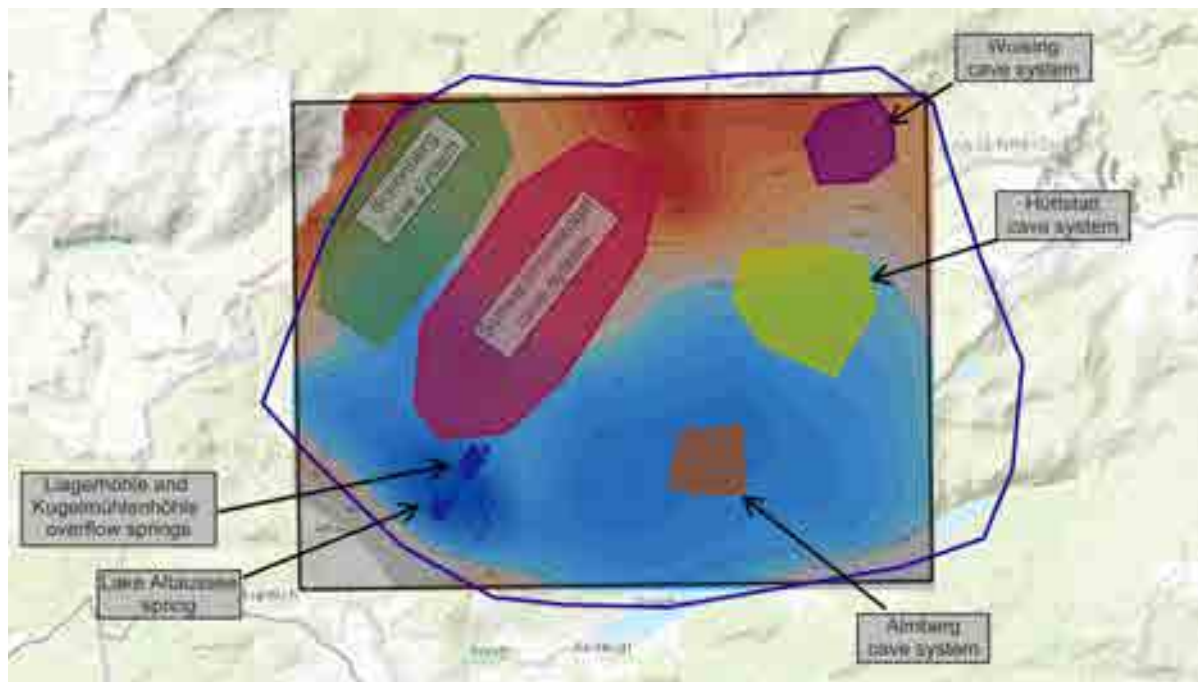


Figure 3.7: Map with results of the VisualKARSYS hydrogeological modelling: contour lines of aquiclude unit, elevations in m a.s.l., and the surface of the low- to normal flow karst groundwater body in light blue at the 700 m a.s.l. mark. The catchment delineated based on the aquiclude in a dark blue polygon stepping over the project boundary, in black. Overlaid coloured polygons of approximate cave system areas for contextualisation, and the locations of the system springs. Background topo map from ArcGIS Online REST service via VisualKARSYS.

4 Discussion

4.1 Discussion of methodology and approach

Depending on the data available and the circumstances of the area of interest, the methodological approach chosen can make a big difference in which results are to be expected. That is why the assumptions and simplifications of the employed methods will be discussed in the following sections.

4.1.1 Water balance modelling

The hydrological and meteorological data that was available for the *Totes Gebirge* plateau and surroundings was not optimal for a hydrological investigation of the Lake Altaussee karst system. As explained in detail above, fast karst conduit flow can reach hundreds of metres per hour in a well-developed karst system, which the *Totes Gebirge* has been shown to be (Harlacher, 2003). This means that temporally high-resolution input and output data is necessary for accurate event-based modelling of the karst response to hydrological events.

For the *Totes Gebirge*, all precipitation (P) and discharge (Q) data was only available on a daily timestep, as daily sums and averages, respectively. This resolution is obviously not sufficient for the present karst system, as Harlacher (2003) shows, if, admittedly, for a smaller catchment: in a matter of hours, the response to a hydrological event could begin and have passed its peak. All of this activity is subsumed in a single value in the available data, making more precise analysis difficult. Further, the spatial distribution of provenance of the precipitation data is not optimal, to say the least. Gößl, the station of lowest elevation, has been shown to be situated in a lee position with regard to the main direction of weather approach, the northwest. In the time span 1901 - 1960, it had one of lowest annual rainfall sums (Dinçer et al., 1972). As Bullmann (2018) showed, the northwestern part of the *Totes Gebirge*, including the valleys “in front” of it from a northwesterly view, receive hundreds of mm of precipitation more per year than does Gößl (see Figure 1.21). The next higher station, Pötschen, is still rather close to the *Totes Gebirge* plateau, yet it too is rained upon a lot

less than the 200 m lower, abandoned weather station of Altaussee-Lichterberg (Bullmann, 2018). This can again be explained by a slight lee position caused by the Sandling mountain to its north. Finally, although the Krippenstein station cannot be said to be sheltered from the main weather direction due to its elevation and north-facing location on the Dachstein massif, it is already at a distance of 13.7 km from Lake Altaussee. In the meteorologically complex context of alpine mountains and valleys, such a distance can already distort the patterns in and volumes of rainfall. As Figure 2.2 shows, the number of days with zero P is not constant between the stations although they are separated from one another by, at most, 20 km. Because any single available weather station has obvious issues with regard to meteorological representation of the plateau in question, the decision to involve all three and, ~~like that~~, get a range of possible values was made. Another reason was the depiction of elevation-dependent orographic precipitation enhancement which, though Mandl et al. (2012) claims it is not to be observed for the area of map sheet 96, is obviously reflected in the P data.

Evapotranspirative (ET) data was missing altogether, the nearest points being from the Upper Austrian Kalkalpen or the Dachstein massif (Schmeiß (1996) and Abel (1970), resp., cited in Harlacher (2003)), the application to the *Totes Gebirge* of which the latter author could not bring into agreement. The 500 mm of flat ET loss per year suggested as a workable hypothesis by two of the supervisors, Philipp Häuselmann and Pierre-Yves Jeannin, was easily applicable without complex estimation methods for soil, vegetation, radiation etc. Furthermore, if compared in percentage of annual P sums (see Table 3.4) to other sources, the approx. 25 % ET loss fits well to the values assumed or estimated by Harlacher (2003) and Winkler (2004) and Bonacci (2001). As Pierre-Yves Jeannin said, in his experience, wherever in the mountains karst catchments are being investigated, 500 mm is a good estimation to begin with. Be it the Hölloch at 2000 m a.s.l. or covered Jurassic karst of Milandre at 400 m a.s.l., that value, in general, does not change that much. The reason given by him for this can be found in the frequency of rainfalls, which are higher at higher elevations, vs. the expected existance of soil cover over the karst. In mountainous regions, the more frequent rainfalls will experience some immediate evaporation from the bare rock, while at lower altitudes, the less frequent events will be stored in the soil and epikarst, some of the water of course being transpired. In any case, in his experience, the ET loss never falls underneath 20 %, meaning an infiltration coefficient of less than 80 %, which fits both to the literature given above and to the values obtained from the methodology applied for this thesis. Compared to the geostatistically interpolated annual potential ET contours, calculated using the Penman approach (Dobesch, 2007) for all of Austria (Fürst, 2007), the flat ET value also seems to fit



well, balancing between the lower values on the higher parts of the plateau and the slightly higher ones in the lower plateau sections.

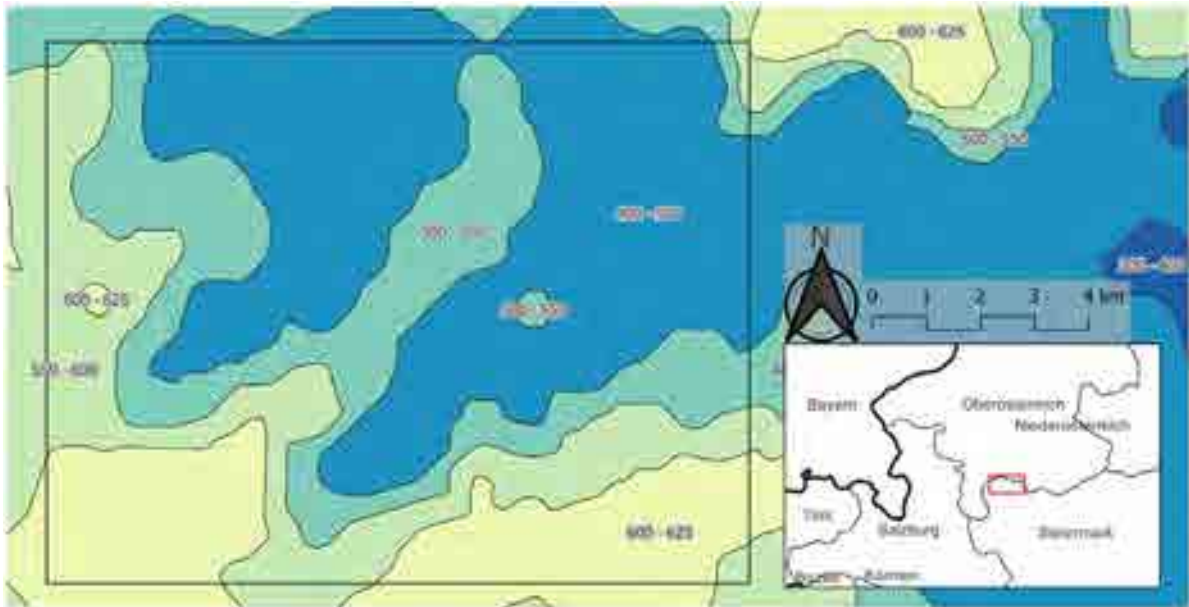


Figure 4.1: Map of the annual potential evapotranspiration contours over area of interest, from the digital Hydrological Atlas of Austria (<https://ehao.boku.ac.at/>).

Improvements in the representativeness of P data could be achieved if, for example, the weather station on the Loser chairlift summit station also collected rainfall data, or the weather station at Lake Altaussee had a longer time series than it has, having been installed in June of 2023. As the latter collects data in the sub-minute resolution range that would be the first step in greatly improving the possibilities in hydrological modelling. However, another important step would also be the increase in temporal resolution of discharge measurement from Lake Altaussee, to an hourly time step, for instance. In the larger context, it would also be of great help in hydrological modelling of the entire *Totes Gebirge* massif if long-term spring monitoring were begun for a range of the larger springs around the plateau, for example some of those identified in Maurin and Zötl (1964) (see Figure 1.22).

For these reasons, any hydrological analysis of the system was by necessity to stay limited to very global, general water balance modelling, similar to those approaches adopted for the *Totes Gebirge* by Winkler (2004) or Harlacher (2003). Benischke et al. (2018) also combined water balancing and hydrogeological modelling in their investigations of Kaisergebirge, Tyrol, Austria. However, because they also carried out extensive field mapping campaigns to gather data about the soil cover and vegetation of the catchment, as well as stable water isotope data, the application of a distributed, physical model was possible. The comparison of

surface stream flow and spring discharge with precipitation levels in the area, as well as the insights into catchment elevation gained from water isotope measurements, allowed them to delineate catchment boundaries with high accuracy. Working on the basis of geological data on stratigraphy and tectonics of the massif and the hydrogeological side with tracer test results, the behaviour of drainage of the entire system was estimated reliably. A similar approach would be applicable for *Totes Gebirge*, but would require a lot of investment in personnel and time for the extensive field work. As Benischke et al. (2018) write in their conclusions, at least a year's worth of discharge and isotope monitoring is necessary to include seasonal dynamics in the model.

Another possible option for characterisation of the karst system at hand is the use of freely available, open-source implementations of a range of statistical, signal and hydrograph analyses. Mentioned previously, KarstID for R and XLKarst for Microsoft Excel (Cinkus et al. (2023) and Bailly-Comte et al. (2023), respectively) are recently published examples that can also be used with daily timestep discharge data. While they are easy to use as such, great care must be taken in the selection of recession curves with which the analysis is performed: the automatic curve selector in XLKarst tends to include very generous recession durations, including smaller peaks that necessarily negatively impact the analysis results.

4.1.2 Geology and hydrogeology

The construction of the necessary geological sections was accompanied by a range of assumptions. First and foremost, on the scale of regional geology, the model of tectonics and paleogeographical provenance of the *Totes Gebirge* advocated for by e.g. Mandl (2000, 2013) and Mandl et al. (2012) and others was adhered to. This implicitly meant interpreting the *Totes Gebirge* massif as a Jurassic gravitativetectonism-activated (?) thrust sheet. Its overthrust plane in the southwest and the west, toward the Hallstatt zone of the Aussee basin, is further assumed to act as an aquiclude following Bögli (1980) and confirmed by Kuffner (1998). However, following Plan et al. (2023), this should not matter for the Lake Altaussee aquifer, as the Schönberg cave system (Teilgruppe 1624 of the Austrian cave cadastral system) is situated inbetween and is drained by apparently bedding-plane-controlled cave conduits mainly to the northeast (Grünbach), secondarily toward the southwest (Naglbründl to Rettenbach), depending on hydrological regime.

Second, the literature on the stratigraphy was believed without much questioning concerning estimates of the thickness of formations. These estimates were followed into the depths of *Totes Gebirge*, drawing the Hauptdolomit from its outcrops in the central northern part of the plateau and the outcrops all along the north face, as continuing all the way to the southwest

at hundreds of meters of depth. This was also done for the Wetterstein dolomite formation, which, because of its even greater depth under surface level, must be taken with an even greater grain of halite.

Thirdly, concerning the faults drawn into the geological sections: as no data regarding their relative importance, depth, dip or movement direction is given, they were included for the sake of qualitative representation. As Schwingenschlögl (1986) observed for *Totes Gebirge* and e.g. Bögli (1980) described in general, fault planes have a strong impact on conduit and cave development. The only fault for which more in-depth data could be found was for the Altaussee-Wildensee-line, mentioned already by G. Geyer (1878) and G. Geyer (1915). Schwingenschlögl (1986) interpreted it to have possibly undergone relative vertical and dextral movement based on its position and strike in relation to the postulated thrust sheet movement direction the *Totes Gebirge* took, as well as the existence of side faults intersecting at 40° to 60°.

4.1.2.1 VisualKARSYS

As explained in the introduction, VisualKARSYS was intended from conception to work as a platform in which any available hydrogeological and hydrological data on a karst system can be put together, in one three-dimensional space, to work out discrepancies in the data itself and to quickly bring all involved parties up to speed. From this shared starting-off point, further investigative methods addressing uncertainties or absences in the data and model can be chosen. With these new inputs, the model can be iterated to attain higher accuracies, or more demanding, e.g. numerical, modelling platforms can be used for more physically-based results Jeannin et al. (2013).

Therefore, the achievable accuracy in the course of this thesis project was, from the beginning, that of an exploratory first study of the Lake Altaussee catchment. Additionally, as described, the geological data available was far from optimal, especially geological map sheet 97 being an interesting fusion of archive material (Moser, 2019) made for even higher uncertainty in the author's construction of geological sections.

On the topic of karst groundwater flow, VisualKARSYS, as mentioned, only calculates flat phreatic surfaces from spring elevations and down to aquicludes level. If the area's karst drainage system is fault conduit-controlled, as implied by Schwingenschlögl (1986) for *Totes Gebirge* and confirmed for the Dachstein massif by F. Bauer and Völkl (1989), the results concerning volume of water stored in the phreatic zone are even less representative of real-world circumstances.

Turning to the present work, some words must also be dedicated to the rather daring

simplification regarding aquiclude definition in the 3D model. As has been explained, VisualKARSYS is a conceptual karst modelling platform that by design needs a geological model to be constructed first and then applies basic karst concepts to. In very tightly folded and faulted geological situations (Jeannin et al., 2013; Malard et al., 2014), the depths of the aquifers, and so too their underlying aquicludes, are small relative to their model domains. Thus, the more-or-less strictly geometric boundaries applied to karst aquifers by VisualKARSYS can more easily be ~~input~~ and manipulated. In the very thick and comparatively evenly bedded karstic rocks of *Totes Gebirge*, there is little variation to the general theme to input. Together with the scarcity of geological data, both of the surface (especially on map sheet 97, see above) and especially in the subsurface - no borehole data is available from the massif itself - not much can be formed apart from a relatively regular basinal structure. If, as in the present case, lithologically obvious aquicludes are even missing as spatially continuous features, little could be done but make bold assumptions for any model to be constructed. This must be kept in mind always when considering the results of such a model; to paraphrase a software adage: “dubious data in - dubious data out.” The VisualKARSYS model results will be discussed in detail further below, including (in)validation using the water balance, available speleological data and by comparison with neighbouring karst massifs.

4.2 Discussion of the results

In the previous section of this chapter, the circumstances and assumptions *ex ante* were discussed and put into context. Now, the focus will shift to the *ex post* interpretation and contextualisation of the modelling results.

4.2.1 Hydrological water balance

A hydrological water budget model was developed following the explanations in Section 2.2.1. Additionally, an estimation based on observed minimal specific karst system discharge was made, as suggested by Pierre-Yves Jeannin and Philipp Häuselmann. The corresponding results were presented in Section 3.1. As mentioned, between these two approaches, the order of magnitude is congruent, approximating the catchment to be around 100 km² in size following the minimum discharge approach, and around 71 km² based on annual P vs Q sums, with the latter having a percentile 25-75 range from 62.8 km² to 76.6 km².

Between the two approaches applied, they are both limited in the strength of their results by their very general, global character. Experiential values play an import role in each, which,

while backed by the decades of experience Pierre-Yves Jeannin and Philipp Häuselmann have between them in this field, still cannot account for every detail in the very heterogeneous world of karst aquifers. Still, the assertion can be made that the catchment area of Lake Altaussee will likely be somewhere in the ranges obtained. Winkler (2004), at least, arrived at a similar order of magnitude using a similarly unspecific approach with 61 km^2 , which he qualified as a minimum size. It must be said, however, that the drainage basin of Augstbach was included in this value. According to Figure 4.3, the Augstbach's orographic catchment size is about 11 km^2 , leaving approximately 50 km^2 for Lake Altaussee. This is clearly smaller than the size arrived at from the methods applied for this thesis. If, however, the catchment sizes derived from the P values from Krippenstein have more merit than given credit for, this is also in the realm of the possible. His assumption of an infiltration rate of 80 % was also at the lower end, compared to e.g. Bonacci (2001), an increase of which would also increase his obtained catchment size.

4.2.2 VisualKARSYS model

Because, as explained above, the generation of comparative slices of the 3D geological model in VisualKARSYS was not reasonably possible, a visual comparison using this method will not be possible here. Instead, in Figure 4.2, two screenshots taken in-platform will be shown and discussed.

As can be seen in Figure 4.2a, the top unit border of the aquiclude does not conform very well to the top of the Hauptdolomit/the bottom of Dachstein Lst. drawn in the geological sections by Schwingenschlögl (1980, 1986). However, it must be said that, firstly, these two sections also do not conform to one another perfectly, and secondly that the older section contains a larger anticline-syncline system with S-N striking cores (see Figure 4.2b) to which the model does not conform. When it comes to section 1 from Schwingenschlögl (1986), the VisualKARSYS model reflects the shape of the Jurassic plateau syncline, the aquiclude unit's top boundary is a few tens of metres too high.

Compared to the cross-section2 depicted in Figure 4.2c, as drawn by the author, the aquiclude unit shows some smaller-scale waves that do not conform to the section's Hauptdolomit top end, but otherwise the forms are similar. On the left side, the aquiclude can be seen to follow the *Totes Gebirge* overthrust plane, which, as explained above, was designated the aquiclude toward the southwest.

Qualitatively, the general trends in the subsurface seem to be followed. Additional new data would not hurt, though, especially in the interest of aquiclude definition.

The catchment area delineated in VisualKARSYS for Lake Altaussee based on the modelled

aquiclude topography has an approximate surface area of 138.0 km^2 . For larger parts of the boundary, its location had to be estimated, as no subsurface aquiclude topography-derived watershed divide was visible inside the project boundary, and therefore had not been modelled. In these cases, the aquiclude elevation contours inside the project domain were used to extrapolate their further shape (see Figure 3.7). Especially in the east of the project scope, a lot of guesswork was involved. This means that the value given above is in itself an estimation, although its order of magnitude should be in the range of reality.

In Figure 4.3, this is compared to the orographic catchment areas given in the Hydrological Atlas of Austria (<https://ehao.boku.ac.at/> (Fürst, 2007)) and in the digital atlas of Styria (GIS-Steiermark, 2023). Obviously, in a karstified area there will be large discrepancies between the actual and the orographically obtained basins. Based on the water balancing done here and elsewhere, the orographic approach cannot account for enough precipitation for the observed lake discharge. However, the author noticed something interesting in the purely surface runoff basin: It is drawn as crossing the Hochklapfsattel, which would actually be expected to act as a watershed divide. Upon contacting Robert Stöffler from the relevant department of the Styrian state administration, unfortunately no data otherwise unavailable has as yet been unearthed that could explain this oddity. As previously explained, the only tracer tests conducted in the central *Totes Gebirge* plateau were those pioneering efforts by Maurin and Zötl (1964) whose validity are unfortunately marred by negligence in preparation and overconfidence in evaluation (F. Bauer and Völkl, 1989).

4.2.2.1 Validation through water balancing

As recommended by Jeannin et al. (2013), the conceptual karst aquifer model obtained from VisualKARSYS was made in parallel with a hydrological water balance aimed at estimating the catchment size of Lake Altaussee. Like this, a validation can be attempted, giving a qualitative assessment of the accuracy of the 3D model.

As mentioned previously, the catchment delineation performed on the basis of the aquiclude topography resulted in a size of 138.0 km^2 , although a healthy amount of uncertainty is implied. When compared to the entire range of hydrologically calculated catchment sizes (30 km^2 to 148 km^2), it falls into the higher end. However, it is almost double the weighted average (71 km^2) and well outside the corresponding range of the 25th and 75th percentile: 62.8 km^2 to 76.6 km^2 . As will be explained below, purely by spatial extent the hydrogeologically delineated catchment is too large, with a manually adjusted version (Figure 4.5) immediately much more in accordance with the hydrological water balance results.

4.2.2.2 Validation by comparison with caves


Based on the map shown in Figure 3.7 in the preceding chapter and existing literature (e.g. E. Geyer et al. (2016), Schneider (2013), and Winkler (2004)), the cave systems known to exist in the area of interest will be examined as to any hints they can give regarding the validity of the VisualKARSYS model.

From northwest to southeast, first in the line is the Schönberg cave system. Its hydrological behaviour and paleokarst development states have been investigated extensively (Plan et al., 2023), showing clearly that drainage directions are mostly toward the north except in high-flow conditions, when the Naglbründl or the Naglsteghöhle become active, feeding the Rettenbach. Although Robert Watson of the CUCC indicated in personal communication (2023) that the cavers active in the area hope to one day find a speleological connection between the Schönberg and Schwarzmooskogel cave systems, as yet no hydraulic flow connection has even been implied.

Concerning the latter, the following: In Figure 4.4 the elevation drawn by Winkler (2004) of the Schwarzmooskogel (SMK) cave system, which includes a potential piezometric surface of the karst groundwater body, was overlayed on a geological slice generated in VisualKARSYS following the approximate trace of the plane onto which the cave elevation was projected. Apart from the unfortunate aesthetics, some information can be gleaned concerning validation of the geological model. In general, the topmost formation was defined as the karst aquifer, and it seems to be able to host the SMK cave system which is said to drain into Lake Altaussee. Unfortunately, based on the nature of the model, it is not possible to ascertain whether the bedding planes which were obviously important for cave development (see Figures 2.9 and 2.10) in SMK are replicated in the VisualKARSYS model. With regard to the SMK's direction of drainage, all available literature indicates that the water which flows through this systems end up in Lake Altaussee (E. Geyer et al., 2016; Seebacher, 2015; Watson, 2023; Winkler, 2004).

Another question entirely is how the drainage of the three smaller cave systems work. While E. Geyer et al. (2016) hypothesize a drainage direction toward Lake Altaussee of the northern part of the Almberg cave system, its southern caves are said to drain southward along the bedding plane dip (Schneider, 2013). This cave system is contained in Plassen Lst. The Woising cave system in the north of the *Totes Gebirge* plateau, straddling the border between Upper Austria and Styria, has also experienced focussed speleological expeditions; unfortunately, no drainage direction has been ascertained as of yet (Kreuß et al., 2017), though the nearby Almsee or the spring in Nesseltal (Harlacher, 2003) would suggest themselves.

Although described in character and examples by E. Geyer et al. (2016), the Hüttstatt

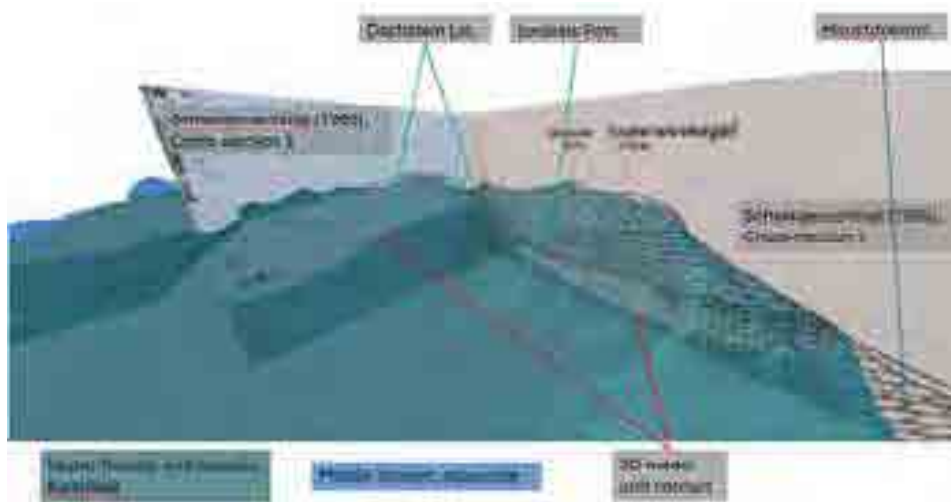
caves around Albert-Appel-Haus are not assigned directions of drainage or even hunches. The comprehensive documentation published by W. Ufrecht in 2012, hinted at by E. Geyer et al. (2016), might contain answers to this question: it was not to be found by the author through even a quite thorough search of the internet. 

As could already be seen in Figure 4.4, the karstified unit of the geological model can comfortably house the vertical extent of the SMK cave system. Beyond this observation, unfortunately, the three-dimensional cave survey data cannot really be used for validation as the author had in mind: bedding planes or fractures that from the cave visualisation obviously acted as inception horizons cannot be compared with any feature of the VisualKARSYS model except for unit mesh boundaries.

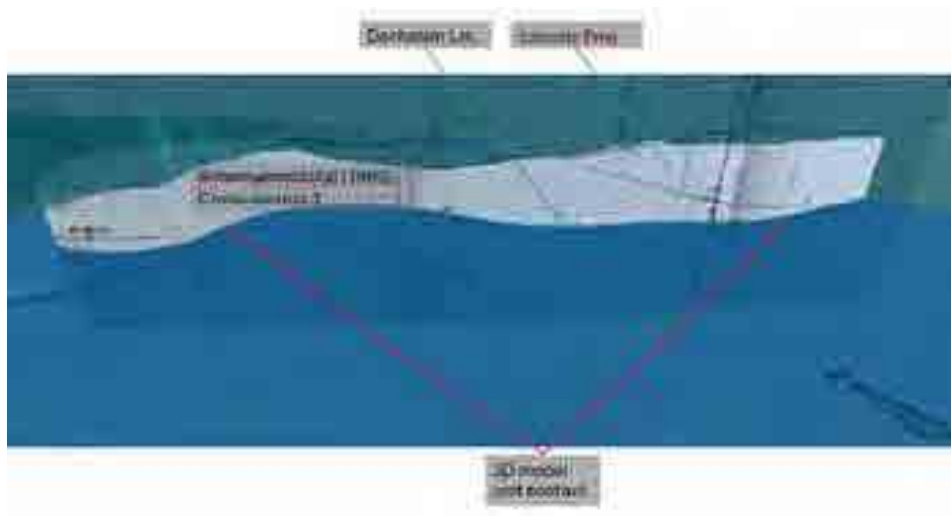
Keeping these points in mind, Figure 4.5 was drawn as an attempt to present the results of this thesis. The catchment boundaries for Lake Altaussee drawn on the basis of the aquiclude topography in VisualKARSYS obviously do not reflect real-world conditions, as they include the Schönberg cave system in the northwest and place the groundwater body as directly touching the Grundlsee to the south which is fed entirely by the Traun-Ursprung spring via Kammer- and Toplitzsee. This clearly shows that subsurface watershed divides exist, but were not simulated by the 3D model. There are probably different reasons for the different parts of the model: the Schönberg caves are heavily influenced by paleokarst levels dipping toward the north (Plan et al., 2023). Toward Grundlsee, however, the situation is less clear. On the one hand, some part of the Jurassic limestone plateau behind Trisselwand probably drains toward Lake Altaussee. However, as a whole, the Jurassic block seems to be formed as a syncline with Dachstein Lst. and probably Hauptdolomit underneath (see above). Proposing one single, continuous catchment boundary seems very daring; potentially, a system of different features and bedding plane dips each have a part to play. Alternatively, Philipp Häuselmann suggested in a meeting (2024) that maybe the Altaussee-Wildensee fault system could be such an efficient system of drainage that hypothetical faults and fissures toward the south were not activated. A paleokarst connection from Lake Altaussee to Grundlsee would also be improbable, in Philipp Häuselmann's opinion, as the water level of the former is said to have been up to 15 m to 20 m lower in its past, probably in the Holocene. This would put it 7 m to 12 m lower than the Grundlsee water surface (708 m a.s.l.), under the assumption that its water table was the same as today.

Although the manually drawn catchment boundary in Figure 4.5 is only to be understood as a qualitative suggestion pending future research, it does seem more realistic than the one based on VisualKARSYS. It also incorporates in its surface area the results of the hydrological water balance modelling, thus representing that part of the methodology too. In a perfect

world, it would also be possible to map tracer test results, proving hydraulic connectivities; this step can only be taken by future hydrogeology enthusiasts.



(a) View onto models and sections from SW.



(b) View onto models and Schwengenschlögl (1980) section 3 from S.



(c) View in model and at section from S.

Figure 4.2: Screenshot of the VisualKARSYS 3D model with (top) the section 3 from Schwengenschlögl (1980) and section 1 from Schwengenschlögl (1986), (bottom) along author's section 2.



Figure 4.3: Map showing comparison between the catchment delineated in VisualKARSYS (in orange) and the orographic catchments covering the surface of the *Totes Gebirge* (in blue polygons), from the digital Hydrological Atlas of Austria (<https://ehao.boku.ac.at/>); the black rectangle is the VisualKARSYS scope.

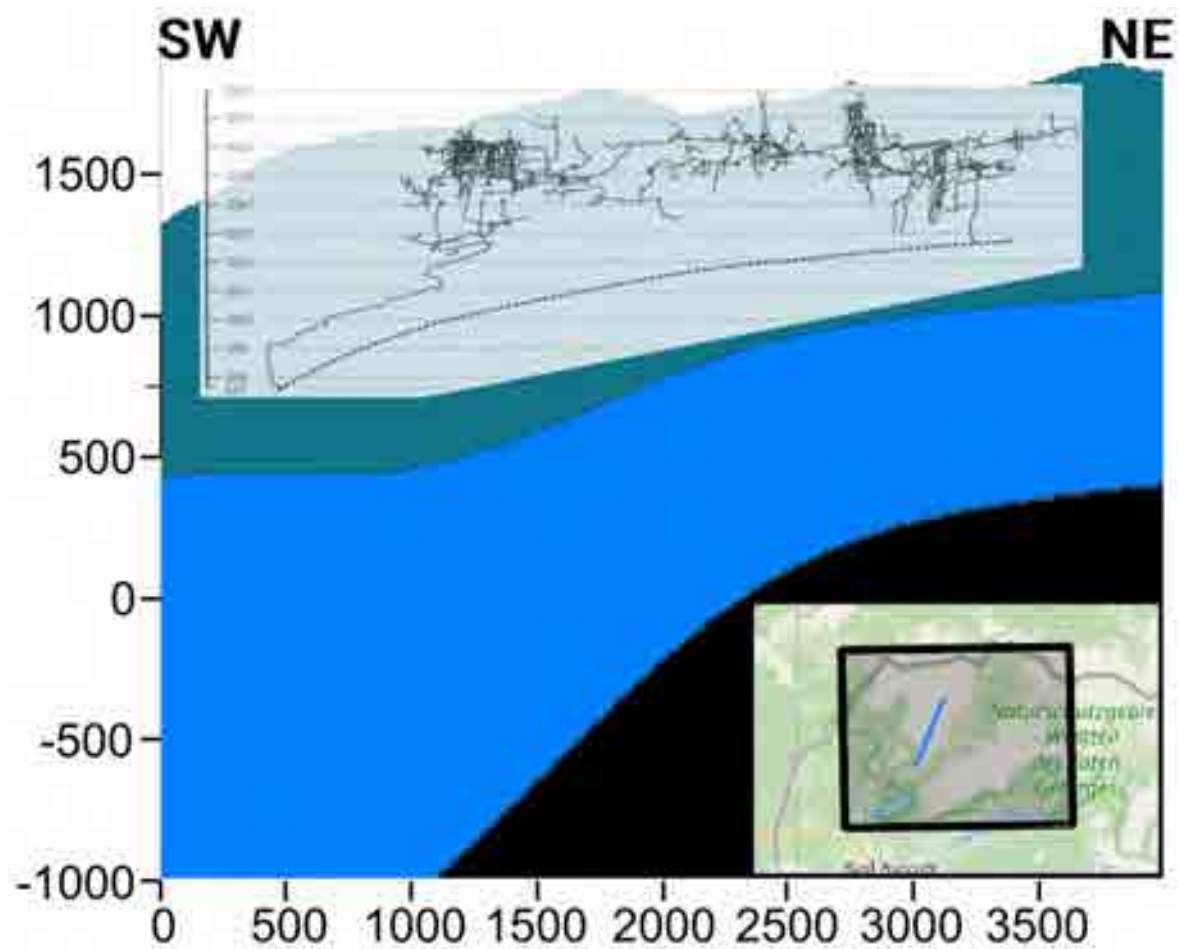


Figure 4.4: Overlay of the elevation of SMK cave system with potential piezometric surface of karst aquifer (Winkler, 2004) over slice generated in VisualKARSYS from 3D model. Because the viewpoint at slices cannot be changed, the SMK elevation had to be modified for visualisation purposes.

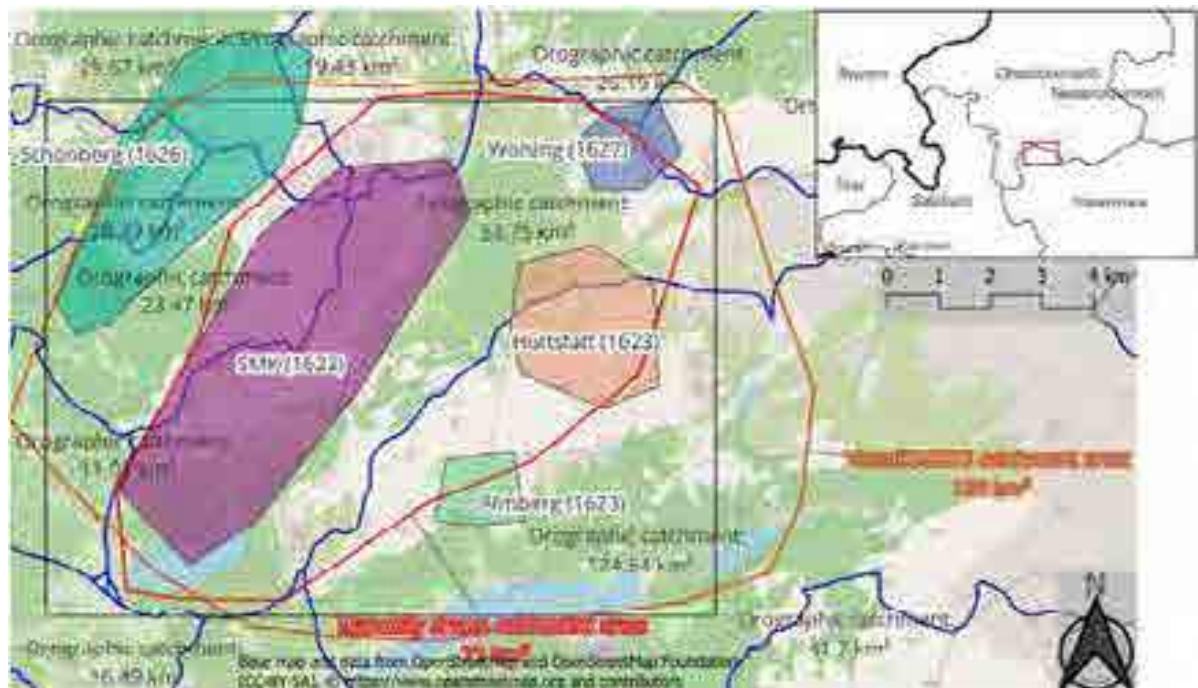


Figure 4.5: Map showing manually delineated catchment area of Lake Altaussee (red stroke polygon) compared to the catchment drawn on the basis of the VisualKARSYS hydrogeological model (orange stroke polygon). Also on the map: approximate areas of the larger cave systems in the area, labelled with their names (SMK: Schwarzmooskogel) and numbers in the Austrian cave cadastre; orographic catchment areas from the digital Hydrological Atlas of Austria (<https://ehao.boku.ac.at/>) as blue polygons with labelling reflecting each catchment's size; spatial scope of the VisualKARSYS project as a black rectangle. Background map: OSM.

5 Conclusions

In conclusion, an attempt was made to model the karst aquifer feeding Lake Altaussee which is situated in the surrounding western *Totes Gebirge*, the largest karstified massif in Austria. On the one hand, two approaches to global hydrological water balancing were followed: the first used annual precipitation sums from three weather stations in the region that each are at a different elevation, combined with an empirical flat evapotranspiration loss per year and annual sums of discharge from the lake. A 48-year time series of catchment sizes per station resulted from this. The second approach used an empirically arrived at value for mountainous karst systems' minimal specific discharge during dry times, which, when used as the denominator for the minimal discharge from Lake Altaussee, returned a catchment size too.

On the other hand, the free, open-access online platform VisualKARSYS for hydrogeological, three-dimensional modelling of karst aquifers was used. Developed by the Swiss Institute for Speleology and Karst Studies (SISKA), it uses implicit geological modelling and basic assumptions about karst hydrogeology to create conceptual groundwater bodies. For this thesis, the available (hydro-)geological data did not quite suffice for robust modelling, calling for the author to construct seven geological cross-sections of the plateau. The resulting 3D subsurface characterisation included a karstified rock mass made up of Middle Triassic (Dachstein) Lst. and Upper Jurassic Lst. (Oberalm Fm., Plassen Lst.). As a simplification, the underlying aquiclude was designated to be Hauptdolomit and the overthrust plane of the *Totes Gebirge* thrust sheet, both of which were represented by one continuous model unit. Based on the location and elevation of the system's permanent spring underneath Lake Altaussee, but modelled as being at the lake's water table, the groundwater body at low to normal hydrological conditions was generated in the trough formed by the aquiclude's topography. This step was repeated once for each of the two overflow springs, Liagerhöhle and Kugelmühlhöhle, although the karst groundwater surface automatically modelled as being flat cannot be so realistically, as the peakflow conditions during activation of the overflow springs implicitly require a large increase in the gradient of the groundwater body.

A catchment delineation was drawn based on the topography of the aquiclude in Visu-

alKARSYS, reaching a size of 138.0 km². However, this catchment included areas known now to drain toward Lake Altaussee, like the Schönberg cave system, and areas for which it does not make sense to be in direct contact with the groundwater body, like Grundlsee to the south. Furthermore, the results of the hydrological water balancing indicated a catchment size in the range of 70 km² to 100 km². With respect to these circumstances, another catchment delineation was drawn manually, covering an area of 71 km². Although this latter basin fits better to real-world conditions and hydrological validation, its precise spatial extent is unclear in the detail. For example, of the four cave systems included, the drainage direction for two is unknown to the author, and half of another is probably toward Grundlsee. These uncertainties and the unsatisfactory data basis for the applied methods point towards areas of research whose results could improve the understanding of the karst aquifer of Lake Altaussee.

5.1 Future outlook

"The resulting 3D conceptual model is thus the hypothesis to be tested (and improved) by any further investigations (i.e. tracing experiments, hydrograph analyses, hydrochemistry, water isotopes, simulations, etc.)." Jeannin et al. (2013, p. 1002)

As can be gathered by the preceeding chapters and the section above, a detailed and more realistic catchment delineation for Lake Altaussee will need more work and more data to base further research on. Above all other suggestions, the current situation of geological data pertaining to *Totes Gebirge* is lacking both in quantity/density and quality, and is quite old (Schönlaub and Draurer, 2001). Although an effort was made by the Geological Survey of Austria for map sheet 97 in the agglomeration of archival material for the GEOFAST map (Moser, 2019), its preliminary status must be underlined and a “proper” geological map produced. Adding to that, the neighbouring sheet 96 (Schäffer, 1982) has some deficiencies in the area of interest (Mandl et al., 2012) and would profit from an overhaul, as provided by Mandl (2013) for the Sandling area or e.g. Fernández et al. (2024) for the regional tectonics of the Hallstatt zone around Altaussee, though focused on an alternative, salt tectonic model. Pertaining to this last point, it must be suggested that deep borehole exploration be performed in the *Totes Gebirge* massif, both to gain an understanding of bedding, faulting and carbonate lithology in depths of interest for karst hydrogeology, and to gather data on the distribution and thickness of underlying Permian evaporites that play such a crucial role in the paleogeology of the Northern Calcareous Alps (NCA). Based on this new geological data, geological sections might be constructed by trained and experienced geologists that better

reflect the actual situation. Armed with so sound a foundation, an updated VisualKARSYS model would surely lead to a robust three-dimensional geological characterisation of the area.

As to the hydrogeological side of VisualKARSYS, modern tracer tests and a re-appraisal of the spore tracing field work from the 1960s (Maurin and Zötl, 1964) would give a much deeper insight into the hydraulic situation of *Totes Gebirge*. An approach could be followed that mirrors the one employed by F. Bauer and Völkl (1989) for the Dachstein massif. However, as Lake Altaussee's karst spring are subaqueous and quite numerous (see Figure 2.13), the dye tracer detection would present significant complications, necessitating underwater sampling stations, not to mention the high cost attached to dye tracing experiments in general. Should a tracing experiment take place it would be advantageous to include the body of expertise which a large number of caving associations (e.g. VHO, ARGE, CUCC and others, see E. Geyer et al. (2016) for further examples) and their members have gathered over decades of caving in the area.

Concerning hydrological research in the area, firstly it would be very useful for karst hydrology in general to have access to temporally higher-resolution data than currently widely available: Both the discharge from Lake Altaussee and all precipitation data are given only in daily steps, averaged or summed, respectively. However, as mentioned previously, karst system discharge can change quickly once rainfall sets in, a dynamic which cannot be followed as closely as necessary for hydraulic applications in the current situation. As of June 2023 a number of meteorological and water parameter measurement instruments were installed either on a platform on the lake's water surface over the largest karst funnel, or the adjacent boat house on the shore, as part of the Lake Altaussee project headed by the Walter Munk Foundation in which context this thesis was also written. In a temporal resolution of seconds, it logs air and water temperature, wind speed and direction, humidity, air pressure, global radiation, and precipitation status, type, intensity and amount. Once a longer time series of data has been acquired, it will surely help increase understanding of the water dynamics of the lake and its surroundings. Speaking of which, the installation of a precipitation measurement instrument on the existing weather station on the mountain station of the chairlift up Loser would be helpful too: it could show differences in rainfall regimes between the plateau and the valley, and of course increase the local spatial distribution of available weather data in any hydrological model.

As an example, it could aid in the following application: Harum et al. (2014) suggest a distributed water balance model, taking into account soil and vegetation, evapotranspiration, percolation and groundwater recharge. A model such as that would probably offer much more nuanced validation for an updated VisualKARSYS model, but would also in itself give more

of an idea of the lake's catchment.

References

- AEIOU (2016). *Geologische Bundesanstalt, GBA (english)*. Austria-Forum, das Wissensnetz. URL: https://austria-forum.org/af/AEIOU/Geologische_Bundesanstalt%2C_GBA/Geologische_Bundesanstalt%2C_GBA_english (accessed on 8/3/2024).
- Alberti, M. and Zanieri, M. (2023). *qProf*. Version 0.5.1. URL: <https://plugins.qgis.org/plugins/qProf/#plugin-details>.
- Autodesk (2023). *AutoCAD*. Version 2023. Autodesk. URL: <https://www.autodesk.com/products/autocad/overview>.
- Baedke S. J. and Krothe N. C. (2001). "Derivation of effective hydraulic parameters of a Karst Aquifer from discharge hydrograph analysis". In: *Water Resources Research* 37.1, pp. 13–19. ISSN: 00431397.
- Bailly-Comte, V. et al. (2023). "XLKarst, an Excel tool for time series analysis, spring recession curve analysis and classification of karst aquifers". In: *Hydrogeology Journal* 31, pp. 2401–2415. ISSN: 1431-2174.
- Bauer, Ch. and Plan, L. (2022). "Karst Landscapes in Austria". In: *Landscapes and Landforms of Austria*. Ed. by Ch. Embleton-Hamann. Cham: Springer International Publishing, pp. 87–104. ISBN: 978-3-030-92813-1.
- Bauer, F. and Völkl, G. (1989). *Die unterirdischen Abflussverhältnisse im Dachsteingebiet und ihre Bedeutung für den Karstwasserschutz*. Wien: Umweltbundesamt.
- Beiwl, C. and Mühlmann, H. (2008). *Atlas der natürlichen Seen Österreichs mit einer Fläche ≥ 50 ha. Morphometrie - Typisierung - Trophie*. ger. Vol. 29. Schriftenreihe des Bundesamtes für Wasserwirtschaft. Wien: Bundesamt für Wasserwirtschaft. 147 pp. ISBN: 3901605290.
- Benischke, R. (2021). "Review: Advances in the methodology and application of tracing in karst aquifers". In: *Hydrogeology Journal* 29.1. PII: 2278, pp. 67–88. ISSN: 1431-2174. DOI: 10.1007/s10040-020-02278-9.
- Benischke, R. et al. (2018). "Sauerstoff-18 - Seehöheneffekt als Zusatzinformation zur Ermittlung der hydrografischen Einzugsgebiete im Karst". In: *Isotopenzusammensetzung in natürlichen Wässern in Österreich - Grundlagen und Anwendungsbeispiele zur Wasser-*

- Isotopenkarte Österreichs 1:500.000*. Ed. by R. Philippitsch and F. Humer. Wien: Bundesministerium für Nachhaltigkeit und Tourismus, pp. 106–110.
- Beven, K. and Binley, A. (1992). "The future of distributed models: Model calibration and uncertainty prediction". In: *Hydrological Processes* 6.3, pp. 279–298. ISSN: 08856087. DOI: 10.1002/hyp.3360060305.
- BFL Bundesamt und Forschungszentrum für Landwirtschaft (1998). *Erläuterungen zur Bodenkarte 1:25.000. Kartierungsbereich 143 BAD AUSSEE Steiermark*. Wien: Bundesministerium für Land- und Forstwirtschaft.
- Birk, S., Liedl, R., and Sauter, M. (2006). "Karst spring responses examined by process-based modeling". eng. In: *Ground water* 44.6. Journal Article Research Support, Non-U.S. Gov't, pp. 832–836. ISSN: 0017-467X. DOI: 10.1111/j.1745-6584.2006.00175.x. eprint: 17087755.
- Bögli, A. (1980). *Karst Hydrology and Physical Speleology*. Berlin, Heidelberg: Springer Berlin Heidelberg. 297 pp.
- Bonacci, O. (2001). "Monthly and annual effective infiltration coefficients in Dinaric karst: example of the Gradole karst spring catchment". In: *Hydrological Sciences Journal* 46.2, pp. 287–299. ISSN: 0262-6667. DOI: 10.1080/02626660109492822.
- Borsato, A. (2001). "Characterisation of a high-altitude alpine karst aquifer by means of temperature, conductivity and discharge monitoring (Centonia spring, Brenta Dolomites, N-Italy)". In: *Sciences et Techniques de l'Environnement* 13, pp. 51–54.
- Bullmann, K. (2018). "Die Niederschlagsverteilung des Inneren Salzkammergutes". Geographie und Raumforschung. Master's thesis. Graz: Karl-Franzens-Universität Graz. 96 pp.
- Çalli, S. S. et al. (2022). "Contribution of the satellite-data driven snow routine to a karst hydrological model". In: *Journal of Hydrology* 607. PII: S0022169422000865, p. 127511. ISSN: 00221694. DOI: 10.1016/j.jhydro1.2022.127511.
- Chen, Z. et al. (2017). "The World Karst Aquifer Mapping project: concept, mapping procedure and map of Europe". In: *Hydrogeology Journal* 25.3. PII: 1519, pp. 771–785. ISSN: 1431-2174. DOI: 10.1007/s10040-016-1519-3.
- Cinkus, G., Mazzilli, N., and Jourde, H. (2023). "KarstID: an R Shiny application for the analysis of karst spring discharge time series and the classification of karst system hydrological functioning". In: *Environmental Earth Sciences* 82. ISSN: 1866-6280.
- CUCC (2018). *Survex*. Version 1.4.3.
- Diem, A., Poulsen, T. M., and Veyret, P. (2024). *Alps*. Encyclopedia Britannica. URL: <https://www.britannica.com/place/Alps> (accessed on 4/3/2024).

- Dinçer, T. et al. (1972). "Das Tote Gebirge als Entwässerungstypus der Karstmassive der nordöstlichen Kalkhochalpen (Ergebnisse von Isotopenmessungen)". In: *Steirische Beiträge zur Hydrogeologie* 24, pp. 71–110.
- Dobesch, H. (2007). "Kapitel 3.2: Mittlere potentielle Jahresverdunstung". In: *Der Hydrologische Atlas Österreichs*. Wien.
- Egger, H. (2007). *Erläuterungen zu Blatt 67 Grünau im Almtal*. Wien: Geologische Bundesanstalt Österreich.
- Egger, H. and van Husen, D. (2007). *Geologische Karte der Republik Österreich 1:50.000 - 67 Grünau im Almtal*. Ed. by Geologische Bundesanstalt. URL: <https://www.geologie.ac.at/en/onlineshop/detail/?id=0&seo=undefined&origId=2056>.
- Encyclopedia Britannica (2024a). *Hydrology*. Encyclopedia Britannica. URL: <https://www.britannica.com/science/hydrology> (accessed on 13/4/2024).
- (2024b). *karst (geology)*. Encyclopedia Britannica. URL: <https://www.britannica.com/science/karst-geology> (accessed on 10/2/2024).
- Esri Inc. (2023). *ArcGIS Pro*. Version 3.2.0. Esri. URL: <https://www.esri.com/en-us/arcgis/products/arcgis-pro/overview>.
- Fernández, O., Grasemann, B., and Sanders, D. (2022). "Deformation of the Dachstein Limestone in the Dachstein thrust sheet (Eastern Alps, Austria)". In: *Austrian Journal of Earth Sciences* 115.1, pp. 167–190. DOI: 10.17738/ajes.2022.0008.
- Fernández, O., Habermüller, M., and Grasemann, B. (2021). "Hooked on salt: Rethinking Alpine tectonics in Hallstatt (Eastern Alps, Austria)". In: *Geology* 49.3, pp. 325–329. ISSN: 0091-7613. DOI: 10.1130/G47981.1.
- Fernández, O. et al. (2023). "Mesozoic paleogeography, structural configuration and evolution of the central Northern Calcareous Alps (Eastern Alps, Austria): Alternative scenarios and discussion". In: *International Journal of Earth Sciences*, pp. 1–43. ISSN: 1437-3254.
- Fernández, O. et al. (2024). "Salt-rich versus salt-poor structural scenarios in the central Northern Calcareous Alps: implications for the Hallstatt facies and early Alpine tectonic evolution (Eastern Alps, Austria)". eng. In: *International Journal of Earth Sciences* 113.2. Journal Article Conflict of interestThe authors declare no conflict of interest., pp. 245–283. DOI: 10.1007/s00531-023-02377-4. eprint: 38500652.
- Fink, M. H. (1978). "Richtlinien für die Erstellung von Karstgefährdungskarten". In: *Die Karstverbreitungs- und Karstgefährdungskarten Österreichs im Maßstab 1:50 000. Ein Beitrag der Karst- und Höhlenforschung zu einem österreichischen Umweltkonzept*. Ed. by H. Trimmel. Wissenschaftliches Beiheft zur Zeitschrift "Die Höhle" 27. Wien, pp. 23–48.

- Ford, D. and Williams, P. W. (2007). *Karst Hydrogeology and Geomorphology*. Chichester: John Wiley. ISBN: 978-0-470-84996-5.
- Frisch, W., Dunkl, I., and Kuhlemann, J. (2000). "Post-collisional orogen-parallel large-scale extension in the Eastern Alps". In: *Tectonophysics* 327, pp. 239–265. ISSN: 00401951.
- Fürst, J. (2007). *Der Hydrologische Atlas Österreichs*. Wien: Austrian Federal Ministry of Agriculture, Forestry, Regions and Water Management. URL: <https://ehao.boku.ac.at/>.
- Ganss, O. (1937). "Zur Geologie des westlichen Toten Gebirges". In: *Jahrbuch der Geologischen Reichsanstalt* 87, pp. 331–374.
- Geyer, E. et al. (2016). "Totes Gebirge". In: *Höhlen und Karst in Österreich*. Ed. by C. Spötl, L. Plan, and E. Christian. Wissenschaftliches Beiheft zur Zeitschrift "Die Höhle" Nr. 61. Linz: Land Oberösterreich Oberösterreichisches Landesmuseum, pp. 599–622. ISBN: 9783854743217.
- Geyer, G. (1878). "Das Todte Gebirge. Eine monographische Abhandlung". In: *Jahrbuch des Oesterreichischen Touristen-Club* 9, pp. 7–200.
- (1915). "Aus den Umgebungen von Mitterndorf und Grundlsee im steirischen Salzkammergut". In: *Jahrbuch der Geologischen Reichsanstalt* 65, pp. 177–238.
- (1916). "Das Gebiet nördlich des Ennstales". In: *Erläuterungen zur Geologischen Karte der im Reichsrath vertretenen Königreiche und Länder der Österr.-Ungar. Monarchie: SW-Gruppe Nr. 20 Liezen*. Spezialkarte der Österr.-Ungar. Monarchie im Maßstabe 1:75000. Wien, pp. 16–56.
- Geyer, T. et al. (2008). "Quantification of temporal distribution of recharge in karst systems from spring hydrographs". In: *Journal of Hydrology* 348.3-4. PII: S0022169407006075, pp. 452–463. ISSN: 00221694. DOI: 10.1016/j.jhydro1.2007.10.015.
- GIS-Steiermark (2023). *Digitaler Atlas des Landes Steiermark*. A17 Landes- und Regionalentwicklung, Referat Statistik und Geoinformation.
- Goldscheider, N., Drew, D., and Worthington, S. (2007). "Introduction". In: *Methods in Karst Hydrogeology*. Ed. by N. Goldscheider and D. Drew. International Contributions to Hydrogeology 26. Leiden: Taylor & Francis/Balkema, pp. 1–7. ISBN: 978-0-20393462-3.
- Goldscheider, N. et al. (2008). "Tracer tests in karst hydrogeology and speleology". In: *International Journal of Speleology* 37.1, pp. 27–40. ISSN: 0392-6672. DOI: 10.5038/1827-806X.37.1.3.
- Gosar, A. et al. (2024). *Slovenia*. Encyclopedia Britannica. URL: <https://www.britannica.com/place/Slovenia#ref477044> (accessed on 10/2/2024).

- Gouy, A. et al. (2024). "KarstNSim: A graph-based method for 3D geologically-driven simulation of karst networks". In: *Journal of Hydrology* 632. ISSN: 00221694.
- Griesmeier, G. and Hornung, T. (2023). *GEOFAST MAPS 1:50.000 - 68 Kirchdorf a. d. Krems*. Ed. by Geologische Bundesanstalt. Wien. URL: <https://www.geologie.ac.at/en/onlineshop/detail/?id=0&seo=undefined&origId=11880>.
- Grottenthaler, W. (1978). "Die Raibler Schichten der Nördlichen Kalkalpen zwischen Salzach und Pyhrnpaß. Lithofazielle, sedimentologische und paläogeographische Untersuchungen". In: *Mitt. Ges. Geol. Bergbaustud. Österr.* 25, pp. 11–33.
- Groves, C. (2007). "Chapter 4: Hydrological methods". In: *Methods in Karst Hydrogeology*. Ed. by N. Goldscheider and D. Drew. International Contributions to Hydrogeology 26. Leiden: Taylor & Francis/Balkema, pp. 45–64. ISBN: 978-0-20393462-3.
- Harlacher, C. (2003). *Chemische und thermische Reaktionen der Wässer von Karstquellen im Hochgebirge (Totes Gebirge, Österreich) auf Niederschlagsereignisse*. In collab. with T. Clemens and M. Sauter. Vol. 84. Berichte der wasserwirtschaftlichen Planung. Graz.
- Hartmann, A. et al. (2014). "Karst water resources in a changing world: Review of hydrological modeling approaches". In: *Reviews of Geophysics* 52.3, pp. 218–242. ISSN: 87551209. DOI: 10.1002/2013RG000443.
- Harum, T. et al. (2014). *Hydrologische Untersuchung Altausseer See. Endbericht*. Graz: Amt der Steiermärkischen Landesregierung Abteilung 15 - Energie, Wohnbau, Technik, Gewässeraufsicht und Gewässerschutz.
- ~~Häuselmann, Ph. and Jeannin, P. Y. (July 26, 2023a). *Personal communication: Simplified hydrological modelling approach for catchment size estimation*. Email. Wien.~~
- ~~– (Dec. 6, 2023b). *Personal communication: Water balance modelling for catchment estimation at Altausseer See*. Email. Wien.~~
- He, Z. H. et al. (2014). "Estimating degree-day factors from MODIS for snowmelt runoff modeling". In: *Hydrology and Earth System Sciences* 18.12, pp. 4773–4789. DOI: 10.5194/hess-18-4773-2014.
- Herlicska, H. and Lorbeer, G. (1994). *Pilotprojekt "Karstwasser Dachstein". Band 1: Karstwasserqualität*. Wien: Umweltbundesamt.
- Hilberg, S. (2016). "Review: Natural tracers in fractured hard-rock aquifers in the Austrian part of the Eastern Alps—previous approaches and future perspectives for hydrogeology in mountain regions". In: *Hydrogeology Journal* 24.5. PII: 1395, pp. 1091–1105. ISSN: 1431-2174. DOI: 10.1007/s10040-016-1395-x.
- Hiscock, K. M. (2005). *Hydrogeology. Principles and practice*. Malden MA: Blackwell Pub. xvi, 389. ISBN: 0632057637.

- Houlding, S. W. (1994). *3D Geoscience Modeling. Computer Techniques for Geological Characterization*. Berlin, Heidelberg: Springer Berlin Heidelberg.
- Hunkeler, D. and Mudry, J. (2007). "Hydrochemical methods". In: *Methods in Karst Hydrogeology*. Ed. by N. Goldscheider and D. Drew. International Contributions to Hydrogeology 26. Leiden: Taylor & Francis/Balkema, pp. 93–121. ISBN: 978-0-20393462-3.
- IAH (2024). *What is Hydrogeology and what do hydrogeologists do?* International Association of Hydrogeologists. URL: <https://iah.org/education/general-public/what-is-hydrogeology> (accessed on 19/2/2024).
- Inkscape Developer Community (2024). *Inkscape*. Version 1.3.2. URL: <https://inkscape.org/>.
- Jacob, C. E. (1940). "On the flow of water in an elastic artesian aquifer". In: *Transactions, American Geophysical Union* 21.2, pp. 574–586.
- Jeannin, P.-Y. (2014). "Karst Hydrogeology". In: *Handbook of engineering hydrology. Book I, Fundamentals and applications*. Ed. by S. Eslamian. Boca Raton, FL: CRC Press/Taylor & Francis Group, pp. 380–406. ISBN: 9781466552418.
- Jeannin, P.-Y. et al. (2013). "KARSYS: a pragmatic approach to karst hydrogeological system conceptualisation. Assessment of groundwater reserves and resources in Switzerland". In: *Environmental Earth Sciences* 69.3. PII: 1983, pp. 999–1013. ISSN: 1866-6280. DOI: 10.1007/s12665-012-1983-6.
- Jeannin, P.-Y. et al. (2015). "Assessing karst-hydraulic hazards in tunneling—the Brunnmühle spring system—Bernese Jura, Switzerland". In: *Environmental Earth Sciences* 74.12. PII: 4655. ISSN: 1866-6280. DOI: 10.1007/s12665-015-4655-5.
- Jeannin, P.-Y. et al. (2021). "Karst modelling challenge 1: Results of hydrological modelling". In: *Journal of Hydrology* 600. PII: S0022169421005552, p. 126508. ISSN: 00221694. DOI: 10.1016/j.jhydro1.2021.126508.
- Jennings, J. N. (1985). *Karst geomorphology*. Oxford: Blackwell. ISBN: 063114031X.
- Kermap (2024). *Nimbo: Earth Online: non-stop satellite monitoring platform*. kermap.com. URL: <https://maps.nimbo.earth> (accessed on 11/4/2024).
- Klimchouk, A. B. (2009). "Principal features of hypogene speleogenesis". In: *Hypogene Speleogenesis and Karst Hydrogeology of Artesian Basins (Simferopol)*. Ed. by A. B. Klimchouk and D. Ford. Special Paper 1. Ukrainian Institute of Speleology and Karstology. Ukrainian Institute of Speleology and Karstology, pp. 7–17.
- Krainer, K. et al. (2021). "Unusual catchment runoff in a high alpine karst environment influenced by a complex geological setting (Northern Calcareous Alps, Tyrol, Austria)". In:

- Hydrogeology Journal* 29.8. PII: 2405, pp. 2837–2852. ISSN: 1431-2174. DOI: 10.1007/s10040-021-02405-0.
- Kresic, N. (1995). "Remote Sensing of Tectonic Fabric Controlling Groundwater Flow in Dinaric Karst". In: *Remote Sens. Environ.* 53, pp. 85–90.
- (2007). "Hydraulic methods". In: *Methods in Karst Hydrogeology*. Ed. by N. Goldscheider and D. Drew. International Contributions to Hydrogeology 26. Leiden: Taylor & Francis/Balkema, pp. 65–92. ISBN: 978-0-20393462-3.
- Kreuß, M., Kalmbach, U., and Heiland, S. (2017). "Das Woising-Höhlensystem im Toten Gebirge, Stmk/OÖ". In: *Die Höhle* 68, pp. 3–13.
- Kuffner, D. (1998). "Höhlenniveaus und Altflächen im westlichen Toten Gebirge". In: *Wissenschaftliche Beihefte zur Zeitschrift "Die Höhle"* 53.
- La Varga, Miguel de, Schaaf, Alexander, and Wellmann, Florian (2019). "GemPy 1.0: open-source stochastic geological modeling and inversion". English. In: *Geoscientific Model Development* 12.1, pp. 1–32. DOI: 10.5194/gmd-12-1-2019. URL: <https://gmd.copernicus.org/articles/12/1/2019/>.
- Laimer, H. J. (2005). "Die Erfassung der Karstgrundwasser-Vulnerabilität mit der Methode „VURAAS“". In: *Grundwasser* 10.3. PII: 93, pp. 167–176. ISSN: 1430-483X. DOI: 10.1007/s00767-005-0093-8.
- Leitner, C. and Spötl, C. (2017). "The Eastern Alps: Multistage Development of Extremely Deformed Evaporites". In: *Permo-Triassic Salt Provinces of Europe, North Africa and the Atlantic Margins. Tectonics and Hydrocarbon Potential*. Ed. by J. I. Soto, J. F. Flinch, and G. Tari. Elsevier, pp. 467–482. ISBN: 9780128094174. DOI: 10.1016/B978-0-12-809417-4.00022-7.
- Linsley, R. K., Kohler, M. A., and Paulhus, J. L. H. (1949). *Applied Hydrology*. McGraw-Hill Engineering Series. McGraw-Hill Book Company, Inc.
- Lobitzer, H. (2012). *Geologische Spaziergänge: Ausseerland, Salzkammergut*. 2. verb. Aufl. Geologische Spaziergänge. Wien: Geologische Bundesanst. 99 pp. ISBN: 978-3-85316-063-3.
- Lopez, S. et al. (2018). "Yet another geological modeling library..." In: *Delivering subsurface models for societal challenges*. 4th meeting of the European 3D Geomodelling community (Orléans). Ed. by BRGM, p. 71.
- Malard, A. and Jeannin, P.-Y. (Oct. 17, 2022). *Visual KARSYS. A web service for modelling karst aquifers in 3D*. La Chaux-de-Fonds (CH): SISKa.
- Malard, A. et al. (2014). "Praxisorientierter Ansatz zur kartographischen Darstellung von Karst-Grundwasserressourcen". In: *Grundwasser* 19.4. PII: 271, pp. 237–249. ISSN: 1430-483X. DOI: 10.1007/s00767-014-0271-7.

- Malard, A. et al. (2015). "An integrated approach for catchment delineation and conduit-network modeling in karst aquifers: application to a site in the Swiss tabular Jura". In: *Hydrogeology Journal* 23.7. PII: 1287, pp. 1341–1357. ISSN: 1431-2174. DOI: 10.1007/s10040-015-1287-5.
- Malard, A. et al. (2023). "Contribution of the dynamic visualization of a 3D hydrogeological conceptual model to the participatory management of groundwater resources". In: *Comptes Rendus. Géoscience* 355.S1, pp. 231–244. DOI: 10.5802/crgeos.152.
- Mandl, G. W. (2000). "The Alpine sector of the Tethyan shelf - Examples of Triassic to Jurassic sedimentation and deformation from the Northern Calcareous Alps". In: *Mitt. Österr. Geol. Ges.* 92, pp. 61–77.
- (2013). "Zur Geologie des Raumes Hütteneckalm-Sandlingalm-Blaa-Alm (Salzkammergut, Österreich) mit kritischen Anmerkungen zur Sandlingalm-Formation". In: *Jahrbuch der geologischen Bundesanstalt* 153, pp. 33–74.
- Mandl, G. W., van Husen, D., and Lobitzer, H. (2012). *Erläuterungen zu Blatt 96 Bad Ischl*. Wien: Geologische Bundesanstalt Österreich.
- Mangin, A. (1975). "Contribution à l'étude hydrodynamique des aquifères karstiques (Contribution to the hydrodynamic study of karst aquifers)". PhD thesis. Dijon, France: Université de Dijon.
- (1984). "Pour une meilleure connaissance des systèmes hydrologiques à partir des analyses corrélatrice et spectrale (For a better understanding of hydrological systems using correlative and spectral analysis)". In: *Journal of Hydrology* 67, pp. 25–43. ISSN: 00221694.
- Mather, J. D., Torrens, H. S., and Lucas, K. J. (2004). "Joseph Lucas (1846–1926) — Victorian polymath and a key figure in the development of British hydrogeology". In: *Geological Society, London, Special Publications* 225, pp. 67–88.
- Maurin, V. and Zötl, J. (1960). *Bericht über karsthydrologische Erhebungen im Toten Gebirge*. Graz: Geologische Bundesanstalt Österreich.
- (1964). "Karsthydrologische Untersuchungen im Toten Gebirge mit besonderer Berücksichtigung der versorgungswasserwirtschaftlichen Belange im Tauplitzgebiet". In: *Österreichische Wasserwirtschaft* 16, pp. 112–123.
- Mazzilli, N. et al. (2017). *KarstMod. A modelling platform for rainfall - discharge analysis and modelling dedicated to karst systems*. Version 2.2.0. Environmental Modelling and Software 122. URL: <https://sokarst.org/en/software-en/karstmod-en/> (accessed on 8/2/2023).
- Microsoft Corporation (2022). *Windows Excel*. Microsoft Corporation.

- Missoni, S. and Gawlick, H.-J. (2011). "Evidence for Jurassic subduction from the Northern Calcareous Alps (Berchtesgaden; Austroalpine, Germany)". In: *International Journal of Earth Sciences* 100.7. PII: 552, pp. 1605–1631. ISSN: 1437-3254. DOI: 10.1007/s00531-010-0552-z.
- Morton, F. (1932). "Interessante Seetypen des steirischen Salzkammergutes". In: *Sonder-Abdruck aus dem Archiv für Hydrobiologie* 24, pp. 263–268.
- Moser, M. (2019). *GEOFAST MAPS 1:50.000 - 97 Bad Mitterndorf*. Ed. by Geologische Bundesanstalt. URL: <https://www.geologie.ac.at/en/onlineshop/detail/?id=0&seo=undefined&origId=2315>.
- Mroczek, Stefan et al. (2023). "Investigating the Eastern Alpine–Dinaric transition with teleseismic receiver functions: Evidence for subducted European crust". In: *Earth and Planetary Science Letters* 609, p. 118096. ISSN: 0012821X.
- Neubauer, F., Genser, J., and Handler, R. (2000). "The Eastern Alps: Result of a two-stage collision process". In: *Mitt. Geol. Ges. Wien* 92, pp. 117–134.
- Oki, T. and Kanae, Sh. (2006). "Global hydrological cycles and world water resources". eng. In: *Science* 313.5790. Journal Article Research Support, Non-U.S. Gov't Review, pp. 1068–1072. ISSN: 1095-9203. DOI: 10.1126/science.1128845. eprint: 16931749. URL: https://www.researchgate.net/publication/6856186_Global_Hydrological_Cycles_and_World_Water_Resources.
- Olarinoye, T. et al. (2020). "Global karst springs hydrograph dataset for research and management of the world's fastest-flowing groundwater". eng. In: *Scientific data* 7.1. Journal Article Research Support, Non-U.S. Gov't The authors declare no competing interests., p. 59. DOI: 10.1038/s41597-019-0346-5. eprint: 32080203.
- Ollivier, Ch. et al. (2021). "An evapotranspiration model driven by remote sensing data for assessing groundwater resource in karst watershed". In: *Science of The Total Environment* 781. PII: S0048969721017745, p. 146706. ISSN: 00489697. DOI: 10.1016/j.scitotenv.2021.146706.
- Pfarr, T., Seebacher, R., and Plan, L. (2023). *Die längsten Höhlen Österreichs / The longest caves in Austria*. Wien: Verband österreichischer Höhlenforscher.
- Pfiffner, O. A. (2015). *Geologie der Alpen*. ger. 3., aktualisierte und erweiterte Auflage. Vol. 8416. Geologie. Pfiffner, Othmar Adrian (VerfasserIn). Bern: Haupt Verlag. 397 pp. ISBN: 9783825286101.
- Piller, W. E. (1976). "Fazies und Lithostratigraphie des gebankten Dachsteinkalkes (Obertrias) am Nordrand des Toten Gebirges (S Grünau/Almtal, Oberösterreich)". In: *Mitt. Ges. Geol. Bergbaustud. Österr.* 23, pp. 113–152.

- Piller, W. E. et al. (2004). *Die stratigraphische Tabelle von Österreich 2004 (sedimentäre Schichtfolgen)*. Wien: Kommission für die paläontologische und stratigraphische Erforschung Österreichs der Österreichischen Akademie der Wissenschaften and Österreichische Stratigraphische Kommission.
- Plan, L. et al. (2009a). "Hypogene Caves in Austria". In: *Hypogene Speleogenesis and Karst Hydrogeology of Artesian Basins* (Simferopol). Ed. by A. B. Klimchouk and D. Ford. Special Paper 1. Ukrainian Institute of Speleology and Karstology. Ukrainian Institute of Speleology and Karstology, pp. 121–127.
- Plan, L. et al. (2009b). "Karst morphology and groundwater vulnerability of high alpine karst plateaus". In: *Environmental Geology* 58.2. PII: 1605, pp. 285–297. ISSN: 0943-0105. DOI: 10.1007/s00254-008-1605-5.
- Plan, L. et al. (2023). "4D flow pattern of the longest cave in the Eastern Alps (Schönberg-Höhle system, Totes Gebirge)". In: *International Journal of Speleology* 52.1, pp. 45–56. ISSN: 0392-6672. DOI: 10.5038/1827-806X.52.1.2471.
- Plöschinger, B. (1980). "Die nördlichen Kalkalpen". In: *Der geologische Aufbau Österreichs*. Ed. by R. Oberhauser. Wien: Springer, pp. 218–264. ISBN: 3-211-81556-2.
- Posit team (2023). *RStudio: Integrated Development Environment for R*. Boston, MA: Posit Software, PBC. URL: <https://www.posit.co/>.
- QGIS Development Team (2023). *QGIS Geographic Information System*. Version 3.22. QGIS Association. URL: <https://www.qgis.org>.
- R Core Team (2023). *R: A Language and Environment for Statistical Computing*. Version 4.3.1. Wien.
- Radulovic, M. and Sekulic, G. (2015). "Determining locations of sublacustrine springs by remote sensing: the Skadar Lake case example Montenegro". In: *Construction of Unique Buildings and Structures* 29, pp. 73–86.
- Riedel, W. (1929). "Zur Mechanik geologischer Brucherscheinungen". In: *Cbl. Min. Geol. Paläont. Stuttgart*, pp. 354–368.
- Riedl, H.-E., Friehs, B., and Hochreiter, M. (2008). *1. Steirischer Seenbericht. Ergebnisse der limnologischen Untersuchungen von 1999 - 2007 unter Berücksichtigung früherer Veröffentlichungen*. Graz: Fachabteilung 17C Referat Gewässeraufsicht der Steiermärkischen Landesregierung.
- Ruttner, F. (1937). "Limnologische Studien an einigen Seen der Ostalpen. Seen des Salzkammergutes, des Ötzer- und Hochschwabgebietes". In: *Archiv für Hydrobiologie* 32.

- Salmen, F. (Jan. 31, 2012). "Polare Kälte in Österreich - aber keine Rekorde". In: *OÖ-Nachrichten*. URL: <https://www.nachrichten.at/oberoesterreich/Polare-Kaelte-in-OEsterreich-aber-keine-Rekorde;art4,809262>.
- Schäffer, G. (1982). *Geologische Karte der Republik Österreich 1:50.000 - 96 Bad Ischl*. Ed. by Geologische Bundesanstalt. Wien.
- Scheidleder, A. (2001). *Pilotprojekt "Karstwasser Dachstein". Band 2: Karsthydrologie und Konstaminationsrisiko von Quellen*. Ed. by A. Scheidleder. Wien: Geologische Bundesanstalt Österreich and Umweltbundesamt.
- Schmalfuss, C. et al. (2023). "Major shifts in sediment provenance revealed by a Pleistocene drill core record from the Eastern Alps (Austria)". In: *EGU General Assembly 2023*.
- Schmid, S. M. et al. (2004). "Tectonic map and overall architecture of the Alpine orogen". In: *Eclogae Geologicae Helvetiae* 97.1. PII: 1113, pp. 93–117. ISSN: 0012-9402. DOI: 10.1007/s00015-004-1113-x.
- Schneider, T.-M. (2013). "Neues aus dem Almborg-Höhlensystem (1624/18), Totes Gebirge - ein Überblick über die laufenden Forschungsarbeiten". In: *Die Höhle* 64.1-4, pp. 72–78.
- Schöllnberger, W. (1973). "Zur Verzahnung von Dachsteinkalk-Fazies und Hallstätter Fazies am Südrand des Toten Gebirges (Nördliche Kalkalpen, Österreich)". In: *Mitt. Ges. Geol. Bergbaustud. Österr.* 22, pp. 95–153.
- Schönlaub, H. P. and Draurer, A. (2001). *GeoAustria: Das strategische Programmpaket der Geologischen Bundesanstalt*. Wien: Geologische Bundesanstalt Österreich.
- Schriebl, A. et al. (2024). *Hydrologische Markierungsversuche in Österreich*. Wien: Geosphere Austria.
- Schuster, R. and Stüwe, K. (2010). "Die Geologie der Alpen im Zeitraffer". In: *Mitteilungen des naturwissenschaftlichen Vereins für Steiermark* 140, pp. 5–21.
- (2022). "Geological and Tectonic Setting of Austria". In: *Landscapes and Landforms of Austria*. Ed. by Ch. Embleton-Hamann. Cham: Springer International Publishing, pp. 3–26. ISBN: 978-3-030-92813-1.
- Schuster, R. et al. (2014). *Rocky Austria. Geologie von Österreich - kurz und bunt*. 2nd ed. Wien.
- Schwingschlögl, R. (1980). *Photogeologie und Bruchtektonik des Totengebirgsplateaus*. Wien.
- (1986). "Photogeologie und Bruchtektonik des Totengebirgsplateaus". In: *Mitt. Ges. Geol. Bergbaustud. Österr.* 32, pp. 79–103.

- Seebacher, R. (2015). "Forschungen in der Liager-Höhle bei Altaussee, Kat. Nr.: 1623/1, und Tauchgänge in der Kugelmühle bei Altaussee, Kat. Nr.: 1623/221, Totes Gebirge, Stmk." In: *Mitt. d. Vereins für Höhlenkunde in Obersteier*, pp. 135–139.
- SISKA (2023). *VisualKARSYS*. La Chaux-de-Fonds (CH): SISKA. URL: <https://www.visualkarsys.com/>.
- Stevanovic, Z. (2015). "Characterization of Karst Aquifer". In: *Karst Aquifers—Characterization and Engineering*. Ed. by Z. Stevanović. Professional Practice in Earth Sciences. Cham: Springer International Publishing, pp. 47–122. ISBN: 978-3-319-12849-8.
- Stundl, K. (1953). "Zur Limnologie steirischer Bergseen". In: *Schweizerische Zeitschrift für Hydrologie* 15.1, pp. 168–189.
- Stüwe, K. and Schuster, R. (2010). "Initiation of subduction in the Alps: Continent or ocean?" In: *Geology* 38.2, pp. 175–178. ISSN: 0091-7613. DOI: 10.1130/G30528.1.
- USACE Hydrologic Engineering Center (2024). *HEC-HMS Technical Reference Manual. Model Classification*. U.S. Army Corps of Engineers Hydrologic Engineering Center. URL: <https://www.hec.usace.army.mil/confluence/hmsdocs/hmstrm/primer-on-models/model-classification> (accessed on 17/4/2024).
- Vacek, M. and Geyer, G. (1916). *Erläuterungen zur Geologischen Karte der im Reichsrath vertretenen Königreiche und Länder der Österr.-Ungar. Monarchie: SW-Gruppe Nr. 20 Liezen*. Wien: Verlag der k. k. Geologischen Reichsanstalt.
- van Husen, D. and Mayr, M. (2007). "The hole of Bad Aussee. An unexpected overdeepened area in NW Steiermark, Austria". In: *Austrian Journal of Earth Sciences* 100.128-136.
- Veress, M. (2022). "A General Description of Karst Types". In: *Encyclopedia* 2.2. PII: encyclopedia2020073, pp. 1103–1118. DOI: 10.3390/encyclopedia2020073.
- Wagner, S. (2021). "Altausseer See- Geomorphologische Kartierung des Seebodens und der Uferzone anhand von photogrammetrischen und Multibeamecholotaufnahmen". Institut für Angewandte Geologie. Master Thesis. Wien: Universität für Bodenkultur. 122 pp.
- Watson, R. (Dec. 22, 2023). *Personal communication: Exploration of Schwarzmooskogel cave system and hope to connect with Schönberg cave system*. Zoom. Online.
- Whitaker, W. and Reid, C. (1899). *The Water Supply of Sussex: From Underground Sources*. London: Memoirs of the Geological Survey of England and Wales, HMSO.
- WHYMAP (2017). *WoKAM (World Karst Aquifer Map)*. Ed. by WHYMAP (World-wide Hydrogeological Mapping and Assessment Programme). Dubrovnik (accessed on. 13/2/2024).
- Wien Geschichte Wiki (2024). *Wasserversorgung*. Stadt Wien (accessed on. 13/3/2024).
- Winding, N. (1985). *Wasservogelzählung - Jänner 1985*.

- Winkler, R. (2004). "Die karsthydrographische Situation im westlichen Toten Gebirge". In: *Der Schwarzmooskogel*. Ed. by R. Winkler. Karst & Höhle 2003/2003. München: VDHK, pp. 117–124.
- Worthington, S. R. H. et al. (2017). "Contrasting definitions for the term 'karst aquifer'". In: *Hydrogeology Journal* 25.5. PII: 1628, pp. 1237–1240. ISSN: 1431-2174. DOI: 10.1007/s10040-017-1628-7.
- Zojer, H. (1978). "Vergleiche von Ergebnissen der Anwendung von Isotopenmethoden in alpinen Karstgebieten". In: *Steirische Beiträge zur Hydrogeologie* 30, pp. 127–138.
- Zötl, J. (1974). *Karsthydrogeologie*. Wien: Springer-Verlag Wien. 308 pp.
- (1985). "Karst water: An important factor for the drinking water supply in Austria". In: *Environ Geol Water Sci* 7, pp. 237–239.

List of Tables

1.1	General characteristics of Lake Altaussee	3
2.1	Overview of the meteorological stations in the region	63
2.2	Summary statistics of precipitation data	65
2.3	Summary statistics of discharge from Lake Altaussee.	66
2.4	List of available boreholes with drilling profile data in area of interest.	72
2.5	P wind correction factors for each P station	78
2.6	Lake Altaussee water table minimum, mean, maximum elevation a.s.l.	84
3.1	Summary statistics of obtained catchment sizes.	97
3.2	Summary statistics on flat ET percentage of annual P.	97
3.3	Summary statistics of obtained catchment sizes from corrected annual P sums.	98
3.4	Summary statistics on flat ET percentage of corrected annual P.	99
3.5	Volumes of VisualKARSYS-derived phreatic zone depending on active spring.	104
A.1	Details of the construction of geological sections	144

List of Figures

1.1	Map of region of interest with shaded relief.	2
1.2	Bathymetry of Lake Altaussee with main karst funnel area.	4
1.3	Phosphorus content of Lake Altaussee compared to trophic state thresholds .	5
1.4	Comparison of NDVI values for February and August 2023 over western <i>Totes Gebirge</i>	7
1.5	World Karst Aquifer Map (WoKAM), developed by the World-wide Hydrogeological Mapping and Assessment Programme (WHYMAP).	10
1.6	European extent of World Karst Aquifer Map (WoKAM).	11
1.7	A map of the Austrian extent of karstifiable rock formations.	12
1.8	Tectonic map of Europe.	15
1.9	Diagram of postulated Pannonian Moho underneath Eastern Alps	18
1.10	Block diagram of current tectonic situation in Alps	20
1.11	Tectonic map of Eastern Alps and NCA	21
1.12	Map showing Rinnerboden and environs with structural geological data points	28
1.13	Block diagram of basic aquifer types	31
1.14	Sectional diagram of a typical karst system's hydrogeological zones.	34
1.15	Block diagram of a typical karst system's hydrogeological zones, inputs and flows.	34
1.16	International distribution of VisualKARSYS projects	46
1.17	Diagram of the water cycle with flux volumes from Oki and Kanae (2006). .	50
1.18	Diagram of the karst hydrologic system by Ford and Williams (2007).	51
1.19	Diagram of the difference in view of a karst system hydrogeology vs hydrology, from Jeannin (2014).	52
1.20	Map of meteorological stations around <i>Totes Gebirge</i>	58
1.21	Precipitation distribution map of <i>Salzkammergut</i> , from Bullmann (2018). . .	59
1.22	Map of springs around <i>Totes Gebirge</i> , from Maurin and Zötl (1960).	60
2.1	Map showing hydrological points of interest and data sources	64
2.2	Overview as boxplot of precipitation data for each station included.	66

2.3	Histogram of daily average discharge from Lake Altaussee	67
2.4	Monthly mean discharge from Lake Altaussee	67
2.5	Development of the annual discharge averages from Lake Altaussee over time	68
2.6	Example of geological map sheet border inconsistencies	70
2.7	Traces of used, existing geological sections	71
2.8	Map with locations of available boreholes.	73
2.9	<i>Schwarzmooskogel</i> (1623) and <i>Schönberg</i> (1626) cave systems visualised. . .	75
2.10	<i>Schwarzmooskogel</i> (1623) cave system visualised with surface terrain	76
2.11	Graph of discharge from Lake Altaussee with flat minimum flow estimation. .	79
2.12	Diagramme of VisualKARSYS workflow	82
2.13	Bathymetry of Lake Altaussee with main karst funnels, geographic means and location of spring for VisualKARSYS.	83
2.14	Stratigraphic formations per map sheet inside scope for section drawing. . .	86
2.15	Iteration on applied hydrostratigraphy for VisualKARSYS model, each as exported directly from the platform.	90
2.16	All section traces of project, with project scope rectangles.	91
2.17	Traces and numbering of constructed sections.	92
3.1	Diagram of results of water balance: catchment size per station and year. . .	96
3.2	Diagram of results of water balance: catchment size per station and year with corrected data.	98
3.3	Geological sections A and D, drawn by author.	101
3.4	Geological sections B and C, drawn by author.	102
3.5	Geological sections 1, 2 and 3, drawn by author.	103
3.6	Screenshots of the 3D model.	106
3.7	Map with VisualKARSYS results and contextualisation.	107
4.1	Map of annual potential evapotranspiration contours over area of interest, from Austrian Hydrological Atlas.	110
4.2	Screenshots of 3D with geological sections for comparison.	119
4.3	Comparison map between catchment delineated in VisualKARSYS and oro- graphic catchments on <i>Totes Gebirge</i>	120
4.4	SMK cave system elevation overlayed on VisualKARSYS generated slice. . .	121
4.5	Map with manual vs VisualKARSYS catchment boundaries, cave system areas and orographic catchments.	122

A.1 Section 1 trace with geological data included in construction. 153

A.2 Section 2 trace with geological data included in construction. 154

A.3 Section 3 trace with geological data included in construction. 155

A.4 Section A trace with geological data included in construction. 156

A.5 Section B trace with geological data included in construction. 157

A.6 Section C trace with geological data included in construction. 158

A.7 Section D trace with geological data included in construction. 159

Appendix A

Table A.1: Details of the construction of geological sections: features included in each section, as seen in corresponding Figures A.1 to A.7 and their type, actual dip direction and dip in Clar notation, apparent dip, normal distance from section trace, elevation above sea level at intersections with traces. EXPLAIN SST, S, M!

Feature number	Feature type	Dip direction and dip (XXX°/YY°)	Apparent dip (ZZ°)	Distance from trace (m)	Elevation of intersection (m a.s.l.)
Section 1		Strike of section trace: 50.5°			
1	bedding plane	251/30-60	28-58	400	1030
2	bedding plane	160/05-30	02-11	525	no intersection
3	bedding plane	180/30-60	20-48	100	875
4	bedding plane	342/30-60	12-32	450	no intersection
5	bedding plane	126/05-30	01-08	400	1475
6	bedding plane	124/05-30	01-09	175	1100
7	bedding plane	100/05-30	03-21	375	no intersection
8	bedding plane	260/05-30	04-27	475	no intersection
9	bedding plane	178/05-30	03-19	175	1750
10	bedding plane	000/05-30	03-20	75	1680
11	bedding plane	140/05-30	00	275	1390
12	fracture	090/90	90	0	1900

Continued on next page

Table A.1 – *Continued from previous page*

Feature number	Feature type	Dip direction and dip (XXX°/YY°)	Apparent dip (ZZ°)	Distance from trace (m)	Elevation of intersection (m a.s.l.)
13	fracture	118/90	90	0	1900
Sst1	bedding plane	338/30	10	25	1530
Sst2	bedding plane	175/40	25	325	no intersection
Section 2		Strike of section trace: 50.5°			
1	bedding plane	000/00-05	00-05	475	no intersection
2	bedding plane	000/00-05	00-05	375	no intersection
3	bedding plane	090/05-30	04-24	450	no intersection
4	bedding plane	150/05-30	01-05	50	no intersection, projected
5	bedding plane	210/05-30	05-28	50	1800
6	bedding plane	125/05-30	01-09	475	1550
7	fracture		0	1275	
8	fracture		0	1400	
9	fracture		0	1400	
10	fracture		0	1425	
11	fracture		0	1650	
12	fracture		0	1700	
13	fracture		0	1750	
Sst1	bedding plane	290/20	11	175	no intersection
Sst2	bedding plane	305/25	07	150	no intersection

Continued on next page

Table A.1 – *Continued from previous page*

Feature number	Feature type	Dip direction and dip (XXX°/YY°)	Apparent dip (ZZ°)	Distance from trace (m)	Elevation of intersection (m a.s.l.)
Sst3	bedding plane	130/55	15	50	1450
Sst4	bedding plane	150/35	07	100	1400
Sst5	bedding plane	240/20	20	150	1400
Sst6	bedding plane	160/30	11	350	no intersection
Sst7	bedding plane	110/15	08	400	no intersection
Sst8	bedding plane	120/50	23	275	no intersection
Sst9	bedding plane	080/70	67	75	1550
Sst10	bedding plane	040/40	40	500	1550
S1	fracture			0	1400
Section 3		Strike of section trace: 50.5°			
1	bedding planes	194/05-30	04-25	225	no intersection
2	bedding planes	201/05-30	04-27	350	no intersection
3	bedding planes	291/85-90	80-90	400	no intersection
4	bedding planes	155/05-30	01-08	275	no intersection
5	bedding planes	163/05-30	02-12	125	1850
6	bedding planes	130/05-30	01-06	300	no intersection
7	bedding planes	135/05-30	00-03	375	no intersection
8	bedding planes	135/05-30	00-03	200	no intersection
9	fracture		90	0	
10	fracture		90	0	

Continued on next page

Table A.1 – *Continued from previous page*

Feature number	Feature type	Dip direction and dip (XXX°/YY°)	Apparent dip (ZZ°)	Distance from trace (m)	Elevation of intersection (m a.s.l.)
11	fracture		90	0	
12	fracture		90	0	
13	fracture		90	0	
14	fracture	0	90	0	
Sst1	bedding planes	140/45	00	450	no intersection
Sst2	bedding planes	150/45	09	325	no intersection
S1	fracture		90	0	
S2	fracture		90	0	
S3	fracture		90	0	
Section A		Strike of section trace: 142°			
1	bedding plane	321/30-60	30-60	175	
			normal projection because of parallelism		
2	bedding plane	307/05-30	05-29	450	
			+/- normal projection because of band of rock		
3	bedding plane	319/60-85	30-60	425	
4	bedding plane	105/05-30	04-25	250	
			3 and 4: Brunnkogel-Ahornkogel anticline		
5	bedding plane	160/05-30	05-29	450	
6	bedding plane	124/05-30	05-29	400	
7	bedding plane	180/30-60	25-54	300	

Continued on next page

Table A.1 – *Continued from previous page*

Feature number	Feature type	Dip direction and dip (XXX°/YY°)	Apparent dip (ZZ°)	Distance from trace (m)	Elevation of inter-section (m a.s.l.)
8	bedding plane	126/05-30	05-29	150	
9	bedding plane	000/00	00	75	
10	bedding plane	291/60-85	56-84	250	
11	bedding plane	194/05-30	03-19	375	
12	bedding plane	291/85-90	84-90	125	
13	bedding plane	208/05-30	02-13	250	
14	fracture	0	90	0	
15	fracture (suspected)	0			
16	fracture		90	0	
17	fracture		90	0	
18	fracture		90	0	
19	fracture		90	0	
20	fracture		90	0	
M1	fracture		90	0	
M2	fracture		90	0	
M3	fracture		90	0	
S1	fracture		90	0	
S2	fracture		90	0	

Section B

Strike of section trace: 142°

1	bedding plane	137/30-60	30-60	475	
---	---------------	-----------	-------	-----	--

Continued on next page

Table A.1 – *Continued from previous page*

Feature number	Feature type	Dip direction and dip (XXX°/YY°)	Apparent dip (ZZ°)	Distance from trace (m)	Elevation of intersection (m a.s.l.)
2	bedding plane	138/05-30	05-30	375	
3	bedding plane	142/30-60	30-60	225	
4	bedding plane	112/05-30	26-56	275	no intersection
5	bedding plane	123/05-30	05-28	175	
6	bedding plane	143/30-60	30-60	475	no intersection
7	bedding plane	125/05-30	05-29	250	
8	bedding plane	133/05-30	05-30	400	
9	fracture		90	0	
10	fracture		90	0	
11	fracture		90	0	
12	fracture		90	0	
13	fracture		90	0	
14	fracture		90	0	
15	fracture		90	0	
16	fracture		90	0	
17	fracture		90	0	
18	fracture		90	0	
19	fracture		90	0	
Section C			Strike of section trace: 142°		
1	bedding plane	186/05-30	04-23	225	1600

Continued on next page

Table A.1 – *Continued from previous page*

Feature number	Feature type	Dip direction and dip (XXX°/YY°)	Apparent dip (ZZ°)	Distance from trace (m)	Elevation of intersection (m a.s.l.)
2	fold core	181/05-20	04-16	450	1650
3	bedding plane	151/30-60	30-60	400	1760
4	bedding plane	161/05-30	05-29	250	1770
5	bedding plane	000/00-05	00-05	425	no intersection
6	bedding plane	180/05-30	04-25	200	no intersection
7	fracture	080	suspected	0	760
8	fracture	090	secured	0	1640
9	fracture	045	secured	0	1730
10	fracture	045	secured	0	1735
11	fracture	120	suspected	0	1890
12	fracture	090	secured	0	1930
13	fracture	320	secured	0	1870
14	fracture	320	secured	0	1785
15	fracture	320	secured	0	1745
16	fracture	030	secured	0	1550
17	fracture	030	secured	0	1460
18	fracture	030	secured	0	1425
19	fracture	080	suspected	0	1720
20	fracture	070	suspected	0	725
S1	fracture	120	suspected	0	1860
S2	fracture	075	suspected	0	1920

Continued on next page

Table A.1 – *Continued from previous page*

Feature number	Feature type	Dip direction and dip (XXX°/YY°)	Apparent dip (ZZ°)	Distance from trace (m)	Elevation of intersection (m a.s.l.)
S3	fracture	065	suspected	0	1920
S4	fracture	250	suspected	0	1875
S5	fracture	210	secured	0	1890
S6	fracture	210	secured	0	1890
Section D		Strike of section trace: 142°			
1	bedding plane	130/60-85	60-85	375	no intersection
2	bedding plane	117/30-60	28-58	50	890
3	bedding plane	145/60-85	60-85	300	
4	bedding plane	300/85-90	85-90	100	
5	bedding plane	000/30-60	25-54	300	
6	bedding plane	218/05-30	01-08	475	
7	bedding plane	090/05-30	03-20	200	
8	bedding plane	130/05-30	05-30	400	
9	bedding plane	150/05-30	05-30	450	
10	bedding plane	177/05-30	04-25	250	
11	bedding plane	295/05-30	05-27	300	
12	bedding plane	180/30-60	25-54	450	
13	fracture			0	
14	fracture			0	
15	fracture			0	

Continued on next page

Table A.1 – *Continued from previous page*

Feature number	Feature type	Dip direction and dip (XXX°/YY°)	Apparent dip (ZZ°)	Distance from trace (m)	Elevation of inter-section (m a.s.l.)
16	fracture			0	
17	fracture			0	
18	fracture			0	
Sst1	bedding plane	215/75	48	100	
Sst2	bedding plane	330/55	55	200	
Sst3	bedding plane	175/40	35	200	
Sst4	bedding plane	338/30	30	100	
Sst5	bedding plane	110/30	26	250	
Sst6	bedding plane	125/35	29	175	
Sst7	bedding plane	165/25	23	300	
Sst8	bedding plane	195/25	16	225	

Figure A.1: Trace of geological section 1 constructed by the author (see Figure 2.17) with numbered data points used from Austrian geological map (A) and fault tectonic map by Schwingenschlögl (1986) (B), respectively, in a 500 m buffer to each side, whose details can be seen in Table A.1.

Figure A.2: Trace of geological section 2 constructed by the author (see Figure 2.17) with numbered data points used from Austrian geological map (A) and fault tectonic map by Schwingenschlögl (1986) (B), respectively, in a 500 m buffer to each side, whose details can be seen in Table A.1.

Figure A.3: Trace of geological section 3 constructed by the author (see Figure 2.17) with numbered data points used from Austrian geological map (A) and fault tectonic map by Schwingenschlögl (1986) (B), respectively, in a 500 m buffer to each side, whose details can be seen in Table A.1.

Figure A.4: Trace of geological section A constructed by the author (see Figure 2.17) with numbered data points used from Austrian geological map (A) and fault tectonic map by Schwingenschlögl (1986) (B), respectively, in a 500 m buffer to each side, whose details can be seen in Table A.1.

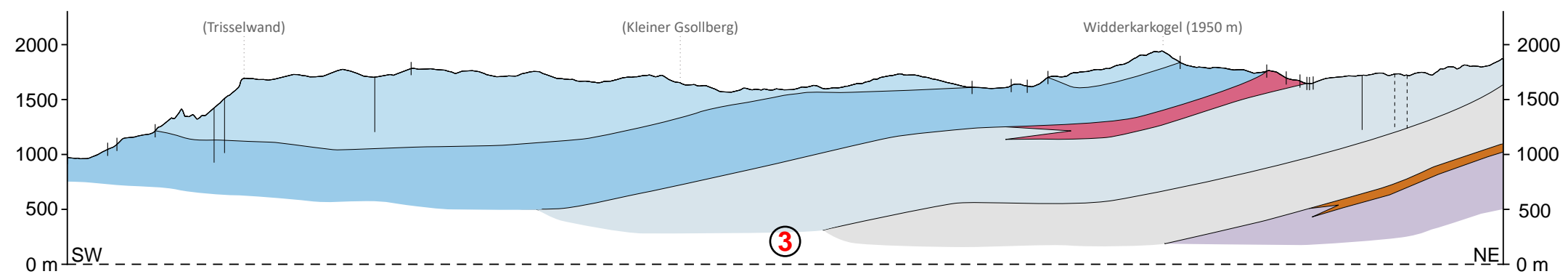
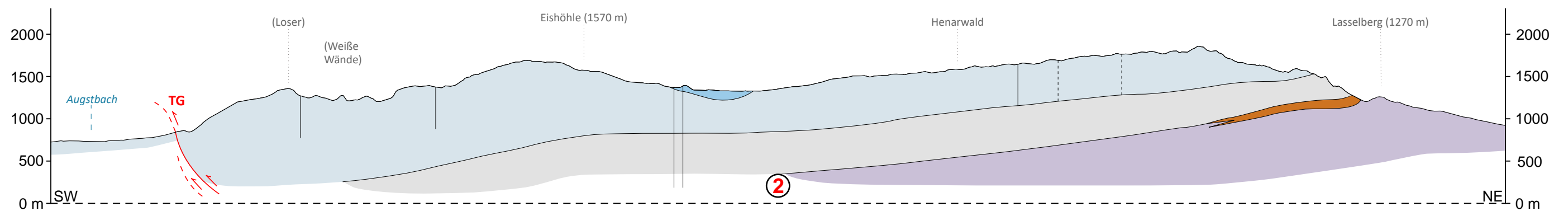
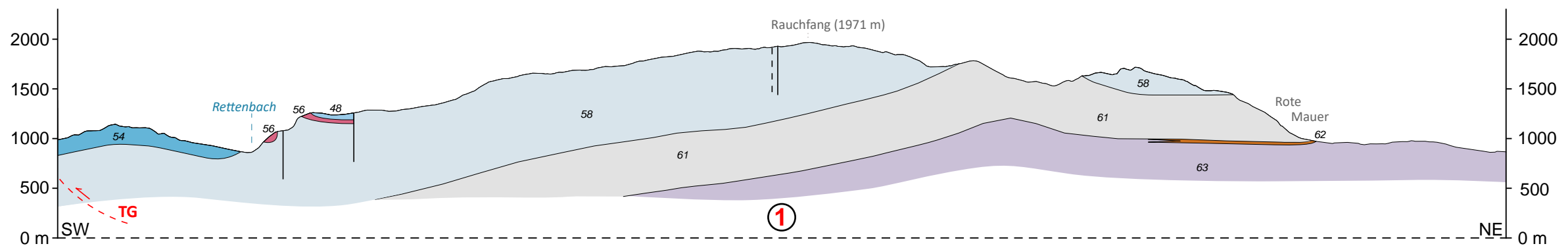
Figure A.5: Trace of geological section B constructed by the author (see Figure 2.17) with numbered data points used from Austrian geological map (A) and fault tectonic map by Schwingenschlögl (1986) (B), respectively, in a 500 m buffer to each side, whose details can be seen in Table A.1.

Figure A.6: Trace of geological section C constructed by the author (see Figure 2.17) with numbered data points used from Austrian geological map (A) and fault tectonic map by Schwingenschlögl (1986) (B), respectively, in a 500 m buffer to each side, whose details can be seen in Table A.1.

Figure A.7: Trace of geological section D constructed by the author (see Figure 2.17) with numbered data points used from Austrian geological map (A) and fault tectonic map by Schwingenschlögl (1986) (B), respectively, in a 500 m buffer to each side, whose details can be seen in Table A.1.



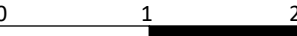
Appendix B

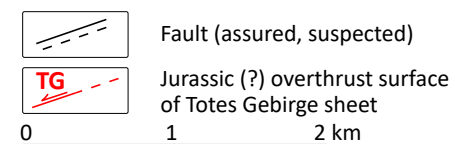
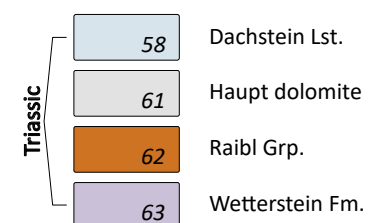
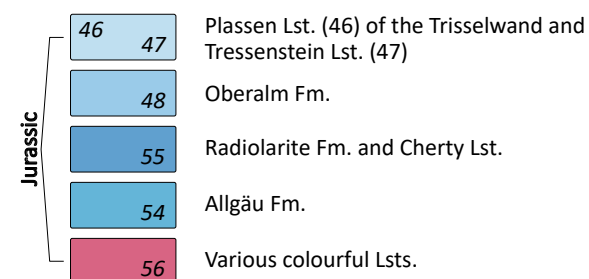
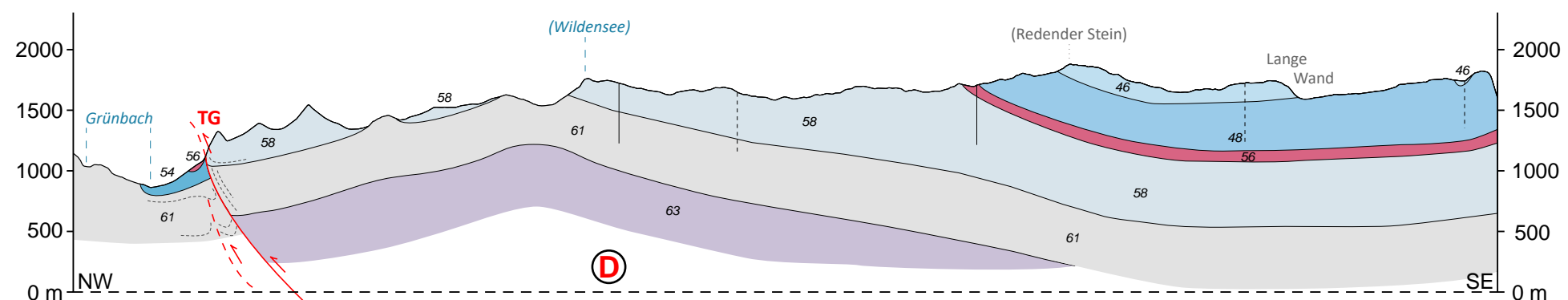
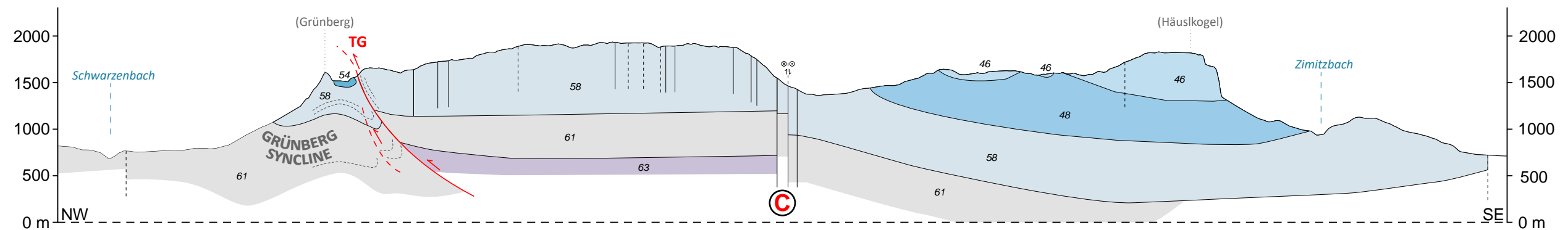
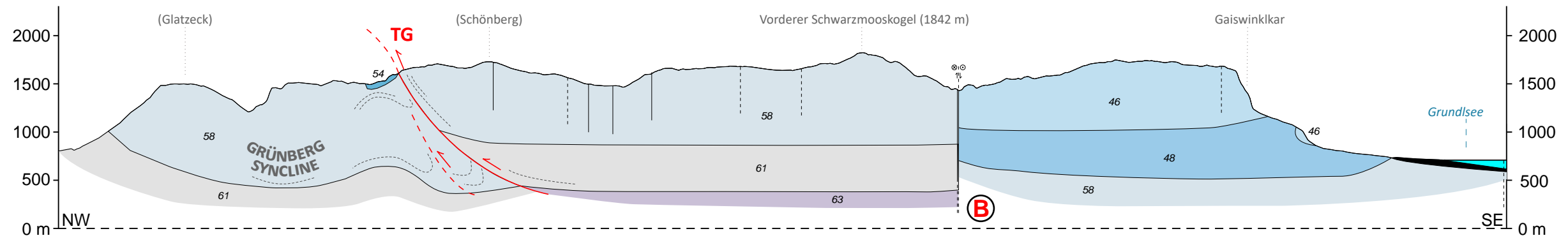
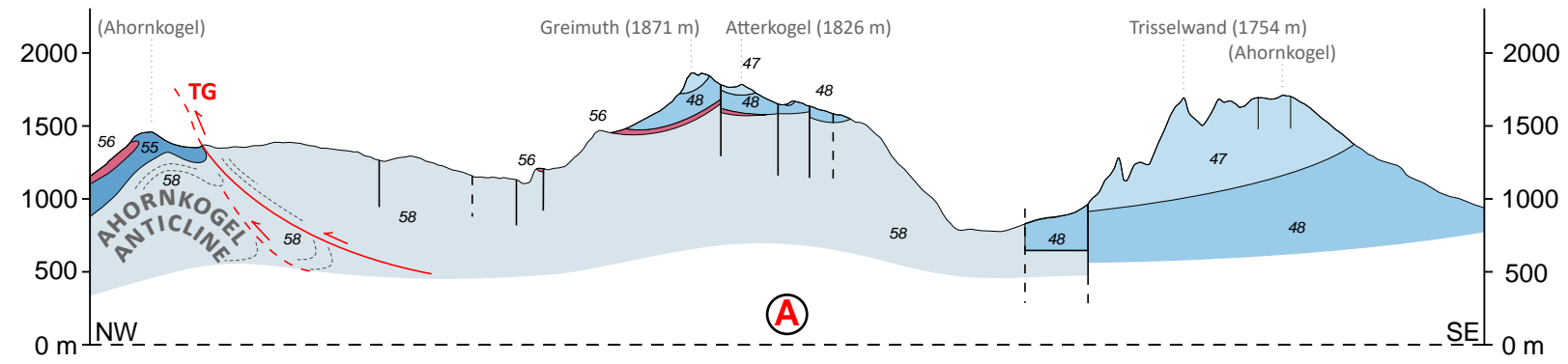
The geological sections drawn by the author are printed in their original scale of 1:50 000 on the following two pages.



- Jurassic**
- 46 47 Plassen Lst. (46) of the Trisselwand and Tressenstein Lst. (47)
 - 48 Oberalm Fm.
 - 55 Radiolarite Fm. and Cherty Lst.
 - 54 Allgäu Fm.
 - 56 Various colourful Lsts.

- Triassic**
- 58 Dachstein Lst.
 - 61 Haupt dolomite
 - 62 Raibl Grp.
 - 63 Wetterstein Fm.

-  Fault (assured, suspected)
 Jurassic (?) overthrust surface of Totes Gebirge sheet
 0 1 2 km
 Drawn by Eric Smit, master thesis 2024
 BOKU University
 Department Civil Engineering and Natural Hazards
 Institute for Applied Geology



Drawn by Eric Smit, master thesis 2024
BOKU University
Department Civil Engineering and Natural Hazards
Institute for Applied Geology